

Technical Report

TR-20-17

July 2021



Evaluation report of Task 9B based on comparisons and analyses of modelling results for the Äspö HRL LTDE-SD experiments

Task 9 of SKB Task Force GWFTS – Increasing the realism in solute transport modelling based on the field experiments REPRO and LTDE-SD

Josep M Soler

Shuo Meng

Luis Moreno

Ivars Neretnieks

Longcheng Liu

Pekka Kekäläinen

Milan Hokr

Jakub Říha

Aleš Vetešník

Dan Reimitz

Jakub Višňák

Dušan Vopálka

Klaus-Peter Kröhn

Yukio Tachi

Tsuyoshi Ito

Urban Svensson

Aitor Iraola

Paolo Trinchero

Mikko Voutilainen

Guido Deissmann

Dirk Bosbach

Dong Kyu Park

Sung-Hoon Ji

Libor Gvoždík

Martin Milický

Michal Polák

Nataliia Makedonska

Stephen P Kuluris

Satish Karra

Hari S Viswanathan

Björn Gylling

G William Lanyon

SVENSK KÄRNBRÄNSLEHANTERING AB

SWEDISH NUCLEAR FUEL
AND WASTE MANAGEMENT CO

Box 3091, SE-169 03 Solna
Phone +46 8 459 84 00
skb.se

SVENSK KÄRNBRÄNSLEHANTERING

Evaluation report of Task 9B based on comparisons and analyses of modelling results for the Äspö HRL LTDE-SD experiments

Task 9 of SKB Task Force GWFTS – Increasing the realism in solute transport modelling based on the field experiments REPRO and LTDE-SD

Josep M Soler¹, Shuo Meng², Luis Moreno², Ivars Neretnieks², Longcheng Liu², Pekka Kekäläinen³, Milan Hokr⁴, Jakub Říha⁴, Aleš Vetešník⁵, Dan Reimitz⁵, Jakub Višňák⁵, Dušan Vopálka⁵, Klaus-Peter Kröhn⁶, Yukio Tachi⁷, Tsuyoshi Ito⁷, Urban Svensson⁸, Aitor Iraola⁹, Paolo Trinchero⁹, Mikko Voutilainen³, Guido Deissmann¹⁰, Dirk Bosbach¹⁰, Dong Kyu Park¹¹, Sung-Hoon Ji¹¹, Libor Gvoždík¹², Martin Milický¹², Michal Polák¹², Nataliia Makedonska¹³, Stephen P Kuluris¹³, Satish Karra¹³, Hari S Viswanathan¹³, Björn Gylling¹⁴, G William Lanyon¹⁵

1 Institute of Environmental Assessment and Water Research, IDAEA-CSIC

2 Royal Institute of Technology, KTH

3 University of Helsinki

4 Technical University of Liberec

5 Czech Technical University in Prague

6 Gesellschaft für Anlagen- und Reaktorsicherheit, GRS

7 Japan Atomic Energy Agency, JAEA

8 Computer-aided Fluid Engineering AB

9 Amphos 21

10 Forschungszentrum Jülich

11 Korea Atomic Energy Research Institute, KAERI

12 PROGEO

13 Los Alamos National Laboratory

14 Gylling GeoSolutions

15 Fracture Systems Ltd

This report concerns a study which was conducted for Svensk Kärnbränslehantering AB (SKB). The conclusions and viewpoints presented in the report are those of the authors. SKB may draw modified conclusions, based on additional literature sources and/or expert opinions.

This report is published on www.skb.se

© 2021 Svensk Kärnbränslehantering AB

Abstract

Task 9B of the SKB Task Force on Modelling of Groundwater Flow and Transport of Solutes (Task Force GWFTS) was the second subtask within Task 9 and focused on the modelling of experimental results from the LTDE-SD in situ tracer test. The test had been performed at a depth of about 410 m in the Äspö Hard Rock Laboratory. Synthetic groundwater containing a cocktail of radionuclide tracers was circulated for 198 days on the natural surface of a fracture and in a narrow slim hole drilled in unaltered rock matrix. Overcoring of the rock after the end of the test allowed for the measurement of tracer distribution profiles in the rock from the fracture surface (A cores) and also from the slim hole (D cores). The measured tracer activities in the rock samples showed long profiles (several cm) for non- or weakly-sorbing tracers (Cl-36, Na-22), but also for many of the more strongly-sorbing radionuclides. The understanding of this unexpected feature was one of the main motivations for this modelling exercise. However, re-evaluation and revision of the data during the course of Task 9B provided evidence that the anomalous long tails at low activities for strongly sorbing tracers were an artefact due to cross-contamination during rock sample preparation. A few data points remained for Cs-137, Ba-133, Ni-63 and Cd-109, but most measurements at long distances from the tracer source (> 10 mm) were now below the reported detection limits.

Ten different modelling teams provided results for this exercise, using different concepts and codes. One additional team provided results related to conceptual development. The tracers that were finally considered were Na-22, Cl-36, Co-57, Ni-63, Ba-133, Cs-137, Cd-109, Ra-226 and Np-237. Three main types of models were used: (1) analytical solutions to the transport-retention equations, (2) continuum-porous-medium numerical models, and (3) microstructure-based models accounting for small-scale heterogeneity (i.e. mineral grains, porosities and/or microfracture distributions) and potential centimetre-scale fractures. The modelling by the different teams led to some important conclusions summarised below.

Concerning Na-22 and Cl-36, which showed long penetration profiles, tracer profiles within ca 30 mm from the tracer source could be interpreted with transport and retention parameters consistent with those obtained from laboratory-scale experiments. A disturbed zone, with a thickness of about 5 mm, could also be identified. This disturbed zone was especially evident in the Cl-36 data. However, some of the measured cores showed rather flat end tails for Na-22, which could not be reproduced by the homogeneous (i.e. constant transport and retention properties) or the continuum-porous-medium models using parameters consistent with those derived from laboratory-scale experiments. Reproduction of those tails by some of the microstructure-based models was performed by implementing fast transport along microfractures and cm-scale fractures.

For the rest of the tracers, which were more strongly sorbing, the profiles did not in general extend beyond 10 mm from the tracer source, with only some data points showing measurable activities further into the rock. Overall, the best fits to the measured profiles within a few mm from the tracer source were achieved by the homogeneous models (constant transport and retention parameters with distance), with apparent diffusion coefficients consistent with laboratory-derived experimental results. Good fits were also achieved by models assuming the presence of a disturbed zone with gradually changing parameters. The fact that most data points above detection limits fell within 5 to 8 mm from the tracer source, and the observations from the Cl-36 data, suggest the existence of a disturbed zone with a thickness of a few mm and characterised by rather constant transport and retention parameters. The longer profiles for Cl-36 and Na-22 advocate for an undisturbed rock matrix (unaffected by borehole drilling or alteration zones next to fractures) beyond these 5 to 8 mm from the tracer source. Additionally, the flat profile tails observed for some of the Na-22 profiles may point to the effect of microfractures and cm-scale fractures on radionuclide transport.

These conclusions could be reached after (1) the re-evaluation and revision of the experimental data (tracer profiles in the rock), and (2) the analysis of the different sets of model results performed by the different teams.

(1) The revision of the experimental data led to the dismissal of most of the measurements showing anomalously high activities far from the tracer source (long flat profile tail ends) for the strongly sorbing tracers, as possible contamination mechanisms during sample preparation were identified.

As an additional consequence, this discovery highlighted the importance of using blank samples in future tracer transport experiments. Using blank samples together with samples from the test rock sections during preparation and analysis will aid in the detection of potential contamination or background effects.

(2) The work performed by the different modelling teams allowed the comparison of many different model concepts, especially in terms of potential zonations of rock properties, such as the presence of a disturbed zone close to the tracer source, the potential effects of micro- and cm-scale fractures, or the implementation of microstructure-based models. An added value was the motivation provided by these exercises to advance in conceptual and numerical model development, which is a key goal of Task 9.

Sammanfattning

Modelleringsuppgiften Task 9B inom SKB:s internationella arbetsgrupp för modellering av grundvattenflöde och transport av lösta ämnen (Task Force GWFTS) var den andra deluppgiften inom Task 9 och fokuserade på modellering av experimentella resultat från LTDE-SD in situ spårämnestest. Experimentet LTDE-SD utfördes på ett djup av cirka 410 m i Äspö Hard Rock Laboratory. Syntetiskt grundvatten innehållande en cocktail av radionuklider cirkulerades 198 dagar i kontakt med en naturlig sprickyta och i ett smalt hål borrar in i en mer opåverkad bergmatris innanför sprickytan. Överborring av bergsektionen efter testets slut möjliggjorde mätning av spårämnesfördelningsprofiler i bergbiten, från sprickytan (A-kärnor) och även från det smala hålet (D-kärnor). De uppmätta radionuklidsaktiviteterna i bergproven påvisade långa profiler (flera cm) för icke- eller svagt sorberande ämnen (Cl-36, Na-22), men också för flera av de starkare sorberande radionukliderna. Förståelsen av detta oväntade resultat var en av de viktigaste motivationerna för denna modelleringsövning. Återbesök och djupare analys av de tidigare erhållna experimentella data, driven av Task 9B, resulterade dock i att de flesta av de anomalt långa lågaktiva svansarna för starkt sorberande spårare försvann. Några datapunkter återstod för Cs-137, Ba-133, Ni-63 och Cd-109, men de flesta mätningar på långa avstånd från spårkällan (> 10 mm) rapporterades nu vara under detektionsgränserna.

Tio olika modelleringsteam har rapporterat resultat för denna övning med olika koncept och koder. Ytterligare ett team tillhandahöll resultat relaterade till konceptuell utveckling. De radionuklider som slutligen modellerades var Na-22, Cl-36, Co-57, Ni-63, Ba-133, Cs-137, Cd-109, Ra-226 och Np-237. Tre huvudtyper av modeller användes: (1) analytiska lösningar av transport-retentionsekvationerna, (2) numeriska poröst medium-kontinuummodeller och (3) mikrostrukturbaserade modeller som redovisar småskalig heterogenitet (dvs mineral Korn, porositeter och/eller mikrosprickfördelningar) och möjliga sprickor i centimeterskala. Modelleringen som utfördes av de olika teamen ledde till några viktiga slutsatser som sammanfattas nedan.

När det gäller Na-22 och Cl-36, som påvisade långa penetrationsprofiler, spårämnesprofiler inom ca 30 mm från spårämneskällan kan modelleras med transport- och retentionsparametrar i överensstämmelse med de som erhållits från experiment i laboratorieskala. En störd zon, med en tjocklek av cirka 5 mm, kunde också identifieras. Inverkan av denna störda zon var särskilt tydlig i data för Cl-36. Vissa av de uppmätta kärnorna påvisade emellertid ganska plana svansar för Na-22, som inte kunde reproduceras av de homogena eller poröst kontinuummodellerna med användning av parametrar som överensstämmer med de härledda från experiment i laboratorieskala. Återgivningen av dessa svansar i några av de mikrostrukturbaserade modellerna utfördes genom att implementera snabba transportvägar längs mikrosprickor och sprickor i cm-skala.

För övriga radionuklider, som sorberade starkare, sträckte sig profilerna inte i allmänhet utöver 10 mm från spårämneskällan, med undantag av bara några datapunkter som påvisade mätbara aktiviteter längre in i bergbiten. Sammanfattningsvis uppnåddes de bästa anpassningarna till de uppmätta profilerna inom några mm från spårämneskällan med de homogena modellerna (konstanta transport- och retentionsparametrar över aktuellt avstånd) med diffusionskoefficienter som överensstämde med laboratoriehärledda experimentella resultat. Goda anpassningar uppnåddes också med modeller som antog förekomsten av en störd zon med gradvis förändrade parametrar. Det faktum att de flesta mätvärden över detektionsgränserna erhöles inom 5 till 8 mm från spårämneskällan, samt observationerna från Cl-36-data, antyder på förekomst av en störd zon med en tjocklek på några mm och kan kännetecknas av ganska konstanta transport- och retentionsparametrar. De längre profilerna för Cl-36 och Na-22 förespråkar en ostörd bergmatris (dvs opåverkad av borrhålsborring eller förändringszoner nära sprickor) bortom dessa 5 till 8 mm från spårämneskällan. Dessutom kan de plana profilsvansarna som observerats för några av Na-22-profilerna peka på effekten av mikrosprickor och sprickor i cm-skala på radionuklidtransport.

Dessa slutsatser kunde nås efter (1) en omvärdering och uppdatering av experimentella data (koncentrationsprofilerna i bergbitarna) och (2) analys av de olika uppsättningarna av modelleringsresultat som levererades av de olika grupperna.

(1) Revidering av de experimentella data ledde till att de flesta mätningarna avvisades som anomalt höga aktiviteter långt från spårämneskällan (långa platta profiländar) för de starkt sorberande spårämnena. Möjliga föroreningsmekanismer under provberedningen identifierades. Som en ytterligare

konsekvens, belyste denna upptäckt vikten av att använda blanka (oexponerade) prover i framtida spårämnes- och transportexperiment. Användandet av blanka prover tillsammans med exponerade prover från testsektionerna under beredning och analys kan hjälpa till att upptäcka potentiell kontaminering eller bakgrundseffekter.

(2) Arbetet som utfördes av de olika modelleringsgrupperna gjorde det möjligt att jämföra många olika modellkoncept, särskilt när det gäller potentiella områden med avvikande bergegenskaper, såsom närvaron av en störd zon nära spårämneskällan, de potentiella effekterna av sprickor i mikro- och centimeter-skalan, eller implementering av mikrostrukturbaserade modeller. Ett mervärde av dessa övningar är avancemanget inom konceptuell och numerisk modellutveckling, vilket är ett centralt mål för Task 9.

Contents

1	Introduction	9
2	Objectives and structure of Task 9B	15
2.1	Task 9B-1	15
2.2	Task 9B-2	15
2.3	Task 9B-3	16
3	Models and parameters	17
3.1	Royal Institute of Technology (KTH)	20
3.2	University of Helsinki (HYRL)	21
3.3	Technical University of Liberec (TUL)	21
3.3.1	Stage 1	22
3.3.2	Stage 2	22
3.4	Czech Technical University in Prague (CTU)	22
3.5	Gesellschaft für Anlagen- und Reaktorsicherheit (GRS)	23
3.6	Japan Atomic Energy Agency (JAEA)	24
3.7	Computer-Aided Fluid Engineering AB (CFE)	24
3.8	Amphos 21 (A21)	25
3.9	Korea Atomic Energy Research Institute (KAERI)	26
3.10	PROGEO	27
3.11	Los Alamos National Laboratory (LANL)	28
4	Results and discussion	29
4.1	Na-22	29
4.2	Cl-36	34
4.3	Co-57	38
4.4	Ni-63	40
4.5	Ba-133	42
4.6	Cs-137	46
4.7	Cd-109	51
4.8	Ra-226	52
4.9	Np-237	54
5	Summary and conclusions	55
	Acknowledgements	59
	References	61
Appendix 1	Summary tables with available measured rock porosities, transport and sorption parameters	63
Appendix 2	Comparison of activity profiles between Data Delivery 11 (start of Task 9B) and Data Delivery 40 (final dataset)	67

1 Introduction

The SKB Task Force on Modelling of Groundwater Flow and Transport of Solutes (Task Force GWFTS) is an international forum in the area of conceptual and numerical modelling of groundwater flow and solute transport in fractured rock. Task 9 focuses on the fractured crystalline host rock surrounding present and future repositories for spent fuel and other radioactive waste. Task 9B was the second subtask within Task 9 and focused on inverse and predictive modelling of experimental results from the in situ tracer test LTDE-SD. The experiment was carried out using radioactive tracers at a depth of about 410 m below sea level within the Äspö Hard Rock Laboratory in Sweden by Geosigma AB, under the direction of SKB (Figure 1-1). It is one of few recent in situ studies focusing on tracer transport in the stagnant pore water of the crystalline rock matrix. Details of the experimental setup and procedures were reported in the task description (Löfgren and Nilsson 2020), together with references to relevant laboratory-based experimental results for porosities, diffusion coefficients and sorption parameters (Vilks et al. 2005, Widstrand et al. 2010). Only a summary is given here.

A borehole (KA3065A03) was drilled to intersect a target fracture in the host granodiorite (196.5 mm diameter at the intersection). The approximate location of the target fracture in the experimental borehole had been predicted prior to its drilling based on a structural model and geometric considerations. The aim was to core drill 50 mm past the fracture surface, thus creating a short core stub. This stub was required in order to pack-off a section of the fracture plane, using a special cup-shaped device, for subsequent performance of the tracer test. However, the drilling continued too far beyond the target fracture, leaving a 16 cm long core stub. The stub surface was located at borehole length 10.72 m (Winberg et al. 2003). Additionally, a 36-mm-diameter slim hole was drilled through the centre of the core stub. During the experiment, synthetic brackish groundwater (Cl-Na-Ca-SO₄ dominated, 5 810 mg/L Cl, ~0.17 M ionic strength, pH ~7, T ~15°C) containing a tracer cocktail was simultaneously circulated on (i) the exposed fracture surface (stub) and (ii) a 300 mm long packed-off section of the slim hole (Widstrand et al. 2010). The hydraulic conditions were stable during the experiment, apart from short pressure disturbances mainly due to injection and sampling occasions in the borehole. The pressure in the test section varied between 3 580 and 3 600 kPa. The experimental setup is shown in Figure 1-2.

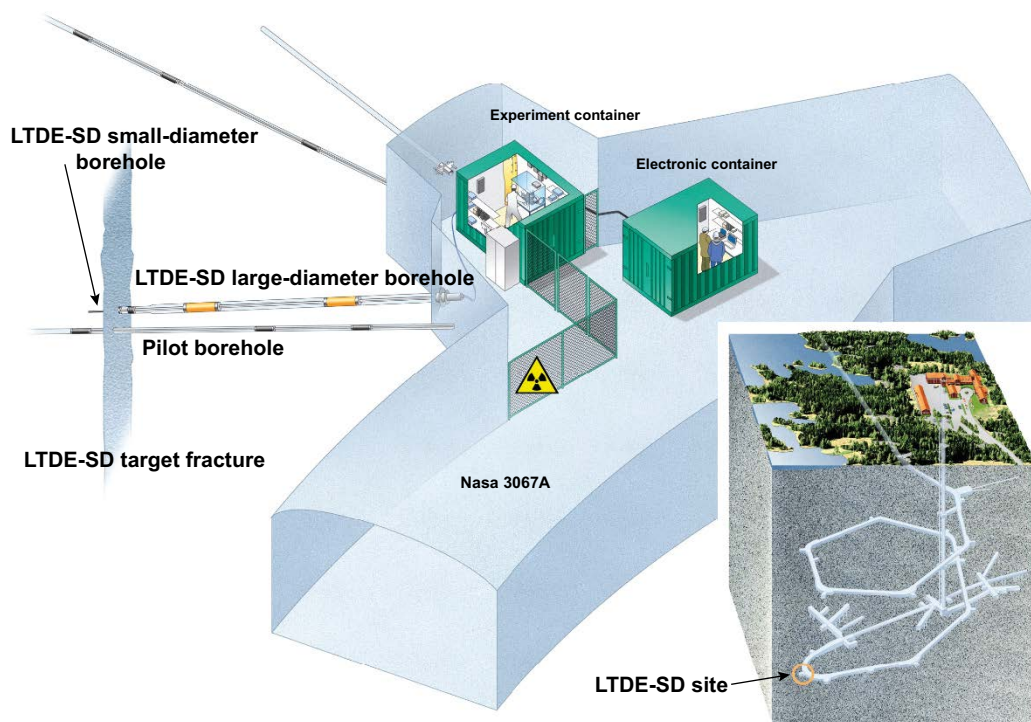


Figure 1-1. Illustration of the LTDE-SD experimental site (after Widstrand et al. 2010).

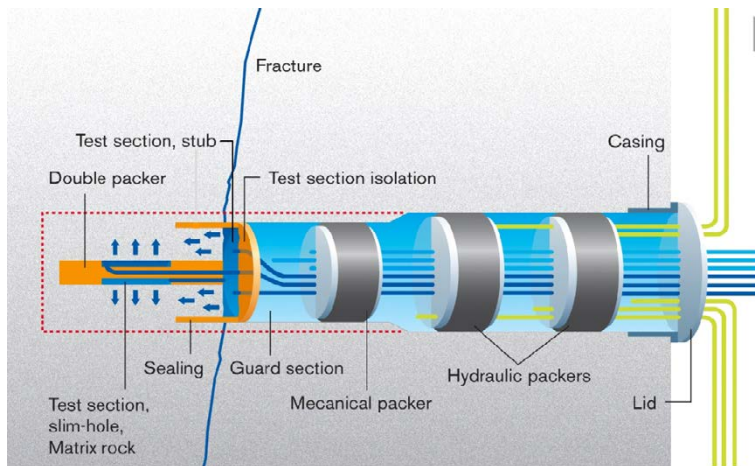


Figure 1-2. Schematic diagram of the LTDE-SD experimental setup (after Widestrand et al. 2010).

A cocktail of both sorbing and non-sorbing tracers was allowed to contact the natural surface of the target fracture, as well as the unaltered rock matrix surrounding the slim hole, for a time period of 198 days. The tracer cocktail contained 22 radionuclides: Na-22, S-35, Cl-36, Co-57, Ni-63, Se-75, Sr-85, Nb-95, Zr-95, Tc-99, Pd-102, Cd 109, Ag-110m, Sn-113, Ba-133, Cs-137, Gd-153, Hf-175, Ra-226, Pa-233, U-236, and Np-237. The injection proceeded as described in Widestrand et al. (2010) and took place on September 27th, 2006.

The experiment was terminated by expelling the tracer cocktail from the borehole system on April 12th, 2007. This was done by rinsing the system with isopropyl alcohol. Thereafter an epoxy resin was injected in order to increase the mechanical strength of the rock prior to overcoring. An additional objective was to protect the water-rock interface of both stub and slim hole test sections from the flushing water used in the overcoring. The tracer content of the outgoing isopropyl alcohol (later with inmixing of epoxy) was monitored (Nilsson et al. 2010).

After termination of the in situ test, the rock volume surrounding the contact sections was overcored and subsequently drilled and sawn into numerous subsamples (Nilsson et al. 2010). The overcoring was performed over a number of days, from April 26th to May 3rd, 2007, producing a 278-mm-diameter core. During the overcoring the tracer activity in the flushing water was controlled. On the 4th of May the large core was transported to the Clab facility (SKB interim storage facility for spent nuclear fuel). Here it was covered with heavy plastic foil to prevent drying. About a month later measurement and geological mapping commenced. After about another month, on the 3rd of August, the large core was covered by a 1–2 mm thick layer of clear epoxy resin. This was primarily done to prevent contamination during further sample preparation, but the resin also prevented drying. On the 6th of August the exposed part of the core was sawn off from the remaining part of the overcored rock. Between the 8th and the 13th of August smaller core samples were drilled from the overcored rock volume. These smaller core samples, having a diameter of 24 mm, were divided into the subclasses A and D, depending on their location (Figure 1-3). A cores correspond to the rock at the target fracture while D cores correspond to rock at the slim hole section. During the drilling of the smaller core samples, cooling water and debris were collected and controlled with respect to their tracer contents. Importantly, cores A20 and A21 (the latter not analysed), were drilled outside of the stub. These cores were not directly exposed to the circulating tracer solution.

A significant time period of about 120 days went by between the termination of the in situ tracer test and the drilling of the smaller core samples. During this time the overcored rock volume was reasonably well protected by heavy plastic foil to prevent it from drying. Hence, further water-phase matrix diffusion could have occurred, although evaporation-induced water flow (advection) would have been prevented.

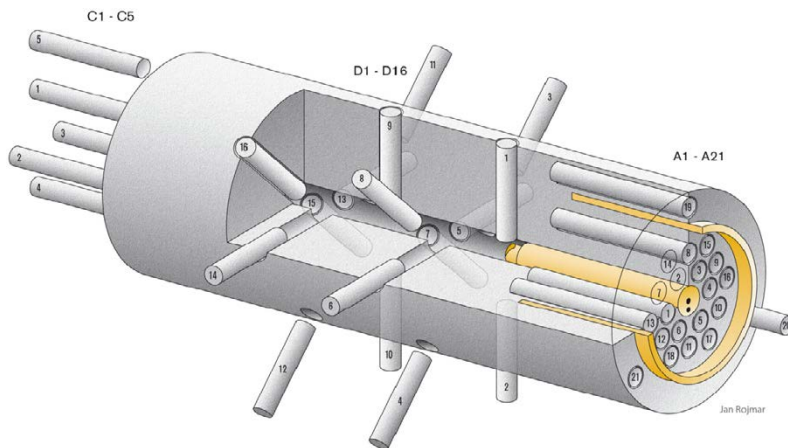


Figure 1-3. Illustration of drill core samples drilled from the overcored rock volume. The A-core samples are drilled from the target fracture and the D-core samples correspond to the slim hole. After Nilsson et al. (2010).

After the drilling of the small-core samples, they were stored in small individual plastics bags, which were reasonably air-tight. This should have prevented, or at least delayed, the drying of the pore water. Physical separation of the core slices was not performed until December 2007 to January 2008 (Nilsson et al. 2010). If the core samples were fully or at least partly saturated up until the slicing, liquid-phase matrix diffusion could have continued for a period of ~240 to ~290 days after the termination of the in situ part of the test. It should be noted that this time exceeds that of the in situ phase (198 days; Figure 1-4).

The measured radionuclide activities in the rock samples at the end of the experiment (rock tracer profiles), and the evolution of the activities in the circulated water during the in situ phase of the experiment, are reported in the task description (Löfgren and Nilsson 2020). The report also includes the geological description of the rock samples (mineralogy, structure) and references to the relevant results from laboratory studies (porosities, sorption distribution coefficients, effective diffusion coefficients; see also Appendix 1).

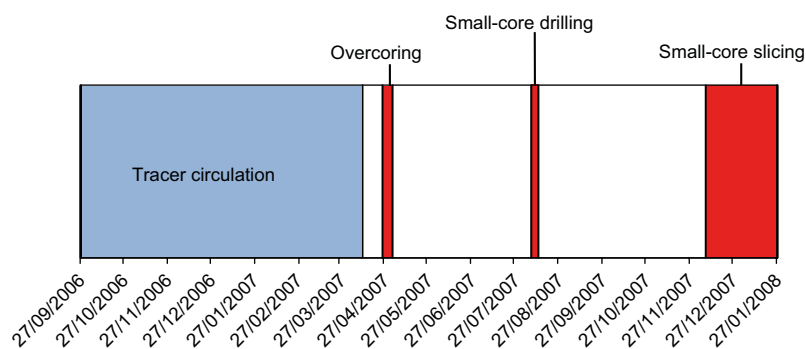


Figure 1-4. Timeline of the in situ, overcoring and small-core drilling and slicing phases of the experiment.

The measurement of the tracer activities in the rock led to the observation of very long profiles (several cm into the rock), not only for non- or weakly-sorbing tracers (Cl-36, Na-22), but for many of the more strongly-sorbing radionuclides (at low activities) as well. This was an unexpected feature which could not be explained based on the available knowledge on transport and sorption properties for this system (Nilsson et al. 2010). Initially, the data set delivered by the principal investigators of the Task Force to the modelling teams consisted of the original measurements performed shortly after the experiment. One of the main objectives of the modelling exercise was to try to understand these apparently anomalous tracer profiles in the rock. However, during the course of Task 9B, the fact that radionuclide activities were observed in core A20, which should not have been exposed to the circulating tracer solution (Figure 1-3), motivated a re-evaluation of the measurement procedures and results and led to the identification of potential contamination by sorbing tracers of many of the samples during sample preparation (contact of high-activity samples with sawing liquids and contamination during crushing of samples; Appendix 12 in Löfgren and Nilsson 2020). Experimental data for sorbing tracers at low activities were completely re-evaluated after the discovery of this issue, which led to the revision of detection limits and the definition of reporting limits (lowest activity values that can be taken into account with some confidence) and risk-of-contamination limits (lowest activity values that can be taken into account with full confidence). In the revised data set (Figure 1-5), the anomalous long tails at low activities were no longer present, although a few data points remained for Cs-137 and Ba-133 (close to reported potential contamination levels), Ni-63 and Cd-109. Profiles for Cl-36 and Na-22 were not affected by this revision. Importantly, most measured data for strongly-sorbing tracers at long distances (> 10 mm) were now below detection limits. The few remaining “tail data” for different tracers are not in the same cores (apparently random distribution), i.e. not related to a possible single structure. As an example, Appendix 2 illustrates the changes in the available rock tracer profile data for Na-22, Cl-36, Ba-133, Cs-137 and Co-57.

Due to the revision of the experimental data during the course of the modelling exercise, some teams did include the anomalous profile tails in their modelling while others did not. The inclusion or not of these tails in the model concepts is a critical factor that will be addressed when discussing the results.

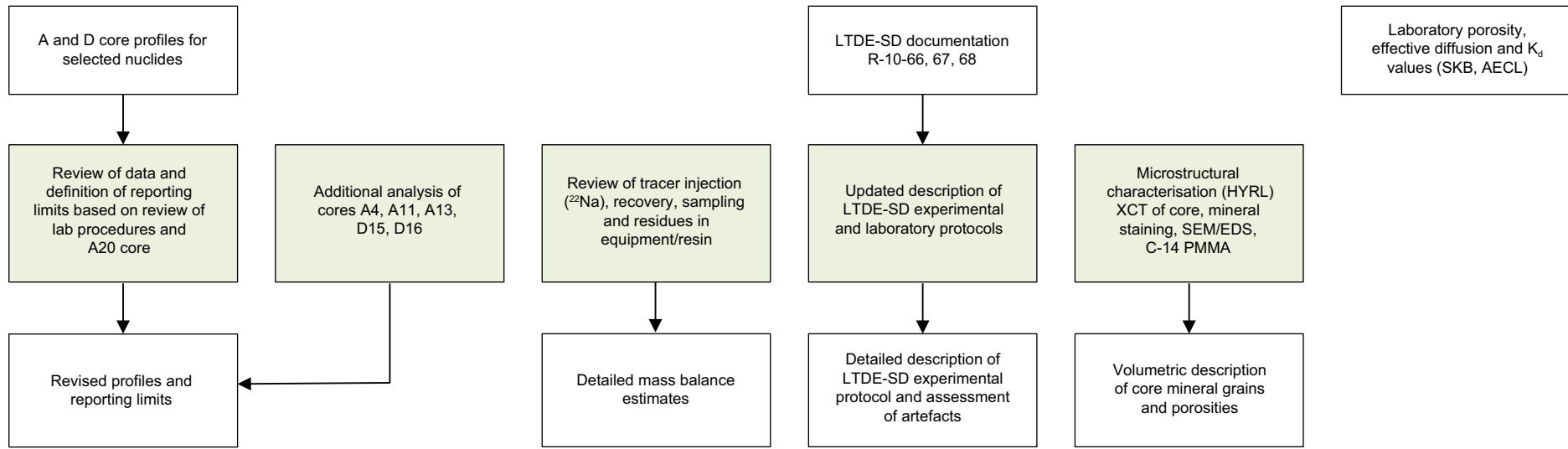


Figure 1-5. Summary of the experimental data available during the modelling exercise, including the re-evaluation of measured tracer profiles in the rock.

2 Objectives and structure of Task 9B

The objective of Task 9B was the quantitative modelling interpretation of the experimental results from LTDE-SD, with the aim of understanding the apparently anomalous tracer profiles (long profile tails for both non-sorbing and sorbing tracers). The use of different concepts by different teams was seen as an opportunity to test different possible explanations concerning rock transport and retention properties.

Task 9B was initially structured into 3 phases, with Tasks 9B-1 and 9B-2 focusing on the modelling of previously measured tracer profiles, and Task 9B-3 designed for the predictive modelling of additional profiles not previously analysed (Table 2-1). However, the distinction between the different phases proved not to be very practical for the modelling groups. Reporting by the different teams did not, in general, follow this structure. In the end, most teams merged the three subtasks into a single modelling exercise, with only two teams providing separate calculations for Task 9B-3 (predictive modelling; see e.g. Meng et al. 2020). These predictive calculations were based on the same concepts and parameter values used by the teams for the modelling of the observed profiles. Since those results did not provide any overly significant new conclusions, and for the sake of conciseness, they are not reported here.

Table 2-1. Rock cores considered in tasks 9B-1, 9B-2 and 9B-3.

	Task 9B-1	Task 9B-2, additional cores	Task 9B-3, predictive modelling
A cores	A6, A9	A1, A5, A8, A10, A12, A15, A16, A17, A20	A4, A11, A13
D cores	D12, D13	D1, D5, D6, D7, D8, D14	D15, D16

2.1 Task 9B-1

Task 9B-1 was intended to include the inverse modelling of a limited number of penetration profiles for a few tracers into a few core samples. Out of the 22 tracers used in the experiment, only the tracers Na-22, Cl-36, Co-57, Ni-63, Ba-133 and Cs-137 produced detectable penetration profiles into the rock of three data points or more. These tracers were to be considered at this stage. Additionally, the individual modelling groups had the freedom to model penetration profiles of Ba-133 in Task 9B-2 instead. To further reduce the number of inversely modelled penetration profiles in Task 9B-1, it was decided to choose only four core samples for the subtask. This also reduced the quantity of sample-specific information on geometry, petrology, microfractures, etc that needed to be assimilated by the modelling groups.

2.2 Task 9B-2

In Task 9B-2, the radionuclides Cd-109, Ag-110m, Gd-153, Ra-226 and Np-237 were also to be modelled. The activities of these radionuclides had been quantitatively recorded in the first rock slice and in some instances also in the second rock slice. For the modelling groups that did not include Ba-133 in Task 9B-1, this nuclide was to be included in Task 9B-2.

In Task 9B-1, the time-dependent data on the evolution of the tracer concentrations in the tracer cocktail (Figure 2-1) were assumed to be accurate without further scrutinising. Activities for most tracers (except Ni-63 and Cd-109) remained approximately constant or decreased only during the first few days. Ag-110m decreased to levels below detection limit very quickly. Activities of Ni-63 and Cd-109 decreased more gradually during the whole experimental period after an initial faster drop.

In Task 9B-2, the overall mass balances of the experiment were to be evaluated for all the included radionuclides. This required keeping track of the amounts of tracers injected into the borehole, withdrawn from the borehole at sampling and experimental termination, attached to experimental equipment and in the epoxy resin, carried away by leakages, and transported into the rock matrix of the overcored rock volume. Mass balance calculations provided an opportunity to scrutinise the reliability of the tracer concentration data.

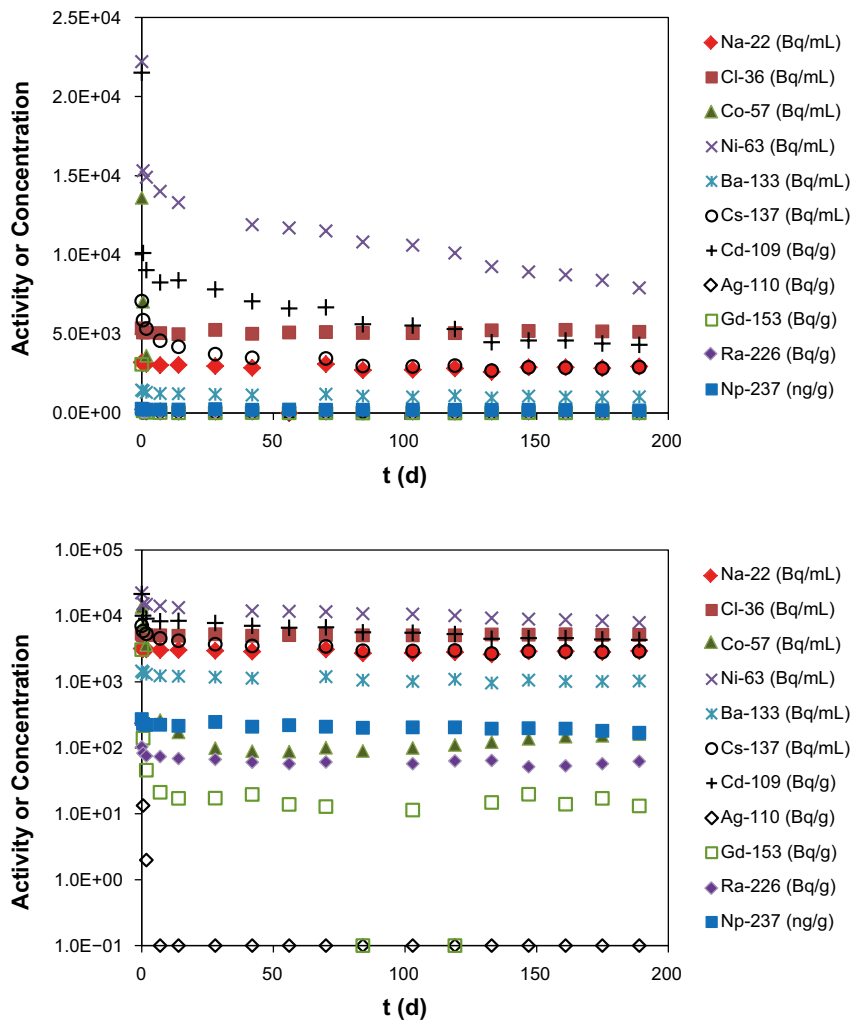


Figure 2-1. Evolution of measured tracer activities in the solution reservoir during the experiment (linear-linear and linear-log plots). Points plotted at 0.1 Bq/g are meant to indicate activities below detection limit. Detection limits for Ag-110m and Gd-153 were ca 1 Bq/g and 10 Bq/g, respectively.

In Task 9B-1 penetration profiles and supporting geological data were only provided for four of the drill core samples from the overcored rock volume, i.e. A6, A9, D12, and D13. These four drill core samples were selected as they displayed significant tracer penetration. Accordingly, there may be a bias towards larger porosities and diffusivities and/or lower or heterogeneous sorption properties. In Task 9B-2, penetration profiles and supporting geological data were supplied for all analysed A and D cores. Penetration profiles were available for ten A cores and eight D cores, although not necessarily for all tracers. The extended set of penetration profiles provided a less biased representation of rock surrounding the test sections, compared to Task 9B-1. Such data could be used to better estimate the tracer amounts that penetrated into the entire rock volume surrounding the test sections. The extended set of data could also be used to evaluate the variability in the tracer penetration pattern.

2.3 Task 9B-3

Task 9B-3 was a continuation of Tasks 9B-1 and 9B-2. The general idea of Task 9B-3 was to use the models developed in Task 9B-1 and 9B-2 and perform predictive modelling of penetration profiles in the rock matrix. At the end of the LTDE-SD experiment, all sample cores were sliced, but not all were fully analysed. Five cores that were not fully analysed in the main LTDE-SD campaign were analysed in a campaign carried out during 2016. Three A cores (A4, A11, and A13) and two D cores (D15 and D16) were part of this campaign. Analyses were performed with respect to their Na-22, Cl-36, Ni-63, Ba-133, and Cs-137 activities and resulted in numerous penetration profiles. These penetration profiles were to be the subject of predictive modelling within Task 9B-3.

3 Models and parameters

Eleven different modelling teams participated in Task 9B. Below is a summary of the models they used. Three main types of models have been applied: (1) Analytical solutions to the transport-retention equations, (2) Continuum-porous-medium-type numerical models, based on the use of Representative Elementary Volumes (REVs), and (3) microstructure-based models, accounting for small-scale heterogeneity (i.e. mineral grains, porosities and/or microfracture distributions) and potential centimetre-scale fractures. Microstructural characterisation was performed at the University of Helsinki and distributed to the modelling teams by the principal investigators of Task 9. Details of the models can be found in the individual reports or journal manuscripts from the teams. The different modelling teams attempted a global fitting to the measured tracer profiles, i.e. a fit to the ensemble of tracer-profile data, except for the two teams using analytical solutions, who performed specific model fits for individual tracer profiles from individual cores.

Some of the teams modelled the whole extended period during which diffusion of tracers could take place, i.e. the in situ phase (198 days, although periods ranging from 189 to 200 days were considered by different teams) and the period until the final slicing of the small core samples (additional 240 to 290 days), while other teams only modelled the in situ phase (see e.g. Tables 4-1 and 4-2). This of course will have some consequences in terms of transport distances and parameters obtained from the model fits to the data. No team reported calculated tracer profiles at different times, but transport distances could be expected to change according to Einstein's equation (i.e. mean transport distance proportional to the square root of the product of apparent diffusion coefficient and time). For a given value of the apparent diffusion coefficient, mean transport distances could be expected to increase by 57 % from 198 to 488 days if the rock samples were fully saturated during the whole period.

- ROYAL INSTITUTE OF TECHNOLOGY (KTH)

Analytical solution (1D linear; numerical inversion from Laplace space). Homogeneous rock properties. Anomalous profile tails for strongly-sorbing tracers not considered. An estimation of tracer mass balances from the experimental measurements was also performed.

- UNIVERSITY OF HELSINKI (HYRL)

Analytical solution (1D linear or radial). Homogeneous rock properties. Anomalous profile tails for strongly-sorbing tracers included through the addition of a constant background (not part of the transport calculations).

- TECHNICAL UNIVERSITY OF LIBEREC (TUL)

1D-linear continuum model, with changes in effective diffusion coefficients (D_e), porosities (ϕ) and sorption distribution coefficients (K_d) with depth. Flow123d code (Březina et al. 2018). Anomalous profile tails for strongly-sorbing tracers taken into account in the calculations.

- CZECH TECHNICAL UNIVERSITY IN PRAGUE (CTU)

1D-linear continuum model with D_e changing with depth. GoldSim code (GoldSim Technology Group 2018). Anomalous profile tails for strongly-sorbing tracers taken into account in the calculations.

- GESELLSCHAFT FÜR ANLAGEN- UND REAKTORSICHERHEIT (GRS)

1D-linear continuum model, with changes in effective diffusion coefficients (D_e) and porosity (ϕ) with depth taken into account. d3f++ code (Schneider 2016). Anomalous profile tails for strongly-sorbing tracers not considered.

- JAPAN ATOMIC ENERGY AGENCY (JAEA)

1D-linear and 1D-radial continuum models, with changes in effective diffusion coefficients (D_e), porosities (ϕ) and sorption distribution coefficients (K_d) with depth. GoldSim code (GoldSim Technology Group 2018). Anomalous profile tails for strongly-sorbing tracers not considered.

- COMPUTER-AIDED FLUID ENGINEERING AB (CFE)

Model developed from a Discrete Fracture Network (micro-DFN) approach, based on rock structure. 3D cylindrical rock domain. Solute transport by particle tracking. DarcyTools code (Svensson and Ferry 2014). Anomalous profile tails for strongly-sorbing tracers taken into account in the calculations.

- AMPHOS 21 (A21)

3D microstructure-based model (square rock prism). PFLOTRAN code (Hammond et al. 2014), run on the JURECA supercomputer (Jülich Supercomputing Centre). Anomalous profile tails for strongly-sorbing tracers not considered.

- KOREA ATOMIC ENERGY RESEARCH INSTITUTE (KAERI)

Microstructure-based model (2D, rectangular section). COMSOL Multiphysics code (Li et al. 2009, Perko et al. 2009). Anomalous profile tails for strongly-sorbing tracers included through the consideration of “tail data” still remaining after data revision.

- PROGEO

3D microstructure-based model, upscaled from a micro-DFN. 3D square rock prism. ConnectFlow (micro-DFN; Hartley 1998, Wood 2018) and MT3DMS (continuous porous medium; Zheng and Wang 1999, Zheng 2010) codes. Anomalous profile tails for strongly-sorbing tracers not considered.

- LOS ALAMOS NATIONAL LABORATORY (LANL)

Discrete Fracture Network (micro-DFN). 3D square rock prism. Solute transport by particle tracking. dfnWorks code (Hyman et al. 2015). Anomalous profile tails for strongly-sorbing tracers not addressed. The calculations were related to conceptual development, not matching exactly the conditions of the in situ experiments. The results are presented in Makedonska et al.¹ and are not included in the compilation of results presented here.

¹ Makedonska N, Kuluris S P, Karra S, Viswanathan H, 2021. Simulation of flow and transport at micro-fractures using discrete fracture network model. Submitted for publication.

Table 3-1. Summary of the model concepts used by the different teams. See subsections 3.1 to 3.11 below for references to symbols.

Team	Model type	Representation of rock	Scale	Duration (days)	Anomalous profiles	References and comments
KTH	Semi-analytic, Laplace	Homogeneous continuum	Infinite 1D	190	No	Meng et al. (2020) Evaluation of tracer mass balances.
HYRL	Analytic	Homogeneous continuum + two-path variant	Infinite 1D	189 + 240–290	Includes background level	Kekäläinen (2021) Evaluation of post-test diffusion. <i>Calibration of D_d and K_d (D_d and ϕ for CI-36).</i> Consistency between core and reservoir data checked separately.
TUL	Numerical, CPM	1D continuum, 3 zones	1D 14.75 cm	189 + 245	Included	Hokr et al. (2020, 2021) Evaluation of mass balances and post-test diffusion. Calibration of ϕ , D_e and K_d Coupling between core and reservoir via multistep.
CTU	Numerical, CPM	1D continuum, variable D_e	1D 6 cm	189 + 121	Included	Hokr et al. (2020, 2021) Evaluation of post-test diffusion. Continuous increase in D_e with distance (power law).
GRS	Numerical, CPM	1D continuum, DZ with varying ϕ and D_e	1D 14 cm	197 + 324	No	Kröhn (2020) Post-test diffusion. Model fit to CI-36 (conservative) ensemble by adjusting τ .
JAEA	Numerical, CPM	1D continuum: Fracture coating + DZ + unaltered rock	1D core scale	200	No	Tachi et al. (2017, 2021 ²) Predictive model approach based on LTD experiment (Tachi et al. 2015) using upscaled laboratory data.
CFE	Numerical, rock microstructure, particle tracking	3D micro-DFN: Intergranular pores + cm-scale fractures	cylinder 14 cm diameter 8 cm long	200	Included	Svensson (2020) Diffusive transport in inter-grain network with sorption on reactive grains. Fast pathways for diffusion filled with non-reactive mineral grains.
A21	Numerical, rock microstructure	3D micro-DFN: Intergranular pores based on HYRL XCT	$1.74 \times 1.74 \times 1.3 \text{ cm}^3$	200	No	Iraola et al. (2017), Trincherro et al. (2017) Fitting by adjusting the local tortuosity (τ) and surface area/volume ratio. Sorption by multisite cation exchange.
KAERI	Numerical, rock microstructure	Homogeneous Heterogeneous Heterogeneous+microfrac.+ vein	$6.0 \times 2.4 \text{ cm}^2$	198 + 265	Included	Park and Ji (2018, 2020) Post-test diffusion. Transport and sorption parameters (ϕ , D_e , K_d) in each structural domain used for fitting.
PROGEO	Numerical, micro-DFN	3D micro-DFN from HYRL micro structure	$10 \times 10 \times 20 \text{ cm}^3$	200	Included	Hokr et al. (2020, 2021) Stochastic 3D micro-fracture networks upscaled to ECPM (multiple realisations changing ϕ , D_p and K_d for microfractures, rock matrix and DZ).
LANL	Numerical, micro-DFN, particle tracking	3D micro-DFN	$5 \times 5 \times 5 \text{ cm}^3$	200	No	Makedonska et al. ³ Higher microfracture density near surface (DZ). Conceptual development.

DZ: Disturbed zone.

²Tachi Y, Ito T, Gylling B, 2021. Modeling the in situ long-term sorption and diffusion experiment (LTDE-SD) at the Äspö Hard Rock Laboratory in Sweden: A scaling approach from laboratory to in situ conditions. Submitted for publication.

³Makedonska N, Kuluris S P, Karra S, Viswanathan H, 2021. Simulation of flow and transport at microfractures using discrete fracture network model. Submitted for publication.

3.1 Royal Institute of Technology (KTH)

Diffusion into A and D cores was modelled accounting for retardation by linear sorption (Meng et al. 2020). Na-22, Cl-36, Ba-133 and Cs-137 were the tracers taken into account. For both A and D cores a 1D-linear geometry was assumed (based on the short transport distances even for the D cores). The diffusion-sorption equation was written as

$$\alpha \frac{\partial c}{\partial t} = D_e \frac{\partial^2 c}{\partial x^2} \quad (3-1)$$

with

$$a = \phi + \rho_d K_d \quad (3-2)$$

and with the following initial and boundary conditions

$$c(x, t = 0) = 0 \quad (3-3)$$

$$c(0, t) = c_b(t) \quad (3-4)$$

$$c(x \rightarrow \infty, t) = 0 \quad (3-5)$$

α is the rock capacity factor (-), c is the tracer activity (concentration) in solution (Bq/m³), t is time (s), D_e is the effective diffusion coefficient (m²/s), x is distance (m), ϕ is porosity (-), ρ_d is bulk dry density (kg/m³), K_d is the sorption distribution coefficient (m³/kg) and c_b is concentration in the reservoir solution (Bq/m³). α and D_e were adjusted for each nuclide in each core.

An analytical solution to the diffusion-sorption equation in Laplace space was numerically inverted to real space. In this conventional matrix diffusion model, the rock was assumed to be a homogeneous porous medium with regard to diffusivity and sorption. Porosity and sorption distribution coefficients were set to be constant. The evolving tracer activities in the fluid reservoir were included through the use of a time-dependent boundary condition. The modelled duration of the experiment was 190 days, corresponding roughly to the in situ part of the test, before overcoring.

For Task 9B-3, predictions of tracer distribution profiles were made based on the conventional matrix diffusion model using mainly experimentally determined parameters. Only Cs-137 was considered for these predictions.

An estimation of mass balances for the different tracers was also performed based on the measured tracer activities (measured in the reservoir solution, rock matrix, in different equipment parts, and activities removed when sampling). For non-sorbing and weakly-sorbing tracers, i.e. Na-22 and Cl-36, their mass balances were very good. In both cases, the location of more than 95 % of the injected tracer was identified at the termination of experiments. The largest part of the recovered tracers was found in the reservoir, which agreed well with expectations. For strongly-sorbing tracers, mass balances were different depending on the type of sorption mechanism. For cation-exchange tracers, i.e. Ba-133, Cs-137 and Ra-226, mass balances were rather acceptable since around 80 % of the tracers were accounted for. For these analysed tracers, most were observed in the reservoir and rock matrix as expected. In contrast, mass balances for surface-complexation ions were rather poor, especially for Co-57, Ni-63, Cd-109 and Gd-153. More than half of the injected tracer activities could not be accounted for.

3.2 University of Helsinki (HYRL)

Model fitting to individual profiles (cores) was performed using an analytical solution of the 1D-linear (A cores) or 1D-radial (D cores) diffusion-sorption equation, assuming linear sorption (Kekäläinen 2021). The diffusion-sorption equation for A cores was written as

$$\frac{\partial c}{\partial t} = D_a \frac{\partial^2 c}{\partial x^2} \quad (3-6)$$

and for D cores as

$$\frac{\partial c}{\partial t} = D_a \left(\frac{\partial^2 c}{\partial r^2} + \frac{1}{r} \frac{\partial c}{\partial r} \right) \quad (3-7)$$

where r is radial distance (m) and D_a is the apparent diffusion coefficient ($D_a = D_e/\alpha$, m²/s). D_a and K_d (D_a and ϕ for Cl-36) were the parameters that were adjusted in the fitting procedure. The modelling took into account the in situ part of the experiment (189 days) and also the extended additional time until the slicing of individual core samples (additional 240 to 290 days). Initial and boundary conditions during the first 189 days were equivalent to those given by Equations (3-3) to (3-5), but a no-flux condition was assumed for the far end of the diffusion domain (instead of zero concentration). A constant average concentration was assumed as boundary condition (reservoir) for the first 189 days, while a no-flux condition was assumed for that same boundary for the additional 240 to 290 days ($\partial c/\partial x = 0$ or $\partial c/\partial r = 0$). Ba-133, Ni-63, Co-57, Ra-226, Cd-109, Cs-137, Na-22 and Cl-36 were the tracers considered. In some cases a two-component approach, assuming two parallel diffusion pathways with the same porosity and sorption properties but different diffusivities, provided a better fit to the data. Homogeneous rock properties, although specific for each core, were assumed. The anomalous profile tails for strongly sorbing tracers were accounted for by adding a constant background activity (not part of the transport calculation).

The consistency of the parameters obtained in the fitting of the models to the tracer profiles with the measured changes in activities in the solution reservoir was checked in separate model calculations. For Ba-133 and Cs-137 those changes were consistent with average values of D_a and K_d obtained in the fitting of the profiles. The modelling was not performed for Na-22 and Cl-36 due to large oscillations in the measured data. The measured data for Co-57 did not match the model results. A good match was obtained for Ni-63, Cd-109 and Ra-226, but with parameter values slightly different from those from the penetration profiles.

3.3 Technical University of Liberec (TUL)

The calculations (Hokr et al. 2020, 2021) were performed using a discontinuous Galerkin numerical approach using the Flow123d code. The diffusion-sorption equations were analogous to those given by Equations (3-1) and (3-2). Initial and boundary conditions were equivalent to those given by Equations (3-3) to (3-5), but a no-flux condition was assumed for the far end of the diffusion domain (instead of zero concentration). Calibration of the models to the global ensemble of the profile data (not to single individual profiles) included the consideration of the anomalous profile tails for strongly sorbing tracers, since it was performed before the revision of the experimental data. Six tracers (Na-22, Cl-36, Co-57, Ni-63, Ba-133 and Cs-137) were considered. The simulations were divided into two stages:

Stage 1 – The task was to replicate the measured concentration (activity) profiles in the rock matrix. Tracer concentrations in the reservoir solution (their evolution over time) were taken from the task description (Löfgren and Nilsson 2020), with the measured values used as input data (time-dependent boundary condition).

Stage 2 – Takes over the parameters from Stage 1. The model was extended by simulating the evolution of tracer concentrations in the reservoir solution. Mass balance was monitored.

3.3.1 Stage 1

Efforts to model the measured profiles were based on the assumption of a disturbed zone (DZ) near the borehole. The rock was considered to be heterogeneous in terms of the parameters continuously changing with increasing depth (distance from borehole/fracture plane). The transport model considered both the A cores (1D linear geometry) and D cores ($\pi/90$ radian circular-sector domain). However, only the 1D linear model was applied when matching the experimental observations (A cores).

The 1D model domain (0.1475 m) was divided into three sub-domains (physical groups) when prescribing the parameters of the model. The boundaries between the sub-domains were defined at depths of 3 and 25 mm (or 3 and 30 mm for Cl-36). The simulation period was 434 days. The rock matrix was in contact with the solution for the first 189 days. For the rest of the period, only diffusion in the matrix itself was simulated, with zero mass flow across the boundary (the total amount of the individual tracers in the matrix no longer changing). This duration covered both the experiment itself and the time between the end of the experiment and the final slicing of the individual core samples.

The transport of tracers (radionuclides) in the rock matrix was controlled by three parameters (porosity – ϕ , effective diffusivity – D_e and distribution coefficient for linear sorption – K_d). Their values were subject to calibration, which was performed manually to reflect the trend of the measured concentration profiles. f , D_e and K_d for all tracers decreased with distance along the domain.

3.3.2 Stage 2

The second stage of the LTDE-SD modelling consisted of extending the model by simulating the evolution of the tracer (radionuclide) solution, with changes being given by diffusion into the rock matrix and also by sampling. After each single run of the transport model, the solution model evaluated the Flow123d outputs (mass flow across the boundary representing the solution-rock interface) and recalculated the masses of the tracers in solution. Before each transport model run, the solution model checked whether a sampling occurred. If so, it adjusted the volume of the solution and the concentration of the tracers dissolved therein. The transport model was applied in this stage to both the A cores (1D linear geometry) and D cores ($\pi/90$ radian circular-sector domain). Model parameters were identical to those of stage 1. The best agreement with the measured concentration values in the reservoir was achieved for Cs-137. The agreement was worse for the other tracers.

3.4 Czech Technical University in Prague (CTU)

For the interpretation of the measured data (ensemble of tracer profiles) from the in situ experiments of LTDE-SD, a model was created in the program environment of GoldSim, as reported in Hokr et al. (2020, 2021). The commercial license (GoldSim + RT (Enterprise)) version 12.0 was used. This model represents diffusion into the rock using a 1D finite volume network. In order to model the heterogeneous nature of the rock environment, the 1D linear domain (60 mm, A cores) was divided into 15 parts. The boundary condition at the input was defined on the basis of experimental concentration data (time-dependent boundary condition). This model was used to optimise the selected transport parameters so that the calculated profile curves represented the shapes of the detected profiles as closely as possible. The diffusion-sorption equations were analogous to those given by Equations (3-1) and (3-2). Initial and boundary conditions were equivalent to those given by Equations (3-3) to (3-5), but a no-flux condition was assumed for the far end of the diffusion domain (instead of zero concentration). The simulation period was 310 days, which included the in situ part of the test and the time between over-coring and the drilling of individual core samples. The rock matrix was in contact with the solution for the first 189 days. For the rest of the period, only diffusion within the matrix itself was simulated (the total amount of the individual tracers in the matrix no longer changing). Only Cl-36 and Na-22 were considered in the modelling.

Optimisation of the values of selected parameters was based on finding the minimum of an objective function, which in this case was the sum of the squared concentration differences between model and experiment in a given rock location (only in places where the experimental data were measured) divided by the experimental values.

Heterogeneity in the model was represented only by changes in the diffusion coefficient D_e , whose value increased with distance from the source. Three parameters were optimised (D_{e0} , α_d , n) for the chosen function for the increase in D_e

$$D_e(d) = D_{e0} + \alpha_d d^n \quad (3-8)$$

where d (m) is distance from the reservoir-rock interface. The minimum difference between the experimental and model data for Cl-36 was reached for $D_{e0} = 1.002 \times 10^{-14} \text{ m}^2/\text{s}$, $\alpha_d = 3.18 \times 10^{-6}$, $n = 3.13$. For Na-22, the parameters were $D_{e0} = 5.314 \times 10^{-14} \text{ m}^2/\text{s}$, $\alpha_d = 3.18 \times 10^{-6}$, $n = 3.13$. K_d and ϕ were fixed for each tracer.

3.5 Gesellschaft für Anlagen- und Reaktorsicherheit (GRS)

The model fit to the ensemble of tracer profiles in the rock was performed using a continuum model considering a disturbed zone (DZ) in addition to unaltered matrix and using the d3f++ code, as reported by Kröhn (2020). Linear geometry was assumed for the modelling of both A and D cores, although the geometry and relatively large domain dimensions (14 cm) were mainly applicable to the A cores. Cl-36, Na-22, Cs-137 and Ba-133 were the tracers that were considered in the calculations.

Modelling proceeded in two steps. In the first step, transport of a non-sorbing tracer was to be modelled in order to find out about the pore space topology. The only candidate was the anion $^{36}\text{Cl}^-$. All other tracers were cations that were prone to sorption. However, an effect from anion exclusion in narrow pore channels on the Cl-36 tracer could not be ruled out entirely.

Without sorption, the only transport-relevant mechanism is diffusion. Fick's second law could therefore be applied in case of Cl-36. The diffusion-sorption equation was written as in Equation (3-1), with $\alpha = \phi$ (no sorption) and with D_e given by

$$D_e = \phi \tau D_0 \quad (3-9)$$

with τ being a geometrical factor. Initial and boundary conditions were equivalent to those given by Equations (3-3) to (3-5), but a no-flux condition was assumed for the far end of the diffusion domain at $x = 14$ cm (instead of zero concentration).

Assuming a homogeneous domain, only the diffusion-limiting factor τ would have to be fitted since the diffusion coefficient is well known and the porosity cancels out. Adding a disturbed zone to the model increased the number of fitting parameters because the factor τ cannot be expected to be the same in both parts of the model, and the same applies to the porosity. Two more parameters concern the disturbed zone. First, there is the unknown depth of the disturbed zone. The assumption was that DZ parameters changed gradually from the sample surface to the unaltered matrix. This transition was formulated as a factor that depended on the distance from the surface and the depth of the disturbed zone. The same type of transition was assumed for the τ factor. As a result, both ϕ and D_e increased along the DZ from the reservoir-rock interface to the unaltered rock matrix.

Once the model was calibrated for Cl-36, migration of the cations should only add sorption (K_d) to the problem (stage 2). It turned out, though, that fitting the model results to the data resulted in very low tortuosity values. As a possible reason, anion exclusion was suspected. K_d values for each tracer were assumed to be constant along the whole rock domain.

The simulation period was 521 days. The rock matrix was in contact with the solution for the first 197 days. Constant tracer activities (representative of those measured during most of this experimental phase) were assumed for the different tracers in the reservoir. For the rest of the period, only diffusion in the matrix itself with zero mass flow across the interface was simulated. The total duration covered both the experiment itself and the time between the end of the experiment and the final slicing of the individual core samples.

3.6 Japan Atomic Energy Agency (JAEA)

Modelling was performed considering 1D-linear (A cores) and 1D-radial (D cores) models using GoldSim, as reported by Tachi et al. (2017, 2021⁴). The diffusion-sorption equations were analogous to those given by Equations (3-1) and (3-2). Initial and boundary conditions were equivalent to those given by Equations (3-3) to (3-5). The simulated time was 200 days, corresponding to the in situ part of the experiment (before overcoring). The evolution of tracer activities in the solution reservoir was also calculated in the model (i.e. activities were not used as a time-dependent boundary condition).

The model concept was based on that developed for modelling performed for the LTD experiment at the Grimsel Test Site (Tachi et al. 2015), which considers the upscaling of transport and retention parameter from laboratory to in situ conditions, with laboratory-derived values corresponding to a disturbed zone. The observed fracture coating (0.5-mm thick) was explicitly considered in the 1D-linear model for the A cores. A disturbed zone (5 mm) was considered for both A cores (between the fracture coating and the unaltered rock matrix) and the D cores. The values for D_e , K_d and ϕ for each tracer decreased linearly with distance in the fracture-coating zone (A cores) and in the disturbed zone (A and D cores). The model concept did not include the modelling of the anomalous tails for strongly sorbing tracers. Results were provided for Cl-36, Ba-133, Na-22, Cs-137, Co-57, Ni-63, Ra-226, Cd-109 and Np-237.

A predictive modelling approach was followed for the whole exercise. In situ porosities and D_e values were determined from the measured depth profiles for Cl and Na, which indicated cation-excess diffusion and anion exclusion. D_e values were scaled for the fracture coating and disturbed zones by considering the difference in porosities and Archie's law. D_e values for each radionuclide (RN) were evaluated by considering the ratios of $D_w(\text{RN})/D_w(\text{HTO})$, where D_w is the diffusion coefficient in free water. K_d parameters were optimised to fit overall trends of tracer depletion and depth profiles for a relatively reliable laboratory dataset (Cs, Ra, Ni). Key uncertainties related to (1) in situ porosity and D_e values, and (2) K_d values for matrix and fracture were evaluated based on uncertainties in the laboratory dataset.

3.7 Computer-Aided Fluid Engineering AB (CFE)

Modelling was performed using a micro-DFN-based approach (Svensson 2020), considering diffusion through intergranular porosity and centimetre-scale deterministic fractures (based on the observations in the rock by the University of Helsinki), with tracer sorption or reactive grains. The deterministic fractures were assumed to be fast pathways for diffusion and filled with non-reactive mineral grains (quartz), playing a key role in the the formation of the anomalous tails for strongly sorbing tracers. The model domain was based on the geometry of the stub section of the experiment (A cores); it was a rock cylinder 14 cm in diameter and 8 cm in length (Figure 3-1). A solution reservoir was included explicitly in the model (in contact with one end of the cylinder). Tracer activities in the reservoir were kept constant. The overall initial and boundary conditions were equivalent to those given by Equations (3-3) to (3-5). However, all external boundaries of the domain were subject to no-flux conditions (instead of zero concentration far from the reservoir). The modelled duration of the experiment was 200 days, equivalent to the in situ stage of the test. Results were calculated for Cl-36, Na-22, Cs-137, Co-57 and Ni-63.

⁴Tachi Y, Ito T, Gylling B, 2021. Modeling the in situ long-term sorption and diffusion experiment (LTDE-SD) at the Äspö Hard Rock Laboratory in Sweden: A scaling approach from laboratory to in situ conditions. Submitted for publication.

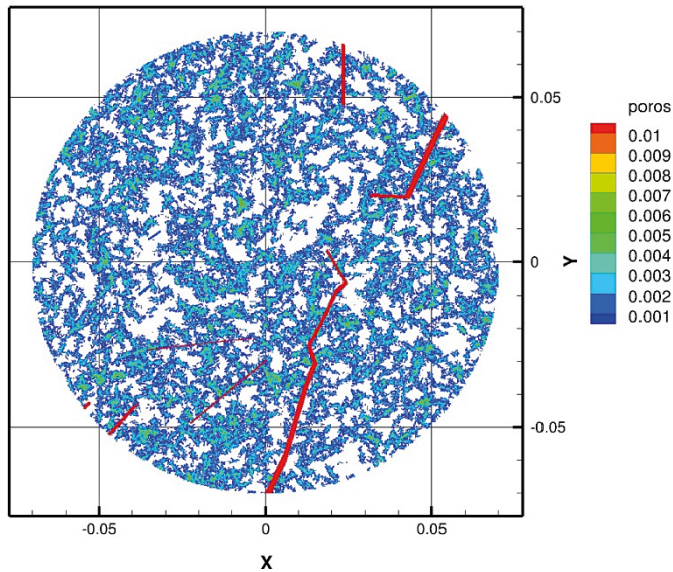


Figure 3-1. Porosity distribution and deterministic fractures in a section of the cylindrical rock domain, at 10 mm from the reservoir-rock interface. Dimensions in m. After Svensson (2020).

3.8 Amphos 21 (A21)

Modelling was performed using an intergranular network (IGN) approach (Iraola et al. 2017, Trincherio et al. 2017), based on the detailed structure and mineralogy of a rock sample from Äspö characterised by X-ray micro-computed tomography at the University of Helsinki. The dimensions of the rock domain ($1.74 \times 1.74 \times 1.3$ cm³ rock prism, Figure 3-2; applicable to both A and D cores) were based on those of the rock sample. Transport was by diffusion through the intergranular pores. Results were calculated for Na-22 and Cs-137. Na-22 was assumed to be conservative, while sorption of Cs-137 on the biotite grains was calculated according to a multisite cation exchange model published in the literature. Only a single effective diffusion coefficient (through a τ factor, see Equation (3-9)) was adjusted when matching model to observations (tracer profiles). This model concept did not consider the anomalous tails for strongly sorbing tracers (Cs-137 in this case). Boundary conditions were no-flux everywhere and the reservoir was explicitly included through appropriate initial conditions. Initial tracer concentrations in the rock were zero. Fitting the model to the evolution of tracer concentrations in the reservoir was performed by adjusting the specific surface area of the reservoir, i.e. the volume of reservoir per unit surface area of exposed rock. The evaluated changes in this parameter did not affect the calculated tracer profiles to any major extent. The modelled duration of the experiment was 200 days, equivalent to the in situ stage of the test.

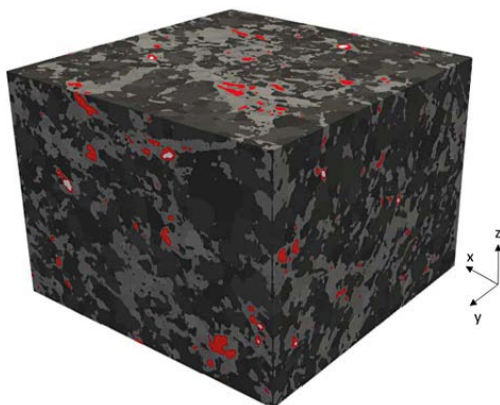


Figure 3-2. Three-dimensional visualisation of the rock-sample domain after mineral segmentation. Biotite grains are displayed in red. Dimensions are 1.74 cm \times 1.74 cm \times 1.3 cm. After Iraola et al. (2017).

3.9 Korea Atomic Energy Research Institute (KAERI)

The modelling from KAERI is reported in Park and Ji (2018, 2020). Three different cases were considered when modelling tracer diffusion and sorption from the reservoir into the rock (Na-22, Cs-137): (1) homogeneous medium; (2) heterogeneous medium considering mineral grains with intragranular porosities and their intergranular pores; and (3) heterogeneous medium considering a single vein and microfractures as well as porous mineral grains and intergranular pores. Sorption was strongly reduced along the vein and the microfractures. A 2D domain was used in all the calculations (ca 60 mm × 24 mm, Figure 3-3; mainly applicable to the A cores). A disturbed zone at the contact with the reservoir was considered in all the cases. The overall initial and boundary conditions were equivalent to those given by Equations (3-3) to (3-5). However, all external boundaries of the domain were subject to no-flux conditions (instead of zero concentration far from the reservoir). A solution reservoir was included explicitly in the model. The total simulation time was set to 463 days, including the in situ period (198 days) and the postexperimental period including overcoring, core sampling and sample slicing (265 days).

The modelling domains for cases 2 and 3 were established using 2D microstructure characterisation results from analyses performed at the University of Helsinki, including chemical staining of minerals and ¹⁴C-PMMA autoradiography of a rock sample from Äspö (the same sample considered by Amphos 21). Sorption (K_d approach) was assumed to occur on plagioclase and biotite grains. Transport and sorption parameters in each different domain were adjusted to match model to observations. The numerical models for cases 1–3 were calibrated by minimising the discrepancies between simulations and observations of the penetration profiles and the changes in concentration in the reservoir for the tracers (Na-22, Cs-137). The results showed that only the calibrated transport parameter values for case 3 were within reported ranges. It was concluded that the sharp decrease in concentrations in the near-surface zone in the observed penetration profiles was likely to result from increased sorption on disturbed biotite grains and the long tails in the observed penetration profiles might originate from diffusion along the vein and microfractures.

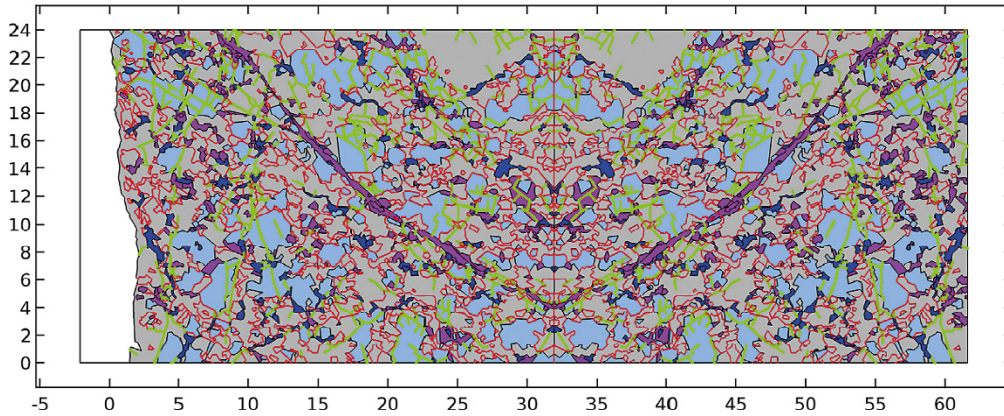


Figure 3-3. Modelling domain for case 3. Dimension are in mm. Biotite is dark blue and plagioclase is sky blue. The red lines are assumed intergranular pores between quartz and feldspars. Intragranular porous structures (including the vein), except for biotite, are drawn in pink. Microfractures are green. After Park and Ji (2018).

3.10 PROGEO

Modelling was performed using a micro-DFN-based model which was based on the analysis of the rock structure observed in ^{14}C -PMMA autoradiographies of 2 rock samples from Äspö taken at the University of Helsinki. Stochastic 3D micro-fracture networks were defined from those images. The domain size was $10 \times 10 \times 20 \text{ cm}^3$ (Figure 3-4; applicable to A cores). The micro-DFN models were then upscaled to a micro-continuum model. Diffusion parameters were calculated for the microfractures and the background rock matrix. A disturbed zone (1 mm) next to the solution reservoir was also defined. The assembled micro-continuum model was simpler than the micro-DFN model, but retained the heterogeneity and properties of the micro-DFN model and was more suitable for transport simulations. The overall initial and boundary conditions were equivalent to those given by Equations (3-3) to (3-5). However, all external boundaries of the domain not in contact with the reservoir were subject to no-flux conditions (instead of zero concentration). The changes in tracer concentrations in the reservoir were also calculated. Results for each model were evaluated and compared with the measured activities in the tracer profiles and in the reservoir. The parameters characterising each model run for each tracer were ϕ , D_p and K_d for microfractures, rock matrix and disturbed zone. The analysis was performed for Na-22, Cl-36 and Cs-137. The modelled duration of the experiment was 200 days, equivalent to the in situ stage of the test.

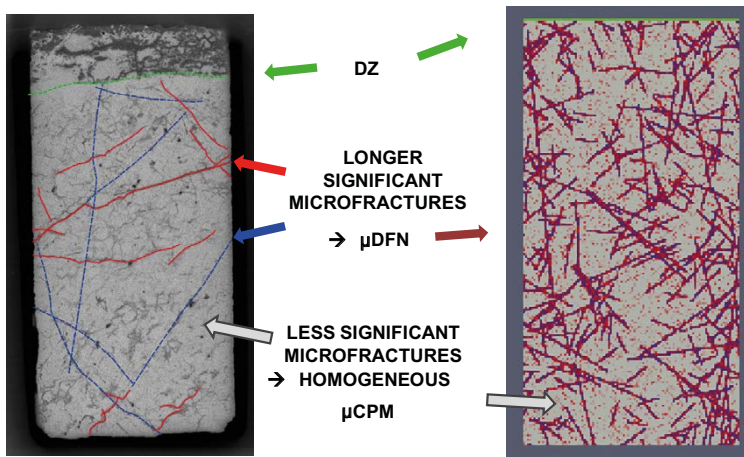


Figure 3-4. Definition of the basic elements characteristic of the rock matrix – DZ, longer significant microfractures and less significant microfractures forming the background of the image. Rock matrix micrograph on the left and a micro-continuum model with a randomly generated network of microfractures in the cross-section on the right. After Hokr et al. (2020).

3.11 Los Alamos National Laboratory (LANL)

Synthetic Discrete Fracture Networks were generated with different configurations of microfracture geometry with decreasing microfracture intensity, where high intensity was assigned near the rock surface where microfractures are formed due to applied stress. The simulation domain size was chosen to be $5\text{ cm} \times 5\text{ cm} \times 5\text{ cm}$ (Figure 3-5). The time domain random walk approach was used to model particles tracking through microfractures, where particles may be driven by advection and diffusion processes.

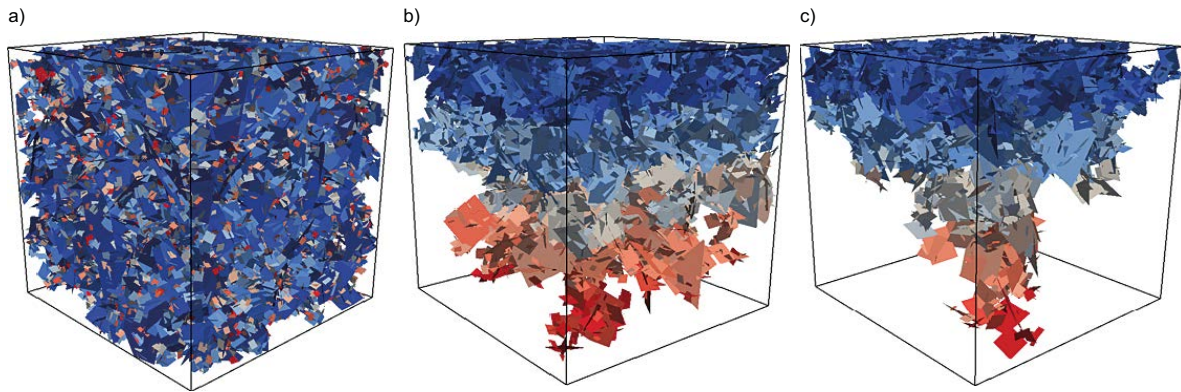


Figure 3-5. DFN configurations in three numerical experiments: a) A DFN realisation of uniform intensity of fracture network. Colors represent individual fractures. b) A DFN realisation where fracture network intensity decreases gradually in vertical direction. Fractures are colored by the vertical layers. c) A DFN realisation where fracture network intensity decreases rapidly in vertical direction. Fractures are colored by vertical layers with different fracture network intensity. After Makedonska et al.⁵

⁵ Makedonska N, Kuluris S P, Karra S, Viswanathan H, 2021. Simulation of flow and transport at microfractures using discrete fracture network model. Submitted for publication.

4 Results and discussion

4.1 Na-22

Figures 4-1 (A profiles) and 4-2 (D profiles) show the measured and calculated Na-22 profiles in the rock. The measurements below the detection limit have been plotted at the very bottom of the figures, since this is relevant information that has to be taken into account (activities are not 10^{-3} Bq/g for these points; see also Appendix 2). For clarity, the results for different types of models are shown in different figures: (a,b) analytical solutions, (c,d) continuum models, and (e,f) microstructure-based models. All plots show all the measured data.

Figures 4-1a,b and 4-2a,b show model results for KTH and HYRL. These two teams used analytical solutions to the diffusion-sorption equations for a homogeneous medium (constant transport and sorption parameters). HYRL assumed a two-component (two parallel diffusion pathways) approach for most of the profiles. In addition, HYRL added a constant background (tail) to account for the activities measured far from the tracer source in the A profiles (further than ca 30 mm). KTH did not try to adjust the model to the points measured far from the tracer source. Only two representative model profiles are shown for each model (the teams did individual model fits for individual profiles) and for each type of profile (A and D cores). Table 4-1 shows ranges of values for the transport and retention parameters used in the models. D_a values are in the range from 1×10^{-13} to 7×10^{-12} m²/s (with smaller values for one of the pathways when a two-component approach was used), which are overall consistent with those that could be expected from the ranges of measured laboratory values for ϕ (Vilks et al. 2005, Widstrand et al. 2010), D_e (HTO, Vilks et al. 2005) and batch-sorption K_d (Na-22, Widstrand et al. 2010) – see Appendix 1.

Figures 4-1c,d and 4-2c,d show model results for TUL, CTU, GRS and JAEA. TUL and CTU only did calculations for A profiles. JAEA provided results for a central case and for upper and lower bounds (dashed red lines in the plots), based on ranges of values for D_e and K_d . Their results clearly show the effect of the fracture coating (increased ϕ , K_d and D_e values) included in the concept for the A profiles (Figure 4-1c,d). The results from TUL and CTU match the highest activities measured far from the tracer source. TUL implemented relatively large D_a values at those distances (ca 6.5×10^{-11} m²/s, Table 4-1). Even larger values were implemented by CTU, reaching values larger than diffusion coefficients in free water. GRS results are similar to those from JAEA, except for the fracture coating effect implemented by JAEA in the A profiles. Both JAEA and GRS implemented a disturbed zone in the profiles. However, while ϕ , K_d and D_e values decrease along the disturbed zone in the JAEA model concept, ϕ and D_e values increase in the GRS model, with constant K_d values. D_a values in the undisturbed matrix are in the 10^{-12} m²/s range for both JAEA and GRS, but the trends from tracer source to undisturbed matrix are different (decreasing for JAEA and increasing for GRS, Table 4-1). JAEA did calculate the evolution of tracer activities in the reservoir during the experiment, while GRS used a constant-activity boundary condition. However, activities in the reservoir did not change significantly during the experiment (Figure 2-1), making the discrimination between the two approaches difficult.

Figure 4-1e,f show model results for CFE, A21, KAERI and PROGEO (only A21 applied the calculations to D profiles; Figures 4-2e and 4-2f). Besides the central prediction shown in the figures, KAERI also performed sensitivity analyses with respect to the different transport and retention parameters, and also with respect to the extension of the disturbed zone assumed in the model (not shown). Two representative curves from PROGEO are shown. Notice that the different model results can be considered to match the measured data, except perhaps one of the PROGEO curves (PG2365). However, the concepts used by the different teams are rather different. The grain-scale heterogeneity implemented in the model from A21 results in an overall constant D_a value (the local pore-scale value was 2.5×10^{-12} m²/s). As shown in previous works (Iraola et al. 2017), this model is expected to behave quasi-homogeneously for non-sorbing tracers, although significant deviations from the homogeneous behaviour could be expected for sorbing tracers due to the implementation of grain-related cation exchange reactions. KAERI assumed the presence of a disturbed zone next to the tracer source. Intragranular and intergranular pores, microfractures and a vein structure were considered in their model. Intragranular porosities and D_e values (quartz, plagioclase, K-feldspar) and mineral-specific sorption parameters (K_d values on biotite and plagioclase) decrease along the disturbed zone, while the transport parameters for microfractures

and vein remain constant (Table 4-2). The vein structure assumed in the model domain (Figure 3-2) is especially responsible for the long transport distances (no sorption in the vein). In the modelling by PROGEO, transport and retention parameters for their assumed disturbed zone, microfractures and matrix were varied to obtain different possible matches to the observed profiles. Different possible combinations were obtained (no a priori concept was implemented for the distribution of values of transport and retention parameters in the different regions). However, for many of the cases, D_a values for fracture or matrix were similar to or larger than diffusion coefficients in free water. This was so for case PG545 (D_a in matrix equal to $9.9 \times 10^{-8} \text{ m}^2/\text{s}$), but not for case PG2365, showing a poorer match to the measured data (Figure 4-3e,f). CFE considered centimetric fractures and matrix in the model concept. In this case, the fractures were assumed to be fast pathways for diffusion (no sorption in the fractures).

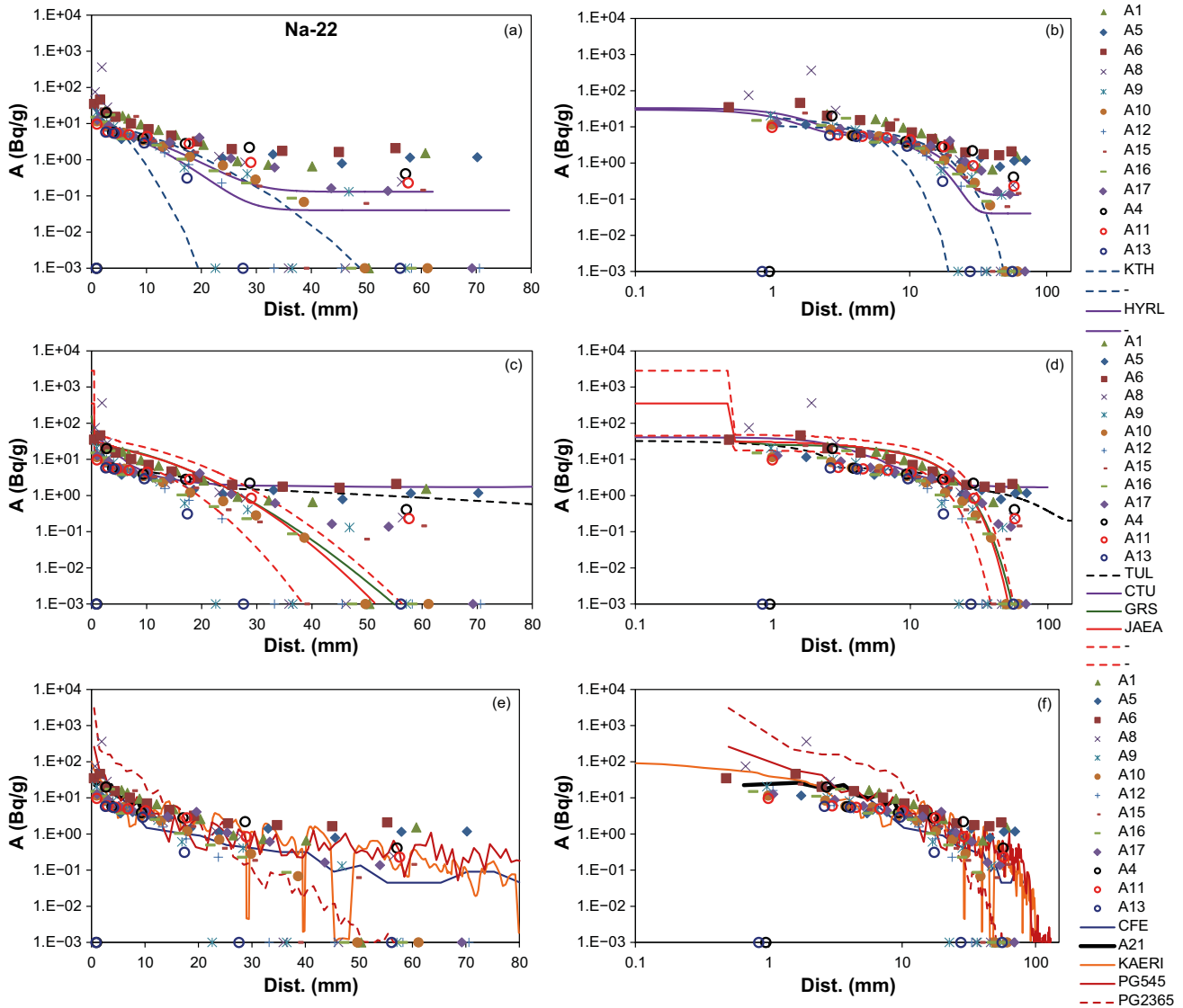


Figure 4-1. Measured (symbols) and calculated (lines) Na-22 tracer profiles for A cores. Activities are in Bq per gram of rock. Three groups of plots are shown: (a,b) homogeneous models, (c,d) continuum-porous-medium models, (e,f) microstructure-based models. All plots show all the measured data, with data plotted at the bottom of the figures (10^{-3} Bq/g) corresponding to measurements below detection limit. For those points, detection limits are mostly below 0.2 Bq/g . They decrease with distance from the tracer source to values less than 0.1 Bq/g . The very first slices in some of the cores have higher detection limits, up to ca 100 Bq/g .

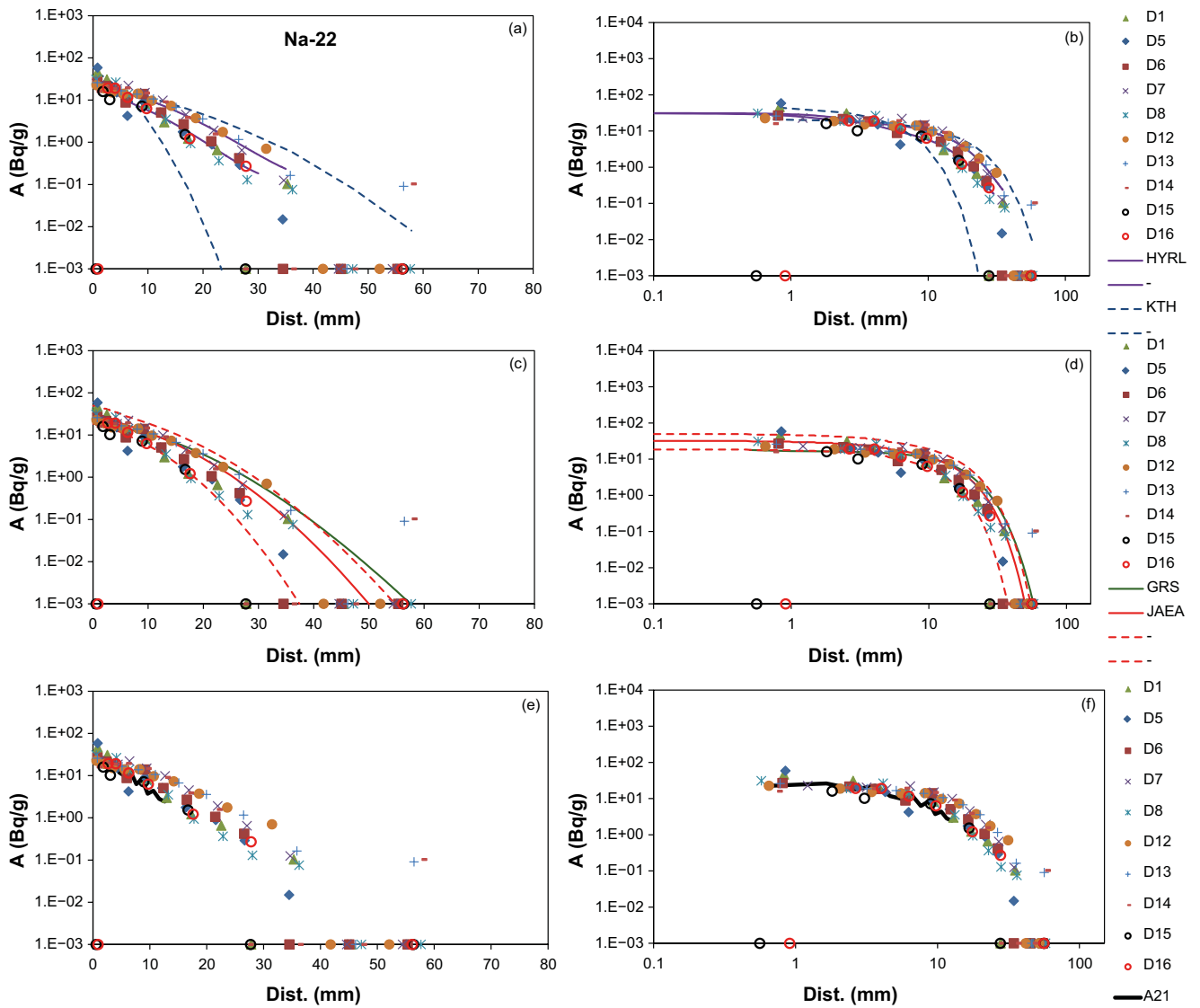


Figure 4-2. Measured (symbols) and calculated (lines) Na-22 tracer profiles for D cores. Activities are in Bq per gram of rock. Three groups of plots are shown: (a,b) homogeneous models, (c,d) continuum-porous-medium models, (e,f) microstructure-based models. All plots show all the measured data, with data plotted at the bottom of the figures (10^{-3} Bq/g) corresponding to measurements below detection limit. For those points, detection limits are mostly below 0.2 Bq/g. They decrease with distance from the tracer source to values less than 0.1 Bq/g. The very first slices in some of the cores have higher detection limits, up to ca 100 Bq/g.

Table 4-1. Na-22 transport and retention parameter values for the different zones implemented in the homogenous and continuum-porous-medium models. Different parameters have been adjusted by different teams. Apparent diffusion coefficients (D_a) have been calculated from the reported parameters in all the cases. D_e : effective diffusion coefficient; ϕ : porosity; K_d : sorption distribution coefficient; α : capacity factor. D_{a1} and D_{a2} stand for D_a values in the two-component model from HYRL.

Team	t (days)	Layer	Na-22 D_e m ² /s	Na-22 ϕ	Na-22 K_d m ³ /kg	Na-22 α	Na-22 D_a m ² /s
KTH	190	1	1.1E-14 – 1.5E-13			0.0085 – 0.1922	1.3E-13 – 7.4E-12
HYRL	429, 479	1			6.9E-6 – 4.9E-5		Da 2.7E-12 – 3.0E-12 Da1 4.0E-14 – 3.0E-14 Da2 1.7E-12 – 5.0E-12
TUL	434	1 (0–3 mm)	2.7E-12 – 4.3E-13	0.02–0.005	~1E-5 – ~1E-6		~5.7E-11 – ~5.6E-11
		2 (3–25 mm, CI 3–30 mm)	4.3E-13 – 1.3E-13	0.005–0.002	~1E-6 – ~1E-9		~5.6E-11 – ~6.5E-11
		3 (35 mm – 14.75 cm)	1.30E-13	0.002	~1E-9		~6.5E-11
CTU	310	1 (0–60 mm)	5.3E-14 – 4.8E-10	0.03	2.72E-05		5.1E-13 – 4.6E-9
GRS	521	DZ A (0–1 mm)	1.85E-15 – 1.65E-12	0.003–0.004	2.9E-04		2.4E-15 – 2.1E-12
		DZ D (0–1 mm)	1.03E-15 – 1.65E-12	0.001–0.004	2.9E-04		1.3E-15 – 2.1E-12
		Matrix (1 mm – 14 cm)	1.65E-12	0.004	2.9E-04		2.1E-12
JAEA	200	A1 – fracture (0–0.5 mm)	3.19E-12 –	0.01 –	3.8E-5 –		2.8E-11 –
		A2 – DZ (0.5–5 mm)	– 8.4E-14	– 0.001	– 6.8E-06		– 4.3E-12
		A3 – undisturbed (5 mm –)	8.40E-14	0.001	6.8E-06		4.3E-12
		D1 – DZ (0–5 mm)	3.19E-12 – 8.30E-14	0.01–0.001	6.9E-6 – 6.8E-6		1.1E-10 – 4.3E-12
		D2 – undisturbed (5 mm –)	8.30E-14	0.001	6.8E-06		4.3E-12

Table 4-2. Na-22 transport and retention parameter values for the different zones implemented in the microstructure-based models. Different parameters have been adjusted by different teams. When possible, apparent diffusion coefficients (D_a) have been calculated from the reported parameters. D_e : effective diffusion coefficient; ϕ : porosity; K_d : sorption distribution coefficient; α : capacity factor; D_p : pore diffusion coefficient.

Team	t (days)	Layer	Na-22 D_e m ² /s	Na-22 ϕ	Na-22 K_d m ³ /kg	Na-22 α	Na-22 D_a m ² /s
CFE	200	Matrix (0–8 cm)	3.50E–13	2.20E–03	2.00E–04		6.5E–13
		Det. fractures (0–8 cm)	$D_p = 4.0E–10$	1	0		4.0E–10
A21	200	Matrix – 13 mm	$D_p = 2.5E–12^*$	0.0026	0.00E+00		2.5E–12*
KAERI	463	DZ (0–6 mm)	Biot intragrain: $\phi^{4/3}D_0$ Non-biot intragrain: $\phi^{4/3}D_0$ Microfrac: $5E–3D_0$ Intergrain pores: $1E–4D_0$ $D_0 = 2.1E–9$ m ² /s	Biot intragrain: 0.03 Non-biot intragrain: $6E–3 – 3E–5$ Intergrain and microfrac: 1.0	Biot: $3.0E–4 – 9.0E–5$ Plag: $5.0E–5 – 2.5E–6$		
		Matrix (6 mm – 60 mm)	Biot intragrain: $\phi^{4/3}D_0$ Non-biot intragrain: $\phi^{4/3}D_0$ Microfrac: $5E–3D_0$ Intergrain pores: $1E–4D_0$ $D_0 = 2.1E–9$ m ² /s	Biot intragrain: 0.03 Non-biot intragrain: $3E–5$ Intergrain and microfrac: 1.0	Biot: $9.0E–5$ Plag: $2.5E–6$		
PROGEO	198	DZ (0–1 mm)	$D_p: 1.3E–10 – 7.1E–6$	$2.3E–8 – 4.0E–2$	$1.9E–5 – 1.2E–3$	$5.2E–2 – 3.29$	$8.4E–15 – 1.8E–10$
		Fractures (1 mm – 20 cm)	$D_p: 5.7E–11 – 4.8E–6$	$2.2E–8 – 5.7E–2$	$5.2E–7 – 5.5E–2$	$1.4E–3 – 150.8$	$7.2E–18 – 8.9E–9$
		Matrix (1 mm – 20 cm)	$D_p: 3.1E–11 – 8.6E–6$	$3.6E–6 – 5.6E–2$	$3.1E–8 – 3.4E–3$	$1.7E–4 – 9.3$	$2.0E–17 – 5.4E–7$

*This value ($D_p = D_a = 2.5 \times 10^{-12}$ m²/s) applies only to the local pore scale (single intergranular volume; porosity equal to 1). It is modified by the geometry of the porous network at the sample scale.
Biot: Biotite. Plag: Plagioclase. Intragrain: Intragranular porosity. Det. Fractures: Deterministic fractures. Microfrac: Microfractures.

4.2 CI-36

Figures 4-3 (A profiles) and 4-4 (D profiles) show the measured and calculated CI-36 profiles in the rock. For clarity, the results for different types of models are shown in different figures: (a,b) analytical solutions, (c,d) continuum models, and (e,f) microstructure-based models. All plots show all the measured data. No results for D profiles were calculated using any of the microstructure-based models.

Figures 4-3a,b and 4-4a,b show model results for KTH and HYRL. These two teams used analytical solutions to the diffusion-sorption equations for a homogeneous medium (constant transport and sorption parameters). HYRL assumed a two-component (two parallel diffusion pathways) approach for all of the profiles. They are clearly visible in the figures (two different segments of the curves before reaching the implemented constant background values). KTH did not try to adjust the model to the points measured far from the tracer source. Only two representative model profiles are shown for each model (the teams did individual model fits for individual profiles) and for each type of profile (A and D cores). Table 4-3 shows ranges of values for the transport and retention parameters used in the models. D_a values from KTH are in the range from ca 9×10^{-14} to 1×10^{-10} m²/s, while those from HYRL are in two narrower ranges (2-component models used here). Values between 5×10^{-14} and 6×10^{-14} m²/s for D_{a1} , providing a good fit for the first few mm in the profiles, and from ca 4×10^{-12} to 9×10^{-12} m²/s for D_{a2} , providing a good fit for distances up to ca 30 mm (flat background values provide a fit for distances beyond 30 mm). D_a values for iodide (comparable to chloride) from the data in Vilks et al. (2005; see Appendix 1, $D_a = D_e/a$) are in the range from ca 1×10^{-11} to 2×10^{-10} m²/s.

Figures 4-3c,d and 4-4c,d show model results for TUL, CTU, GRS and JAEA. TUL and CTU only did calculations for A profiles. JAEA provided results for a central case and for upper and lower bounds, based on ranges of values for ϕ and D_e . In this case there is no great effect of the fracture coating on the calculated A profiles, but the effect of the disturbed zone (5 mm) is obvious. The results from TUL match the highest activities measured far from the tracer source, with a D_a value of 1.2×10^{-10} m²/s for distances larger than 35 mm from the tracer source, which is within the range of values deduced from the data in Vilks et al. (2005; see Appendix 1). CTU implemented large D_a values at those distances (Table 4-3), reaching values even larger than diffusion coefficients in free water, and resulting in very flat profile tails. Note also that CTU implemented a small K_d value of 10^{-8} m³/kg (instead of zero), based on values reported by Nilsson et al. (2010). GRS results are somewhat similar to those from JAEA, but reflecting the thinner disturbed zone considered in the model (1 mm) and with a slightly steeper profile. D_a values in the undisturbed matrix for JAEA and GRS are 6.2×10^{-11} m²/s and 7.9×10^{-12} m²/s, respectively. They are in the low end of values deduced from the data in Vilks et al. (2005). Like in the case of Na-22, while ϕ and D_e values decrease along the disturbed zone in the JAEA model concept, ϕ and D_e values increase in the GRS model. Also, activities in the reservoir did not change significantly during the experiment (Figure 2-1), making the discrimination between the two concepts difficult.

Figure 4-3e,f show model results for CFE and PROGEO (A profiles only). Two representative curves from PROGEO are shown. They both match reasonably well the measured profiles. Transport and retention parameters for their assumed disturbed zone, microfractures and matrix were varied to obtain different possible matches to the observed profiles (Table 4-4). Different possible combinations were obtained (no a priori concept was implemented for the distribution of values of transport and retention parameters in the different regions, including the use of positive K_d values). However, for all reported cases, D_a values for fracture or matrix were similar to or larger than diffusion coefficients in free water. CFE considered centimetric fractures and matrix in the model concept. In this case, D_p values (no sorption; $D_p = D_a$) were similar for matrix (1.6×10^{-10} m²/s) and fractures (4.0×10^{-10} m²/s).

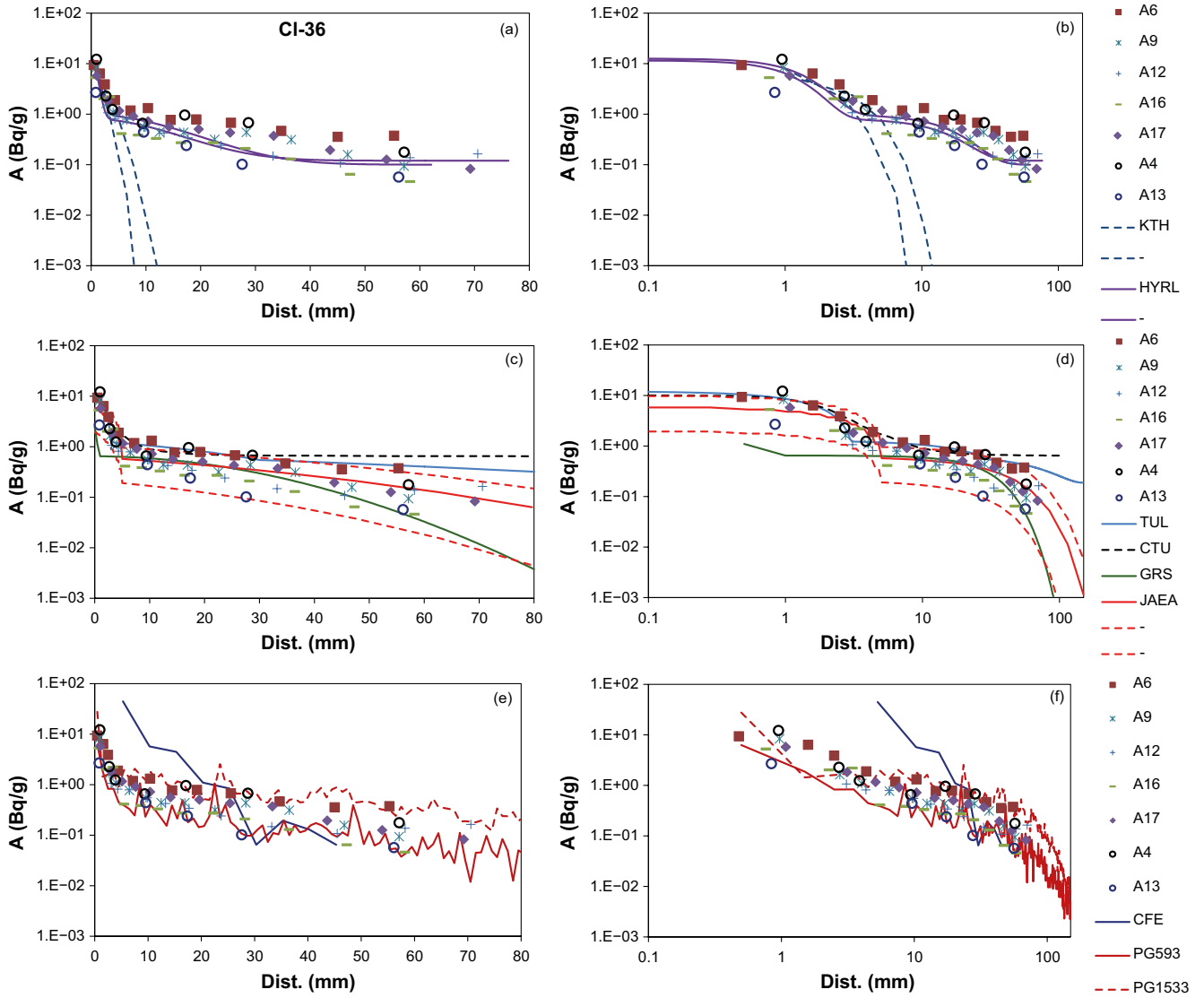


Figure 4-3. Measured (symbols) and calculated (lines) Cl-36 tracer profiles for A cores. Activities are in Bq per gram of rock. Three groups of plots are shown: (a,b) homogeneous models, (c,d) continuum-porous-medium models, (e,f) microstructure-based models. All plots show all the measured data.

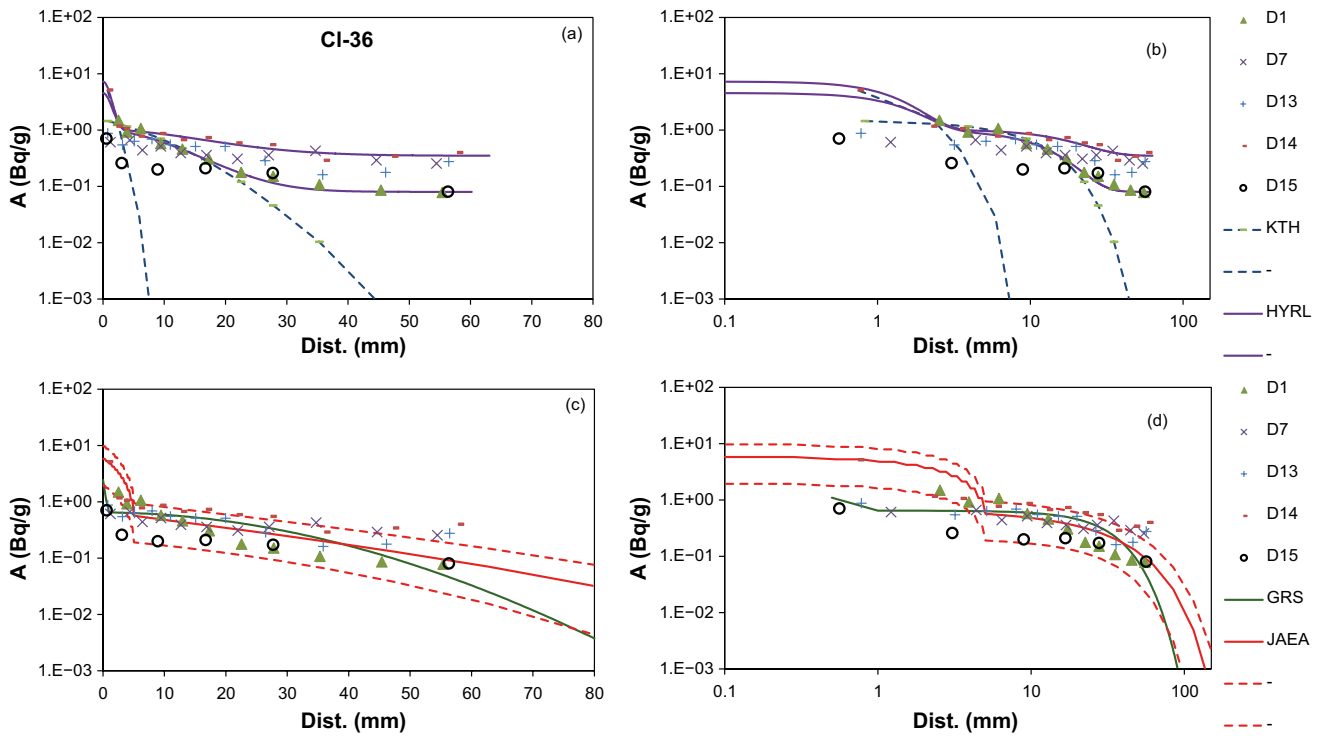


Figure 4-4. Measured (symbols) and calculated (lines) $Cl-36$ tracer profiles for D cores. Activities are in Bq per gram of rock. Two groups of plots are shown: (a,b) homogeneous models, (c,d) continuum-porous-medium models. No results from microstructure-based models were reported. All plots show all the measured data.

Table 4-3. CI-36 transport and retention parameter values for the different zones implemented in the homogenous and continuum-porous-medium models. Different parameters have been adjusted by different teams. Apparent diffusion coefficients (D_a) have been calculated from the reported parameters in all the cases. D_e : effective diffusion coefficient; ϕ : porosity; K_d : sorption distribution coefficient; α : capacity factor. D_{a1} and D_{a2} stand for D_a values in the two-component model from HYRL.

Team	t (days)	Layer	CI-36 D_e m ² /s	CI-36 ϕ	CI-36 K_d m ³ /kg	CI-36 α	CI-36 D_a m ² /s
KTH	190	1	3.8E-16 – 3.6E-14		0	0.0003 – 0.0104	9.1E-14 – 1.2E-10
HYRL	429,479	1		0.00109–0.00136	0		Da1 5.0E-14 – 6.0E-14 Da2 4.3E-12 – 9.0E-12
TUL	434	1 (0–3 mm)	3.1E-12 – 6.3E-13	0.01–0.001	0		3.1E-10 – 6.3E-10
		2 (3–25 mm, CI 3–30 mm)	6.3E-13 – 5.8E-14	0.001–0.0005	0		6.3E-10 – 1.16E-10
		3 (35 mm – 14.75 cm)	5.8E-14	0.0005	0		1.16E-10
CTU	310	1 (0–60 mm)	1.0E-14 – 4.8E-10	0.03	1.0E-08		3.3E-13 – 1.6E-8
GRS	521	DZ A (0–1 mm)	2.84E-15 – 6.32E-15	0.003–0.0008	0		9.5E-13 – 7.9E-12
		DZ D (0–1 mm)	1.58E-15 – 6.32E-15	0.001–0.0008	0		1.6E-12 – 7.9E-12
		Matrix (1 mm – 14 cm)	6.32E-15	0.0008	0		7.90E-12
JAEA	200	A1 – fracture (0–0.5 mm)	4.72E-12 –	0.01 –	0		4.7E-10 –
		A2 – DZ (0.5–5 mm)	– 1.85E-14	– 0.0003	0		– 6.2E-11
		A3 – undisturbed (5 mm –)	1.85E-14	0.0003	0		6.2E-11
		D1 – DZ (0–5 mm)	4.72E-12 – 1.85E-14	0.01–0.0003	0		4.7E-10 – 6.2E-11
		D2 – undisturbed (5 mm –)	1.85E-14	0.0003	0		6.20E-11

Table 4-4. CI-36 transport and retention parameter values for the different zones implemented in the microstructure-based models. Different parameters have been adjusted by different teams. Apparent diffusion coefficients (D_a) have been calculated from the reported parameters. D_e : effective diffusion coefficient; ϕ : porosity; K_d : sorption distribution coefficient; α : capacity factor; D_p : pore diffusion coefficient.

Team	t (days)	Layer	CI-36 D_e m ² /s	CI-36 ϕ	CI-36 K_d m ³ /kg	CI-36 α	CI-36 D_a m ² /s
CFE	200	Matrix (0–8 cm)	3.50E-13	2.20E-03	0		1.6E-10
		Det. fractures (0–8 cm)	$D_p = 4.0e-10$	1	0		4.0E-10
PROGEO	198	DZ (0–1 mm)	$D_p: 4.8e-12 – 8.3e-8$	$2.1e-7 – 1.6e-3$	$1.6e-8 – 3.0e-6$	$3.3e-4 – 8.3e-3$	$4.7e-12 – 2.8e-10$
		Fractures (1 mm – 20 cm)	$D_p: 1.7e-12 – 3.9e-8$	$2.9e-5 – 2.0e-3$	$1.8e-8 – 2.7e-7$	$7.8e-5 – 2.7e-3$	$1.2e-12 – 1.4e-8$
		Matrix (1 mm – 20 cm)	$D_p: 4.3e-11 – 1.0e-6$	$1.1e-7 – 6.3e-3$	$1.4e-8 – 2.4e-2$	$3.9e-5 – 65.8$	$1.1e-19 – 3.7e-8$

4.3 Co-57

Figure 4-5 shows the measured and calculated Co-57 profiles in the rock. The measurements below the detection limit have been plotted at the very bottom of the figures, since this is relevant information that has to be taken into account (activities are not 10^{-3} Bq/g for these points). It is important to mention that several data points further than ca 7 mm from the tracer source, and defining conceivable long flat profile tails, were discarded during data revision and are not shown here (see Appendix 2). Additionally, potential contamination levels were set at 3 Bq/g. Modelling results were provided by HYRL (A and D profiles), TUL (A profiles), JAEA (A and D profiles) and CFE (A profiles).

HYRL used an analytical solution to the diffusion-sorption equations for a homogeneous medium (constant transport and sorption parameters), assuming here a two-component (two parallel diffusion pathways) approach for the profiles. In addition, HYRL added a constant background (tail) to account for the activities measured far from the tracer, based largely on data points that were later discarded during data revision. Notice that most points further than ca 3 mm from the tracer source show measurements below detection limit (plotted at 10^{-3} Bq/g). Only one (A cores) or two (D cores) representative model profiles are shown for each type of profile (HYRL performed individual model fits for individual profiles). Table 4-5 shows ranges of values for the transport and retention parameters used in the models. D_a values from HYRL are in the 10^{-14} m²/s range, which would be consistent with high-end laboratory D_e values for HTO (Vilks et al. 2005) and rock-matrix batch sorption K_d values for Co-57 (Widestrand et al. 2010) – see Appendix 1.

TUL also tried to fit the flat profiles extending for long distances (data points later discarded). For that purpose, D_a values in the 10^{-12} m²/s range had to be implemented starting just after ca 2 mm from the tracer source. The bend in the curve at 3 mm corresponds to the changes in parameter values (zonation) implemented at that point (Table 4-5).

JAEA provided results for a central case and for upper and lower bounds, based on ranges of values for D_e and K_d . The model concept did not try to account for any possible profile tails far from the tracer source. Their results show some effect from the fracture coating (increased ϕ , K_d and D_e values) included in the concept for the A profiles. However, D_a values in the fracture coating, disturbed zone and undisturbed rock matrix are all about 10^{-15} m²/s for the A profiles, with values up to 4×10^{-14} m²/s in the disturbed zone for the D profiles. Most measured data points would fall into this assumed disturbed zone. The D_a value in the undisturbed matrix is 1.3×10^{-15} m²/s (central case).

The model from CFE considered centimetric fractures and matrix, with no sorption along the fractures. Fast diffusion along the fracture would in this concept explain the points measured far from the tracer source (data discarded during data revision).

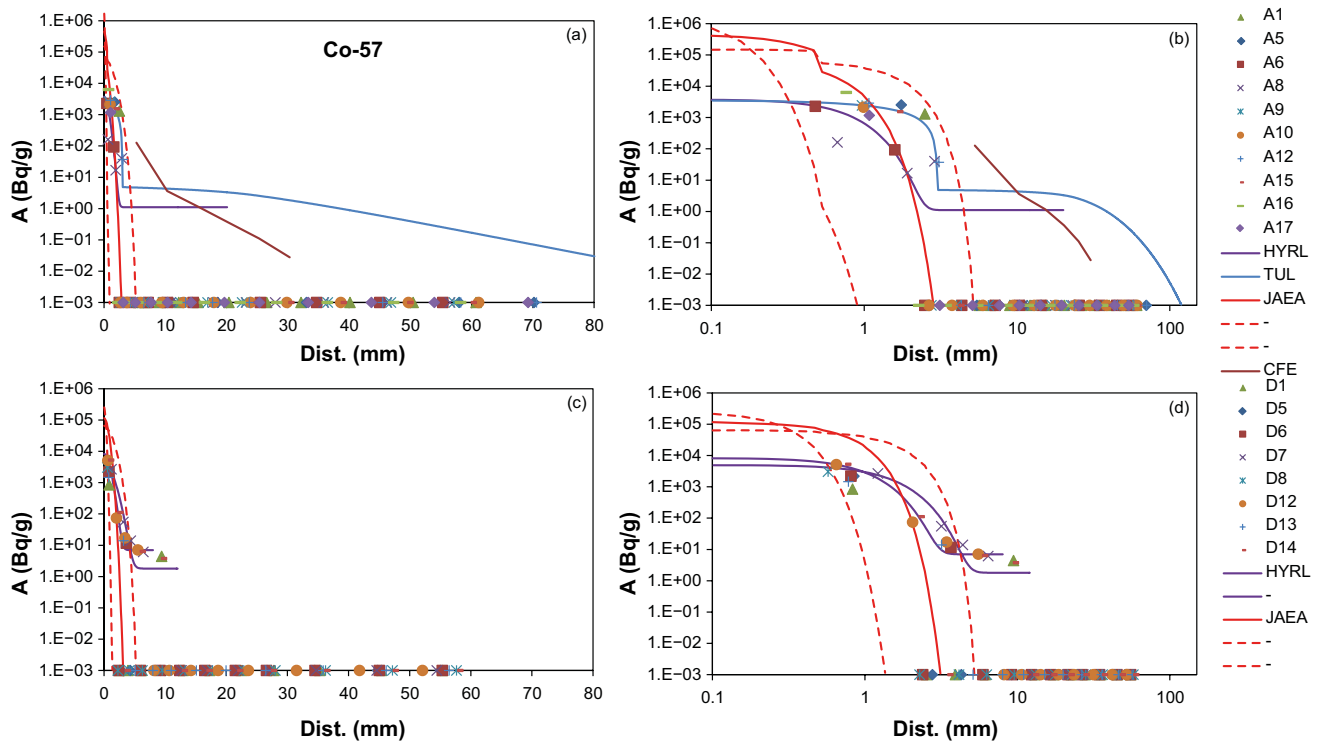


Figure 4-5. Measured (symbols) and calculated (lines) Co-57 tracer profiles for A cores (a,b) and D cores (c,d). Activities are in Bq per gram of rock. All plots show all the measured data, with data plotted at the bottom of the figures (10^{-3} Bq/g) corresponding to measurements below detection limit. For those points, detection limits are always below 20 Bq/g and decrease with distance from the tracer source to values less than ca 1 Bq/g. Measurements that were judged to be caused by contamination, with activities less than ca 2 Bq/g, are not shown.

Table 4-5. Co-57 transport and retention parameter values for the different zones implemented in the models. Different parameters have been adjusted by different teams. Apparent diffusion coefficients (D_a) have been calculated from the reported parameters in all the cases. D_e : effective diffusion coefficient; ϕ : porosity; K_d : sorption distribution coefficient.

Team	t (days)	Layer	Co-57 D_e m ² /s	Co-57 ϕ	Co-57 K_d m ³ /kg	Co-57 D_a m ² /s
HYRL	429, 479	1			$4.5e-2 - 1.2e-1$	$1.0e-14 - 4.0e-14$
TUL	434	1 (0–3 mm)	$2.7e-12 - 4.3e-13$	0.02–0.005	$\sim 2e-2 - \sim 3e-5$	$\sim 5.0e-14 - \sim 5.0e-12$
		2 (3–25 mm, Cl 3–30 mm)	$4.3e-13 - 1.3e-13$	0.005–0.002	$\sim 3e-5$	$\sim 5.0e-12 - \sim 1.6e-12$
		3 (35 mm – 14.75 cm)	$1.30E-13$	0.002	$\sim 3e-5$	$\sim 1.6e-12$
JAEA	200	A1 – fracture (0–0.5 mm)	$1.68E-12 -$	0.01 –	0.42 –	$1.5E-15 -$
		A2 – DZ (0.5–5 mm)	$- 4.41E-14$	- 0.001	- $1.3E-02$	- $1.3E-15$
		A3 – undisturbed (5 mm –)	$4.41E-14$	0.001	$1.3E-02$	$1.3E-15$
		D1 – DZ (0–5 mm)	$1.68E-12 - 4.41E-14$	0.01–0.001	$1.6E-2 - 1.3E-2$	$3.9E-14 - 1.3E-15$
		D2 – undisturbed (5 mm –)	$4.41E-14$	0.001	$1.3E-02$	$1.3E-15$
CFE	200	Matrix (0–8 cm)	$3.50E-13$	$2.20E-03$	0.1	$1.3E-15$
		Det. fractures (0–8 cm)	$D_p = 4.0E-10$	1	0	$4.0E-10$

4.4 Ni-63

Figure 4-6 shows the measured and calculated Ni-63 profiles in the rock. The measurements below the detection limit have been plotted at the very bottom of the figures, since this is relevant information that has to be taken into account (activities are not 10^{-3} Bq/g for these points). It should also be mentioned that a few data points further than ca 4 mm from the tracer source, and defining potential long flat profile tails, were discarded during data revision and are not shown here. However, there is still an almost flat tail remaining for one of the measured profiles (core D12). Notice that other points at similar distances show readings below detection limits (Figure 4-6). Modelling results were only provided by HYRL (A and D profiles), TUL (A profiles), JAEA (A and D profiles) and CFE (A profiles).

HYRL used an analytical solution to the diffusion-sorption equations for a homogeneous medium (constant transport and sorption parameters; only a single diffusion pathway). In addition, HYRL added a constant background (tail) to account for the activities measured far from the tracer. Only one (A cores) or two (D cores) representative model profiles are shown for each type of profile (HYRL performed individual model fits for individual profiles). Table 4-6 shows ranges of values for the transport and retention parameters used in the models. D_a values from HYRL are in the 10^{-14} m²/s range, which, like Co-57, would be consistent with high-end laboratory D_e values for HTO (Vilks et al. 2005) and rock-matrix batch sorption K_d values for Ni-63 (Widstrand et al. 2010) – see Appendix 1.

JAEA provided results for a central case and for upper and lower bounds, based on ranges of values for D_e and K_d . The model concept did not try to account for any possible profile tails far from the tracer source. Their results clearly show the effect of the fracture coating (increased ϕ , K_d and D_e values) included in the concept for the A profiles (Figure 4-1c,d). The D_a value in the undisturbed matrix is 3.8×10^{-15} m²/s (central case), which is slightly smaller than the values obtained by HYRL, but consistent with the upscaling concept used by JAEA. Values in the disturbed zone (5 mm) are more similar to those used by HYRL (Table 4-6). Most of the measured data points would fall into this assumed disturbed zone.

Like in the case of Co-57, TUL also tried to fit the flat profiles extending for long distances. For that purpose, D_a values in the 10^{-11} m²/s range had to be implemented starting just after ca 2 mm from the tracer source. The kink in the curve at 3 mm corresponds to the changes in parameter values (zonation) implemented at that point (Table 4-6). The model from CFE considered centimetric fractures and matrix, with no sorption along the fractures. Fast transport along the fracture would be responsible for those points measured at large distances from the tracer source (data discarded during data revision).

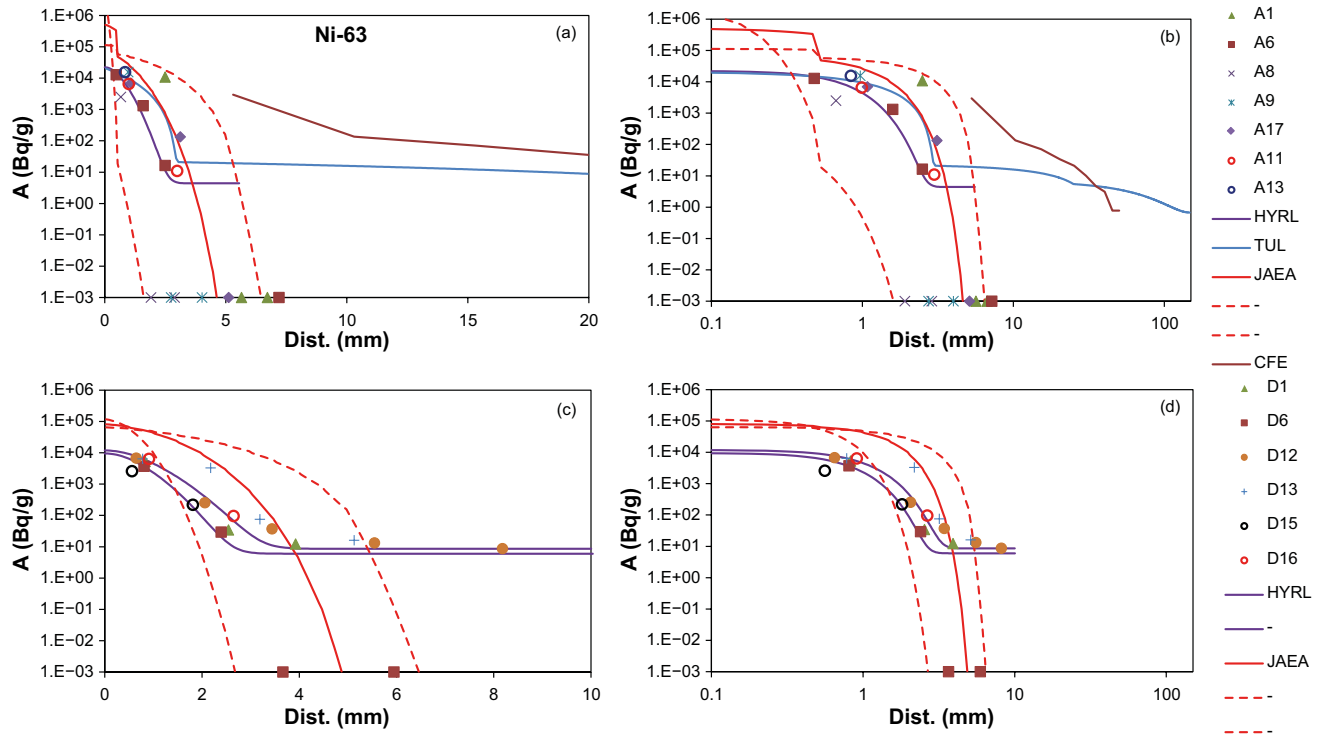


Figure 4-6. Measured (symbols) and calculated (lines) Ni-63 tracer profiles for A cores (a,b) and D cores (c,d). Activities are in Bq per gram of rock. All plots show all the measured data, with data plotted at the bottom of the figures (10^{-3} Bq/g) corresponding to measurements below detection limit. For those points, detection limits are always below 8 Bq/g. Measurements that were judged to be caused by contamination, with activities less than ca 7 Bq/g, are not shown.

Table 4-6. Ni-63 transport and retention parameter values for the different zones implemented in the models. Different parameters have been adjusted by different teams. Apparent diffusion coefficients (D_a) have been calculated from the reported parameters in all the cases. D_e : effective diffusion coefficient; ϕ : porosity; K_d : sorption distribution coefficient.

Team	t (days)	Layer	Ni-63 D_e m ² /s	Ni-63 ϕ	Ni-63 K_d m ³ /kg	Ni-63 D_a m ² /s
HYRL	429, 479				1.6E-3 – 3.7E-3	1.1E-14 – 3.0E-14
TUL	434	2.7E-12 – 4.3E-13	2.7E-12 – 4.3E-13	0.02–0.005	~2E-3 – ~1E-6	~5.0E-13 – ~5.6E-11
		4.3E-13 – 1.3E-13	4.3E-13 – 1.3E-13	0.005–0.002	~1E-6 – ~1E-9	~5.6E-11 – ~6.5E-11
		1.30E-13	1.30E-13	0.002	~1E-9	~6.5E-11
JAEA	200	A1 – fracture (0–0.5 mm)	1.63E-12 –	0.01 –	8.1E-2 –	7.5E-15 –
		A2 – DZ (0.5–5 mm)	– 4.29E-14	– 0.001	– 4.2E-03	– 3.8E-15
		A3 – undisturbed (5 mm –)	4.29E-14	0.001	4.2E-03	3.8E-15
		D1 – DZ (0–5 mm)	1.63E-12 – 4.29E-14	0.01 – 0.001	0.005 – 4.2E-3	1.2E-13 – 3.8E-15
		D2 – undisturbed (5 mm –)	4.29E-14	0.001	4.2E-03	3.8E-15
CFE	200	Matrix (0–8 cm)	3.50E-13	2.20E-03	3.00E-02	4.3E-15
		Det. fractures (0–8 cm)	$D_p = 4.0E-10$	1	0	4.0E-10

4.5 Ba-133

Figures 4-7 (A profiles) and 4-8 (D profiles) show the measured and calculated Ba-133 profiles in the rock. The measurements below the detection limit have been plotted at the very bottom of the figures, since this is relevant information that has to be taken into account (activities are not 10^{-3} Bq/g for these points). Most data points with measured activities at distances further than ca 5 mm from the tracer source and defining conceivable long flat profile tails were discarded during data revision and are not shown here (see Appendix 2). However, there are still two data points (cores A11 and D15) showing measurable activities at distances further than 10 mm. Still, the great majority of measurements at those distances, after revision, show readings below detection limits. Potential contamination levels were set at 0.3 (sliced samples) to 0.4 (crushed samples) Bq/g.

For clarity, the results for different types of models are shown in different figures: (a,b) analytical solutions and (c,d) continuum models. All plots show all the measured data. No results from any microstructure-based models were made available.

Figures 4-7a,b and 4-8a,b show model results for KTH and HYRL. These two teams used analytical solutions to the diffusion-sorption equations for a homogeneous medium (constant transport and sorption parameters). In addition, HYRL (only single-component models for this tracer) added a constant background (tail) to account for the activities measured far from the tracer source in the A profiles (further than ca 5 mm). KTH did not try to adjust the model to the points measured far from the tracer source. Only two representative model profiles are shown for each model (the teams did individual model fits for individual profiles) and for each type of profile (A and D cores). Table 4-7 shows ranges of values for the transport and retention parameters used in the models. D_a values are in the range from 1×10^{-14} to 1×10^{-13} m²/s, which are consistent with those that could be expected from laboratory D_e values for HTO (Vilks et al. 2005) and rock-matrix batch sorption K_d values for Ba-133 (Widstrand et al. 2010) – see Appendix 1.

Figures 4-7c,d and 4-8c,d show model results for TUL (A profiles), GRS (A and D profiles) and JAEA (A and D profiles). JAEA provided results for a central case and for upper and lower bounds, based on ranges of values for D_e and K_d . Their results clearly show the effect of the fracture coating (increased ϕ , K_d and D_e values) included in the concept for the A profiles (Figure 4-7c,d). The results from TUL match the highest activities measured far from the tracer source. TUL had to implement large D_a values at those distances (ca 6.5×10^{-11} m²/s, Table 4-7). Results from GRS show profiles that are less steep than those shown by the measurements, extending also to slightly larger distances. Most measured data points would fall within the disturbed zone assumed in the JAEA model (5 mm), with D_a values largely in the 10^{-14} m²/s range (similar to the values obtained by KTH and HYRL in their homogeneous models) or slightly larger (D profiles). However, the profiles calculated by JAEA tend to be slightly steeper than those shown by the measurements. The calculated steepness of the profiles is probably given by the way transport and retention parameter values decrease along the disturbed zone. The value in the undisturbed matrix is 1.5×10^{-14} m²/s. The value from GRS for the undisturbed matrix (beyond 1 mm from the tracer source) is 1.8×10^{-13} m²/s (consistent with the slightly longer transport distances), with smaller values in the disturbed zone. Both JAEA and GRS implemented a disturbed zone in the profiles. However, while ϕ , K_d and D_e values decrease along the disturbed zone in the JAEA model concept, ϕ and D_e values increase in the GRS model, with constant K_d values. While GRS used a constant-activity boundary condition for the tracer source, JAEA did calculate the evolution of activities in the reservoir during the experiment, matching reasonably well the measured data, and supporting D_a values in the 10^{-14} m²/s range close to the tracer source. However, the overall fit to the profile data was best for the homogeneous models from KTH and HYRL.

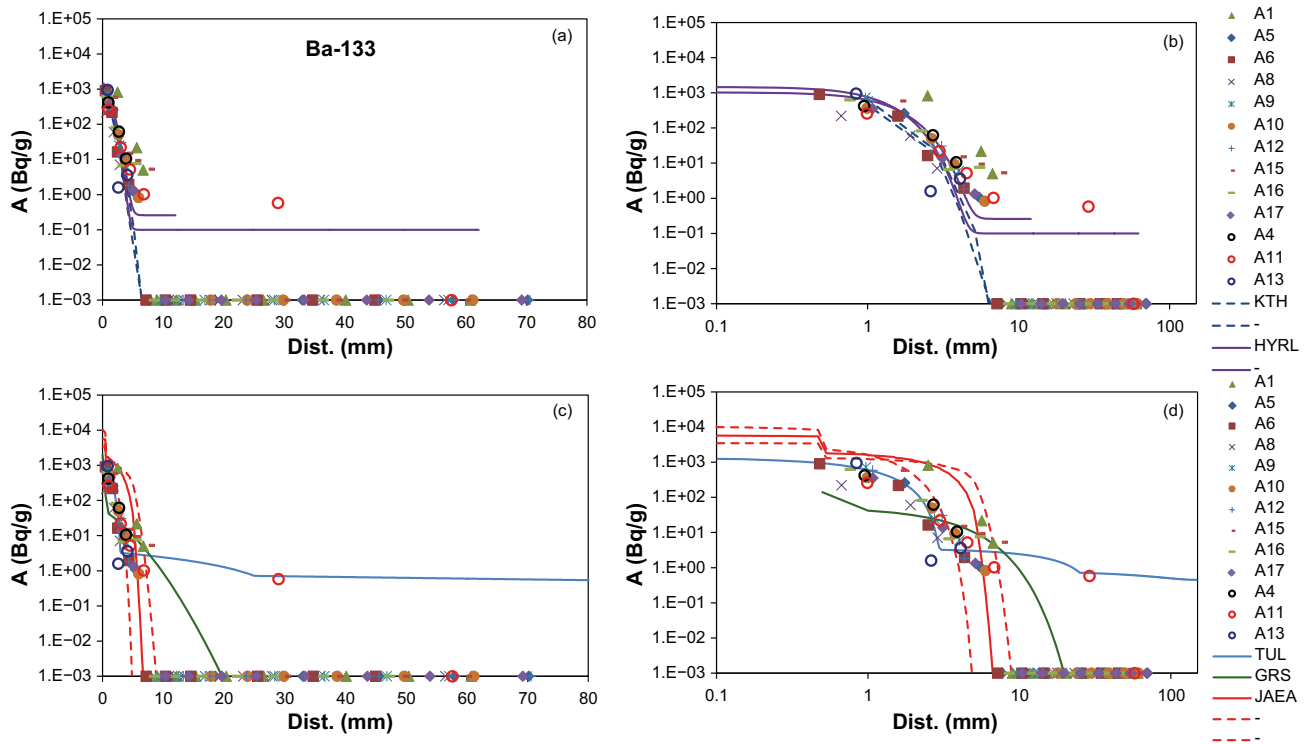


Figure 4-7. Measured (symbols) and calculated (lines) Ba-133 tracer profiles for A cores. Activities are in Bq per gram of rock. Two groups of plots are shown: (a,b) homogeneous models, (c,d) continuum-porous-medium models. No results from microstructure-based models were reported. All plots show all the measured data, with data plotted at the bottom of the figures (10^{-3} Bq/g) corresponding to measurements below detection limit. For those points, detection limits are always below 0.8 Bq/g and decrease with distance from the tracer source to values less than ca 0.2 Bq/g. Measurements that were judged to be caused by contamination, with activities less than 0.4 Bq/g, are not shown.

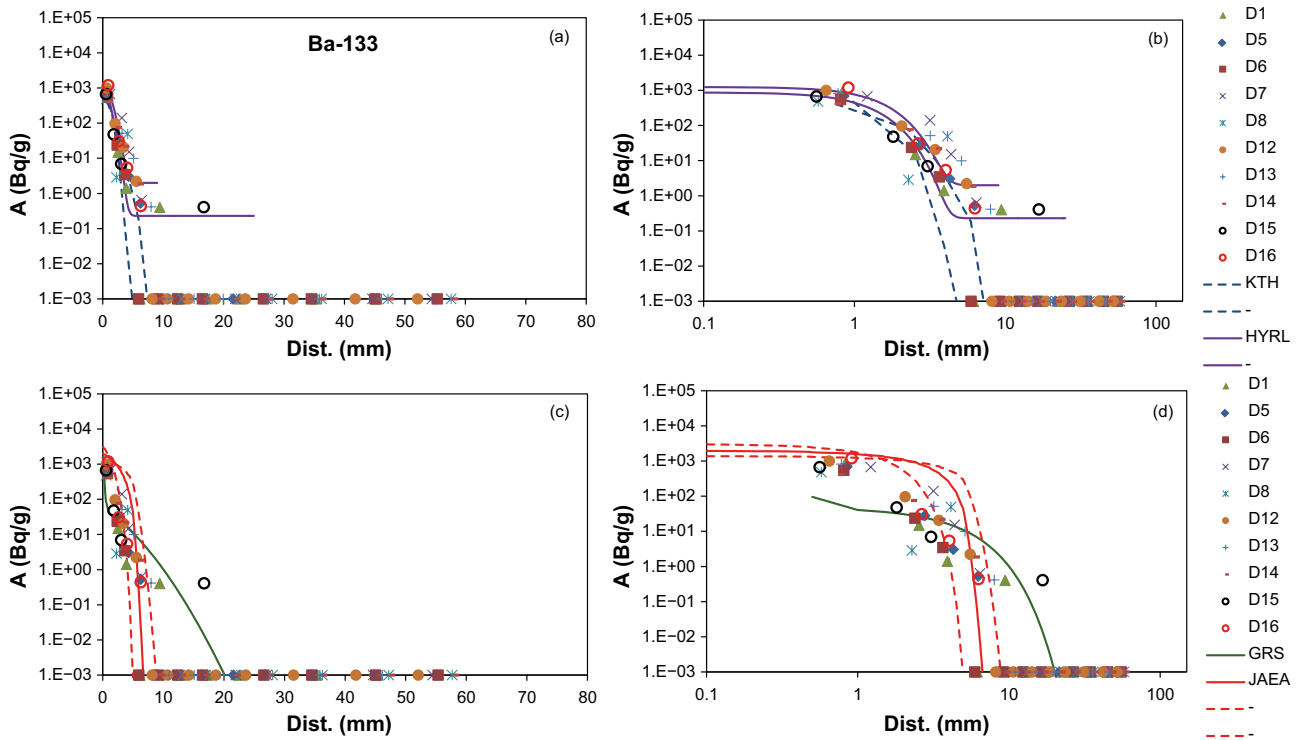


Figure 4-8. Measured (symbols) and calculated (lines) Ba-133 tracer profiles for D cores. Activities are in Bq per gram of rock. Two groups of plots are shown: (a,b) homogeneous models, (c,d) continuum-porous-medium models. No results from microstructure-based models were reported. All plots show all the measured data, with data plotted at the bottom of the figures (10^{-3} Bq/g) corresponding to measurements below detection limit. Detection limits are always below 0.8 Bq/g and decrease with distance from the tracer source to values less than ca 0.2 Bq/g. Measurements that were judged to be caused by contamination, with activities less than 0.4 Bq/g, are not shown.

Table 4-7. Ba-133 transport and retention parameter values for the different zones implemented in the models. Different parameters have been adjusted by different teams. Apparent diffusion coefficients (D_a) have been calculated from the reported parameters in all the cases. D_e : effective diffusion coefficient; ϕ : porosity; K_d : sorption distribution coefficient; α : capacity factor.

Team	t (days)	Layer	Ba-133 D_e m ² /s	Ba-133 ϕ	Ba-133 K_d m ³ /kg	Ba-133 α	Ba-133 D_a m ² /s
KTH	190	1	3.2E-14 – 8.0E-13			0.902 – 7.552	1.3E-14 – 1.3E-13
HYRL	429, 479	1			4.3E-4 – 3.0E-3		1.2E-14 – 1.0E-13
TUL	434	1 (0–3 mm)	2.7E-12 – 4.3E-13	0.02–0.005	~1E-3 – ~1E-6		~9.9E-13 – ~5.6E-11
		2 (3–25 mm, CI 3–30 mm)	4.3E-13 – 1.3E-13	0.005–0.002	~1E-6 – ~3E-9		~5.6E-11 – ~6.5E-11
		3 (35 mm – 14.75 cm)	1.30E-13	0.002	~3E-9		~6.5E-11
GRS	521	DZ A (0–1 mm)	1.17E-15 – 1.04E-12	0.003–0.004	2.10E-03		2.0E-16 – 1.8E-13
		DZ D (0–1 mm)	6.50E-16 – 1.04E-12	0.001–0.004	2.10E-03		1.2E-16 – 1.8E-13
		Matrix (1 mm – 14 cm)	1.04E-12	0.004	2.10E-03		1.80E-13
JAEA	200	A1 – fracture (0–0.5 mm)	2.04E-12 –	0.01 –	0.011 –		6.9E-14 –
		A2 – DZ (0.5–5 mm)	– 5.35E-14	– 0.001	– 1.30E-03		– 1.5E-14
		A3 – undisturbed (5 mm –)	5.35E-14	0.001	1.30E-03		1.5E-14
		D1 – DZ (0–5 mm)	2.04E-12 – 5.35E-14	0.01–0.001	1.48E-3 – 1.30E-3		5.1E-13 – 1.5E-14
		D2 – undisturbed (5 mm –)	5.35E-14	0.001	1.30E-03		1.5E-14

4.6 Cs-137

Figures 4-9 (A profiles) and 4-10 (D profiles) show the measured and calculated Cs-137 profiles in the rock. All plots show all the measured data. The measurements below the detection limit have been plotted at the very bottom of the figures, since this is relevant information that has to be taken into account (activities are not 10^{-3} Bq/g for these points). Most data points with measured activities at distances further than ca 5 mm from the tracer source were discarded during data revision and are not shown here (see Appendix 2), but there are still a few data points, corresponding to cores A11, A15 and D6, showing measurable activities at distances further than 10 mm. Still, most measurements at those distances, after revision, show readings below detection limits. Potential contamination levels were set at 1.5 (sliced samples) to 2.0 (crushed samples) Bq/g.

For clarity, the results for different types of models are shown in different figures: (a,b) analytical solutions, (c,d) continuum models, and (e,f) microstructure-based models.

Figures 4-9a,b and 4-10a,b show model results for KTH and HYRL. These two teams used analytical solutions to the diffusion-sorption equations for a homogeneous medium (constant transport and sorption parameters). HYRL assumed either a one-component or a two-component (two parallel diffusion pathways) approach, depending on the individual profile that was modelled. In addition, HYRL added a constant background (tail) to account for the activities measured far from the tracer source (before data revision). KTH did not try to adjust the model to the points measured far from the tracer source. Only a few model profiles are shown for each model (the teams did individual model fits for individual profiles) and for each type of profile (A and D cores). Table 4-8 shows ranges of values for the transport and retention parameters used in the models. D_a values are in the 10^{-14} m²/s range, except for the cases where HYRL added a second diffusion pathway, with values in the 10^{-12} m²/s range. In those cases, the second pathway accounted for the transition between the data points close to the tracer source (within ca 5 mm) and those in the tails (further than ca 10 mm). D_a values in the 10^{-14} m²/s range are consistent with high-end laboratory D_e values for HTO (Vilks et al. 2005) and rock-matrix batch sorption K_d values for Cs-137 (Widstrand et al. 2010) – see Appendix 1.

Figures 4-9c,d and 4-10c,d show model results for TUL, GRS and JAEA. TUL only did calculations for A profiles. JAEA provided results for a central case and for upper and lower bounds, based on ranges of values for D_e and K_d . The results from TUL match the highest activities measured far from the tracer source. TUL had to implement large D_a values (in the 10^{-11} m²/s range) at those distances (Table 4-8). Results from GRS show a good match to the data close to the tracer source (less than ca 8 mm), with a D_a value of 4.4×10^{-14} m²/s in the undisturbed rock matrix beyond the disturbed zone (1 mm). For JAEA, most measured data points would fall within the assumed disturbed zone (5 mm), with D_a values largely in the 10^{-15} m²/s range for A cores and in the 10^{-14} m²/s range (10^{-13} to 3×10^{-15} m²/s) for D cores. Like in the case of Ba-133, the calculated profiles tend to be slightly steeper than those shown by the measurements.

Figures 4-9e and 4-9f show model results for CFE, A21, KAERI and PROGEO (only A21 applied the calculations to D profiles; Figures 4-10e and 4-10f). Besides the central prediction shown in the figures, KAERI also performed sensitivity analyses with respect to the different transport and retention parameters, and also with respect to the extension of the disturbed zone assumed in the model (not shown). Two representative curves from PROGEO are shown. Notice that, like in the case of Na-22, the different model results can be considered to match the measured data. In this case the CFE results overestimate the measured activities close to the tracer source by ca an order of magnitude. However, the concepts used by the different teams are rather different. Also, KAERI and CFE tried to match the data measured far from the tracer source, while A21 and PROGEO did not. Again, despite some remaining data points, most data measured at distances further than ca 10 mm from the tracer source were discarded during data revision.

The grain-scale heterogeneity implemented in the model from A21 results in an overall constant D_a value. This model could be considered to be similar to a homogeneous model, except for the implementation of the heterogeneity (sorption by cation exchange only on the biotite grains). KAERI assumed the presence of a disturbed zone next to the tracer source. Intragranular and intergranular pores, microfractures and a vein structure were considered in their model. Intragranular porosities and D_e values (quartz, plagioclase, K-feldspar) and mineral-specific sorption parameters (K_d values on biotite and plagioclase) decrease along the disturbed zone, while the transport parameters for

microfractures and vein remain constant (Table 4-9). The vein structure assumed in the model domain (Figure 3-2) is especially responsible for the long transport distances (no sorption in the vein). In the modelling by PROGEO, transport and retention parameters for their assumed disturbed zone, microfractures and matrix were varied to obtain different possible matches to the observed profiles. Different possible combinations were obtained (no a priori concept was implemented for the distribution of values of transport and retention parameters in the different regions). CFE considered centimetric fractures and matrix in the model concept. In this case, the fractures were assumed to be fast pathways for diffusion (no sorption in the fractures).

Like with Ba-133, the overall fit to the profile data was very good for the homogeneous models from KTH and HYRL, although in this case the results from JAEA (central case, A cores), A21 and PROGEO can be considered equally good.

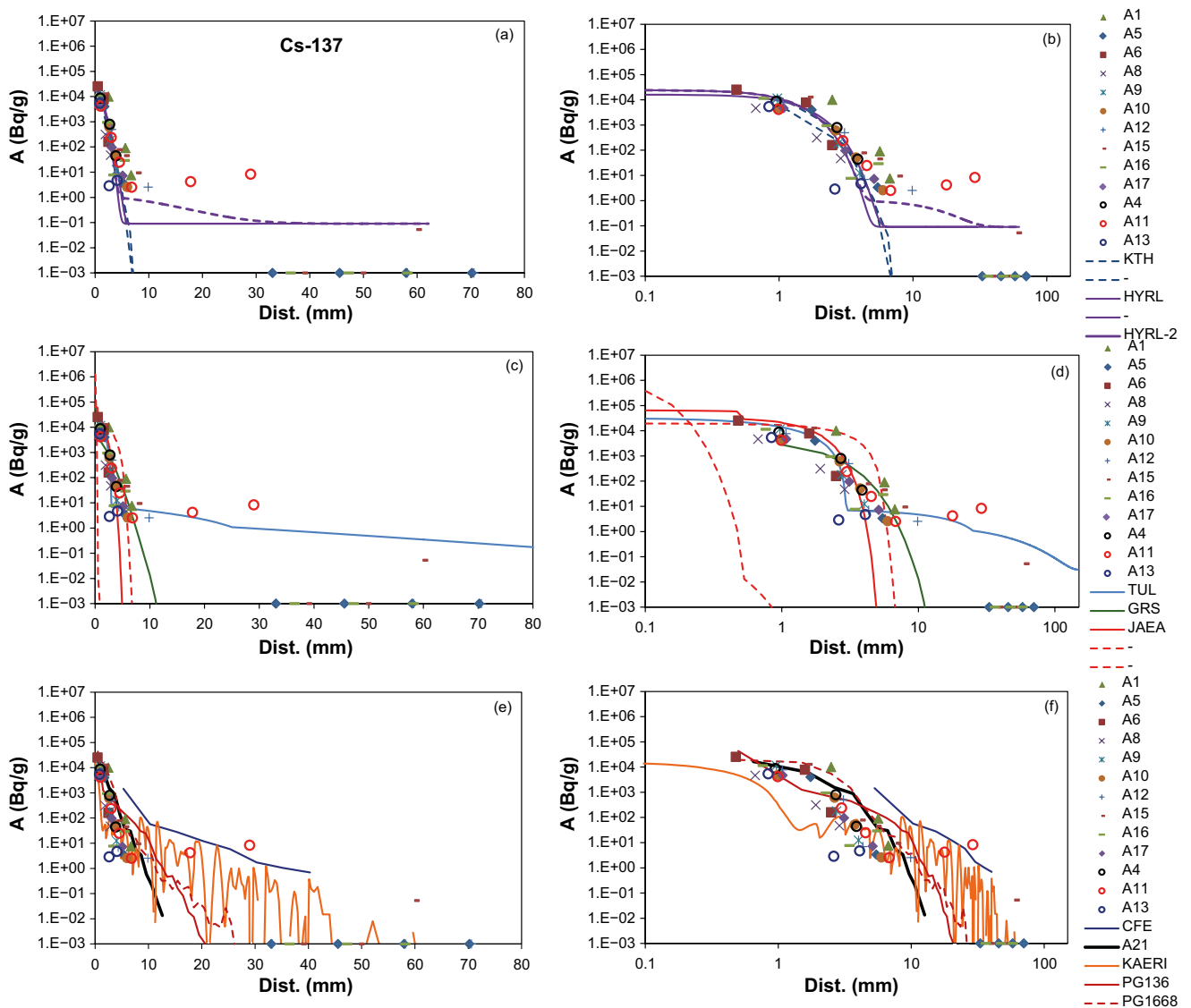


Figure 4-9. Measured (symbols) and calculated (lines) Cs-137 tracer profiles for A cores. Activities are in Bq per gram of rock. Three groups of plots are shown: (a,b) homogeneous models, (c,d) continuum-porous-medium models, (e,f) microstructure-based models. HYRL and HYRL-2 refer here to one- and two-component models from HYRL. All plots show all the measured data, with data plotted at the bottom of the figures (10^{-3} Bq/g) corresponding to measurements below detection limit. For those points, detection limits are always below 0.2 Bq/g and decrease with distance from the tracer source to values less than 0.05 Bq/g. Many measurements with activities less than 2 Bq/g were judged to be caused by contamination. They are not shown.

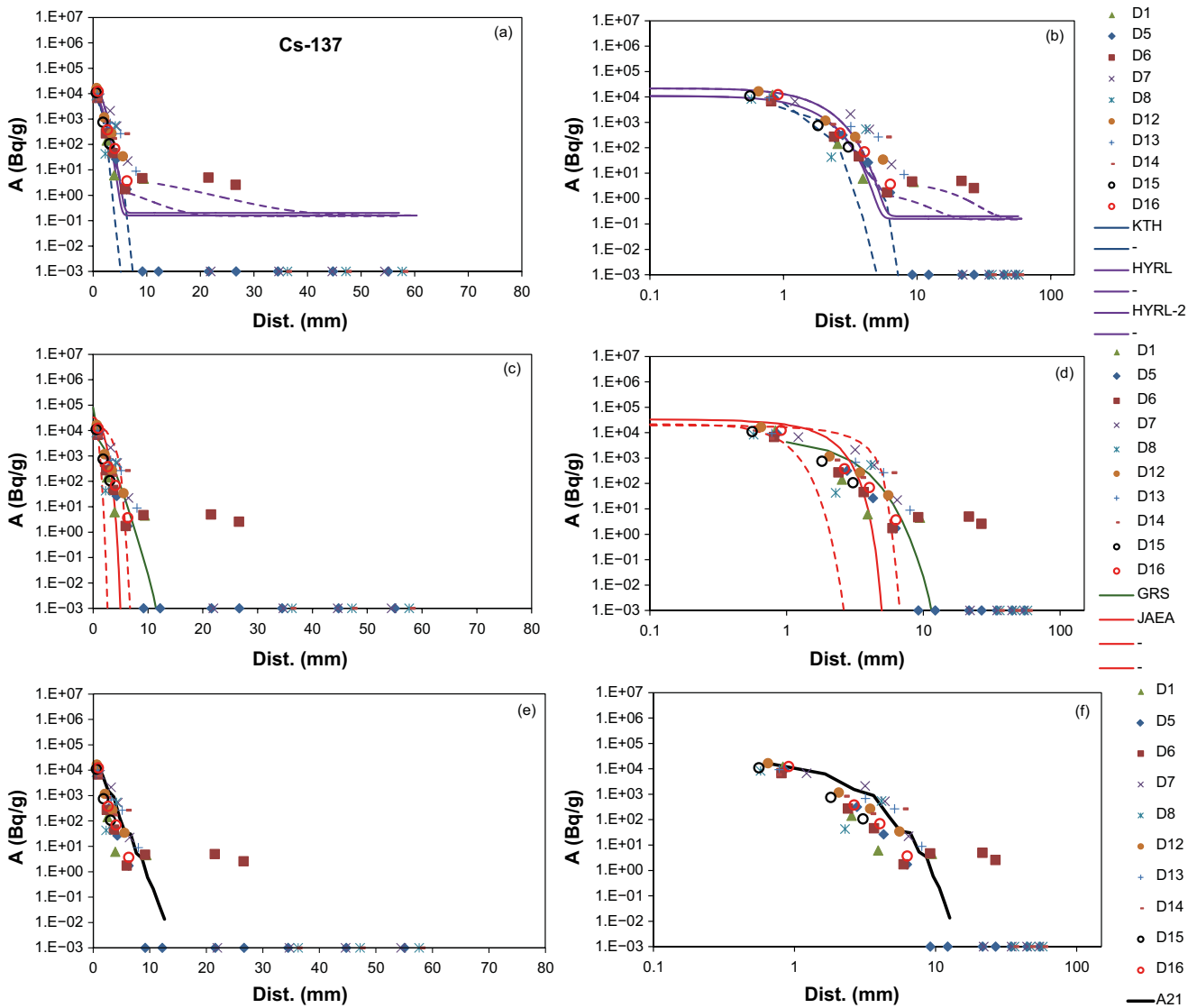


Figure 4-10. Measured (symbols) and calculated (lines) Cs-137 tracer profiles for D cores. Activities are in Bq per gram of rock. Three groups of plots are shown: (a,b) homogeneous models, (c,d) continuum-porous-medium models, (e,f) microstructure-based models. HYRL and HYRL-2 refer here to one- and two-component models from HYRL. All plots show all the measured data, with data plotted at the bottom of the figures (10^{-3} Bq/g) corresponding to measurements below detection limit. For those points, detection limits are always below 0.2 Bq/g and decrease with distance from the tracer source to values less than 0.05 Bq/g. Many measurements with activities less than 2 Bq/g were judged to be caused by contamination. They are not shown.

Table 4-8. Cs-137 transport and retention parameter values for the different zones implemented in the homogenous and continuum-porous-medium models. Different parameters have been adjusted by different teams. Apparent diffusion coefficients (D_a) have been calculated from the reported parameters in all the cases. D_e : effective diffusion coefficient; ϕ : porosity; K_d : sorption distribution coefficient; α : capacity factor. D_{a1} and D_{a2} stand for D_a values in the two-component model from HYRL.

Team	t (days)	Layer	Cs-137 D_e m ² /s	Cs-137 ϕ	Cs-137 K_d m ³ /kg	Cs-137 α	Cs-137 D_a m ² /s
KTH	190	1	1.7E-13 – 2.8E-12			7.72 – 29.4	1.0E-14 – 9.7E-14
HYRL	429, 479	1			5.0E-4 – 2.5E-2		Da 1.5E-14 – 6.0E-14 Da1 9E-14 – 7E-14 Da2 1.0E-12 – 7.0E-12
TUL	434	1 (0–3 mm)	2.7E-12 – 4.3E-13	0.02–0.005	~1E-2 – ~1E-6		~1.0E-13 – ~4.3E-13
		2 (3–25 mm, Cl 3–30 mm)	4.3E-13 – 1.3E-13	0.005–0.002	~1E-6 – ~3E-9		~4.3E-13 – ~6.5E-11
		3 (35 mm – 14.75 cm)	1.30E-13	0.002	~3E-9		~6.5E-11
GRS	521	DZ A (0–1 mm)	2.95E-15 – 2.62E-12	0.003–0.004	2.20E-02		5.0E-17 – 4.4E-14
		DZ D (0–1 mm)	1.64E-15 – 2.62E-12	0.001–0.004	2.20E-02		2.8E-17 – 4.4E-14
		Matrix (1 mm – 14 cm)	2.62E-12	0.004	2.20E-02		4.40E-14
JAEA	200	A1 – fracture (0–0.5 mm)	4.97E-12 –	0.01 –	0.30 –		6.1E-15 –
		A2 – DZ (0.5–5 mm)	– 1.31E-13	– 0.001	– 0.016		– 3.0E-15
		A3 – undisturbed (5 mm –)	1.31E-13	0.001	0.016		3.0E-15
		D1 – DZ (0–5 mm)	4.97E-12 – 1.31E-13	0.01–0.001	0.018–0.016		1.0E-13 – 3.0E-15
		D2 – undisturbed (5 mm –)	1.31E-13	0.001	0.016		3.0E-15

Table 4-9. Cs-137 transport and retention parameter values for the different zones implemented in the microstructure-based models. Different parameters have been adjusted by different teams. When possible, apparent diffusion coefficients (D_a) have been calculated from the reported parameters. D_e : effective diffusion coefficient; ϕ : porosity; K_d : sorption distribution coefficient; α : capacity factor; D_p : pore diffusion coefficient.

Team	t (days)	Layer	Cs-137 D_e m ² /s	Cs-137 ϕ	Cs-137 K_d m ³ /kg	Cs-137 α	Cs-137 D_a m ² /s
CFE	200	Matrix (0–8 cm)	3.50E-13	2.20E-03	5.00E-02		2.6E-15
		Det. fractures (0–8 cm)	$D_p = 4.0E-10$	1	0		4.0E-10
A21	200	Matrix – 13 mm	$D_p = 2.5E-12^*$	0.0026	Cat. Ex. model		
KAERI	463	DZ (0–6 mm)	Biot intragrain: $\phi^{4/3} \cdot D_0$ Non-biot intragrain: $\phi^{4/3} \cdot D_0$ Microfrac: $5E-3 \cdot D_0$ Intergrain pores: $1E-4 \cdot D_0$ $D_0 = 2.1E-9$ m ² /s	Biot intragrain: 0.03 Non-biot intragrain: $6E-3 - 3E-5$ Intergrain and microfrac: 1.0	Biot: $8.0E-2 - 8.0E-4$ Plag: $1.0E-4 - 5.0E-6$		
		Matrix (6 mm – 60 mm)	Biot intragrain: $\phi^{4/3} \cdot D_0$ Non-biot intragrain: $\phi^{4/3} \cdot D_0$ Microfrac: $5E-3 \cdot D_0$ Intergrain pores: $1E-4 \cdot D_0$ $D_0 = 2.1E-9$ m ² /s	Biot intragrain: 0.03 Non-biot intragrain: $3E-5$ Intergrain and microfrac: 1.0	Biot: $8.0E-4$ Plag: $5.0E-6$		
PROGEO	198	DZ (0–1 mm)	$D_p: 5.0E-10 - 3.1E-6$	$3.4E-6 - 3.4E-2$	$2.7E-3 - 1.2E-2$	7.4 – 32.9	$9.6E-14 - 2.3E-12$
		Fractures (1 mm – 20 cm)	$D_p: 1.4E-10 - 2.6E-6$	$5.1E-7 - 3.8E-5$	$2.0E-5 - 1.0E-1$	$5.5E-2 - 274.1$	$1.1E-18 - 9.7E-14$
		Matrix (1 mm – 20 cm)	$D_p: 3.9E-10 - 4.5E-9$	$9.6E-5 - 1.6E-2$	$1.3E-5 - 5.2E-3$	$3.6E-2 - 14.3$	$6.3E-13 - 1.2E-11$

*This value ($D_p = 2.5 \times 10^{-12}$ m²/s) applies only to the local pore scale (single intergranular volume; porosity equal to 1). It is modified by the geometry of the porous network at the sample scale. Biot: Biotite. Plag: Plagioclase. Intragrain: Intragranular porosity. Det. fractures: Deterministic fractures. Microfrac: Microfractures. Cat. Ex. Model: Cation exchange model.

4.7 Cd-109

Figure 4-11 shows the measured and calculated Cd-109 profiles in the rock. The measurements below the detection limit have been plotted at the very bottom of the figures, since this is relevant information that has to be taken into account (activities are not 10^{-3} Bq/g for these points). All measured data points are within a distance of 2.5 mm from the tracer source, except for 2 points (core D5). All the other points measured at distances larger than ca 2.5 mm from the tracer source show readings below detection limit. Modelling results were only provided by HYRL (a single A profile) and JAEA (A and D profiles).

HYRL used an analytical solution to the diffusion-sorption equations for a homogeneous medium (constant transport and sorption parameters), without the addition of any constant background activity. The D_a value obtained by HYRL was 1.8×10^{-14} m²/s. This value is consistent with low-end laboratory D_e values for HTO (Vilks et al. 2005) and rock-matrix batch sorption K_d values for Cd-109 (Widstrand et al. 2010) – see Appendix 1.

JAEA provided results for a central case and for upper and lower bounds, based on ranges of values for D_e and K_d . The model concept did not try to account for any possible profile tails far from the tracer source (only 2 data points). Their results show the effect from the fracture coating (increased ϕ , K_d and D_e values) included in the concept for the A profiles. D_a values in the fracture coating and disturbed zone are mainly in the 10^{-14} m²/s range (Table 4-10). Almost all measured data points are within the 5-mm disturbed zone assumed by JAEA, except for 2 points (core D5). The D_a value for the undisturbed matrix was 8.4×10^{-15} m²/s (central case).

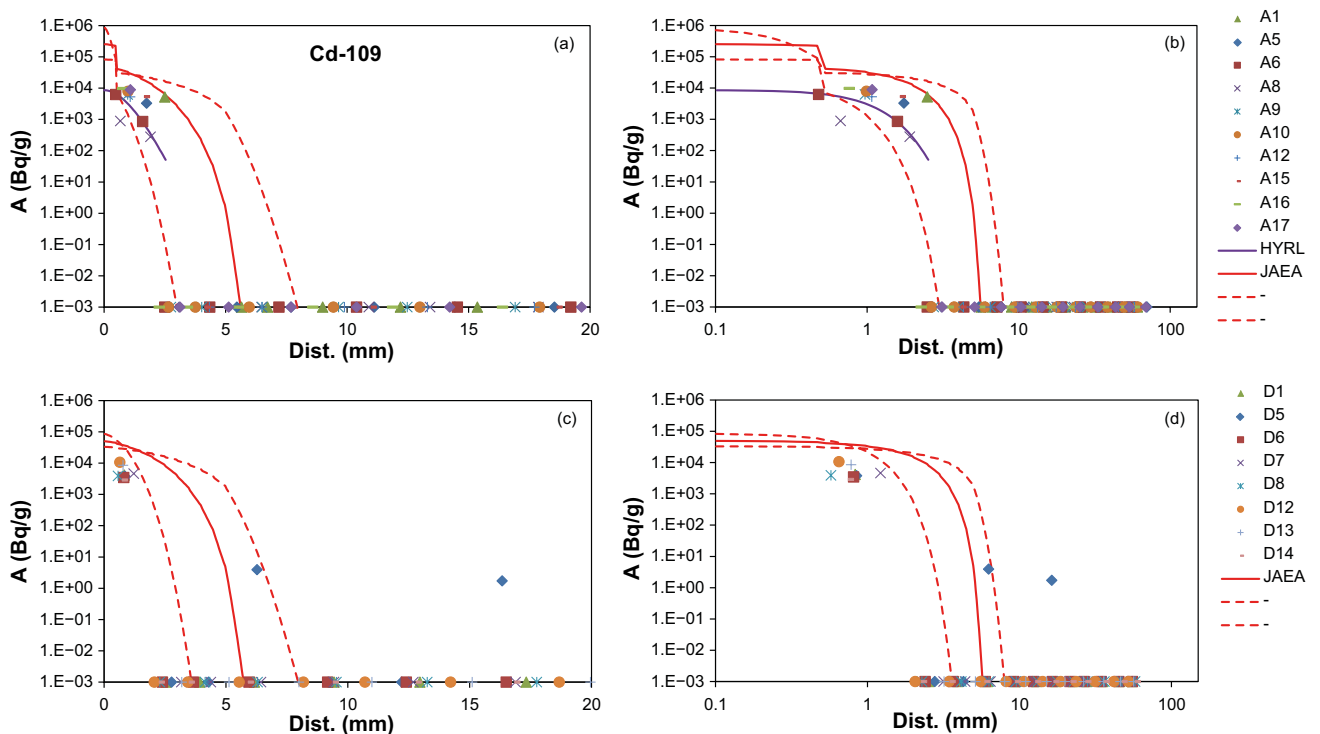


Figure 4-11. Measured (symbols) and calculated (lines) Cd-109 tracer profiles for A cores (a,b) and D cores (c,d). Activities are in Bq per gram of rock. All plots show all the measured data, with data plotted at the bottom of the figures (10^{-3} Bq/g) corresponding to measurements below detection limit. For those points, detection limits are always below 250 Bq/g and decrease with distance from the tracer source to values less than 20 Bq/g.

Table 4-10. Cd-109 transport and retention parameter values for the different zones implemented in the models. Different parameters have been adjusted by different teams. Apparent diffusion coefficients (D_a) have been calculated from the reported parameters in all the cases. D_e : effective diffusion coefficient; ϕ : porosity; K_d : sorption distribution coefficient.

Team	t (days)	Layer	Cd-109 D_e m ² /s	Cd-109 ϕ	Cd-109 K_d m ³ /kg	Cd-109 D_a m ² /s
HYRL	429, 479				2.80E-03	1.80E-14
JAEA	200	A1 – fracture (0–0.5 mm)	1.72E-12 –	0.01 –	0.04 –	1.6E-14 –
		A2 – DZ (0.5–5 mm)	– 4.53E-14	– 0.001	– 2.0E-03	– 8.4E-15
		A3 – undisturbed (5 mm –)	4.53E-14	0.001	2.0E-03	8.4E-15
		D1 – DZ (0–5 mm)	1.72E-12 – 4.53E-14	0.01–0.001	2.6E-3 – 2.0E-3	2.5E-13 – 8.4E-15
		D2 – undisturbed (5 mm –)	4.53E-14	0.001	2.0E-03	8.4E-15

4.8 Ra-226

Figure 4-12 shows the measured and calculated Ra-226 profiles in the rock. The measurements below the detection limit have been plotted at the very bottom of the figures, since this is relevant information that has to be taken into account (activities are not 10^{-3} Bq/g for these points). Most data points with measured activities at distances further than ca 5 mm from the tracer source and defining conceivable long flat profile tails were discarded during data revision and are not shown here. Only a single point corresponding to core D12 shows measurable activity at a distance of 18.7 mm from the tracer source. All the other points measured at distances larger than 5 mm show readings below detection limit. Modelling results were only provided by HYRL (two A profiles) and JAEA (A and D profiles).

HYRL used an analytical solution to the diffusion-sorption equations for a homogeneous medium (constant transport and sorption parameters), with the addition of a constant background activity accounting for the points originally measured far from the tracer source. D_a values range between 2.0×10^{-14} m²/s and 3.0×10^{-14} m²/s (Table 4-11). These values are overall consistent with laboratory D_e values for HTO (Vilks et al. 2005) and rock-matrix batch sorption K_d values for Ra-226 (Widestrand et al. 2010) – see Appendix 1.

JAEA provided results for a central case and for upper and lower bounds, based on ranges of values for D_e and K_d . The model concept did not try to account for any possible profile tails far from the tracer source. Their results show the effect from the fracture coating (increased ϕ , K_d and D_e values) included in the concept for the A profiles. D_a values in the fracture coating and disturbed zone are mainly in the 10^{-14} m²/s range, with a value of 5.1×10^{-15} m²/s for the undisturbed matrix (Table 4-11). Almost all measured data points are within the 5-mm disturbed zone assumed by JAEA, except for one point (core D12).

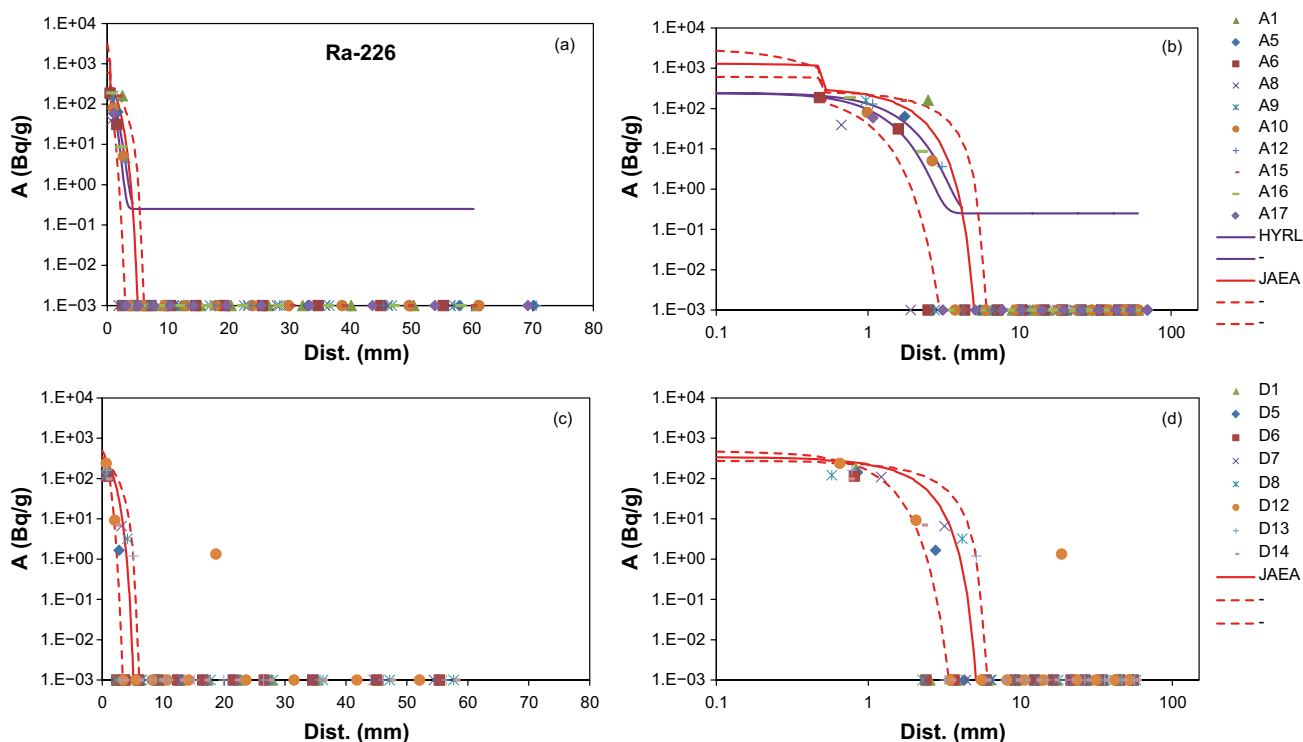


Figure 4-12. Measured (symbols) and calculated (lines) Ra-226 tracer profiles for A cores (a,b) and D cores (c,d). Activities are in Bq per gram of rock. All plots show all the measured data, with data plotted at the bottom of the figures (10^{-3} Bq/g) corresponding to measurements below detection limit. For those points, detection limits are always below 15 Bq/g and decrease with distance from the tracer source to values less than 1 Bq/g.

Table 4-11. Ra-226 transport and retention parameter values for the different zones implemented in the models. Different parameters have been adjusted by different teams. Apparent diffusion coefficients (D_a) have been calculated from the reported parameters in all the cases. D_e : effective diffusion coefficient; ϕ : porosity; K_d : sorption distribution coefficient.

Team	t (days)	Layer	Ra-226 D_e m ² /s	Ra-226 ϕ	Ra-226 K_d m ³ /kg	Ra-226 D_a m ² /s
HYRL	429, 479				6.0E-3 – 7.0E-3	2.0E-14 – 3.0E-14
JAEA	200	A1 – fracture (0–0.5 mm)	2.13E-12 –	0.01 –	4.3E-2 –	1.83E-14 –
		A2 – DZ (0.5–5 mm)	– 5.61E-14	– 0.001	– 4.1E-03	– 5.1E-15
		A3 – undisturbed (5 mm –)	5.61E-14	0.001	4.1E-03	5.1E-15
		D1 – DZ (0–5 mm)	2.13E-12 – 5.61E-14	0.01–0.001	4.6E-3 – 4.1E-3	1.7E-13 – 5.1E-15
		D2 – undisturbed (5 mm –)	5.61E-14	0.001	4.1E-03	5.1E-15

4.9 Np-237

Figure 4-13 shows the measured and calculated Np-237 profiles in the rock. Notice that there is only one single measurement of the very first slice available per core. Tracer profiles cannot really be defined from the measured data. Modelling results were only provided by JAEA (A and D profiles), including a central case and upper and lower bounds (from ranges of values for D_e and K_d). The results show the effect from the fracture coating (increased ϕ , K_d and D_e values) included in the concept for the A profiles. Table 4-12 shows the transport and retention parameters used in the fracture coating (A profiles), disturbed zone and undisturbed rock matrix. The values in the different zones cover the whole range of values calculated from laboratory D_e values for HTO (Vilks et al. 2005) and rock-matrix batch sorption K_d values for Np-237 (Widestrand et al. 2010) – see Appendix 1.

Table 4-12. Np-237 transport and retention parameter values for the different zones implemented in the model by JAEA. Apparent diffusion coefficients (D_a) have been calculated from the reported parameters. D_e : effective diffusion coefficient; ϕ : porosity; K_d : sorption distribution coefficient.

Team	t (days)	Layer	Np-237 D_e m ² /s	Np-237 ϕ	Np-237 K_d m ³ /kg	Np-237 D_a m ² /s
JAEA	200	A1 – fracture (0–0.5 mm)	1.02E-12 –	0.01 –	6.9E-3 –	5.5E-14 –
		A2 – DZ (0.5–5 mm)	– 2.69E-14	– 0.001	– 4.0E-05	– 2.5E-13
		A3 – undisturbed (5 mm –)	2.69E-14	0.001	4.0E-05	2.5E-13
		D1 – DZ (0–5 mm)	1.02E-12 – 2.69E-14	0.01–0.001	6.6E-5 – 4.0E-5	5.4E-12 – 2.5E-13
		D2 – undisturbed (5 mm –)	2.69E-14	0.001	4.0E-05	2.5E-13

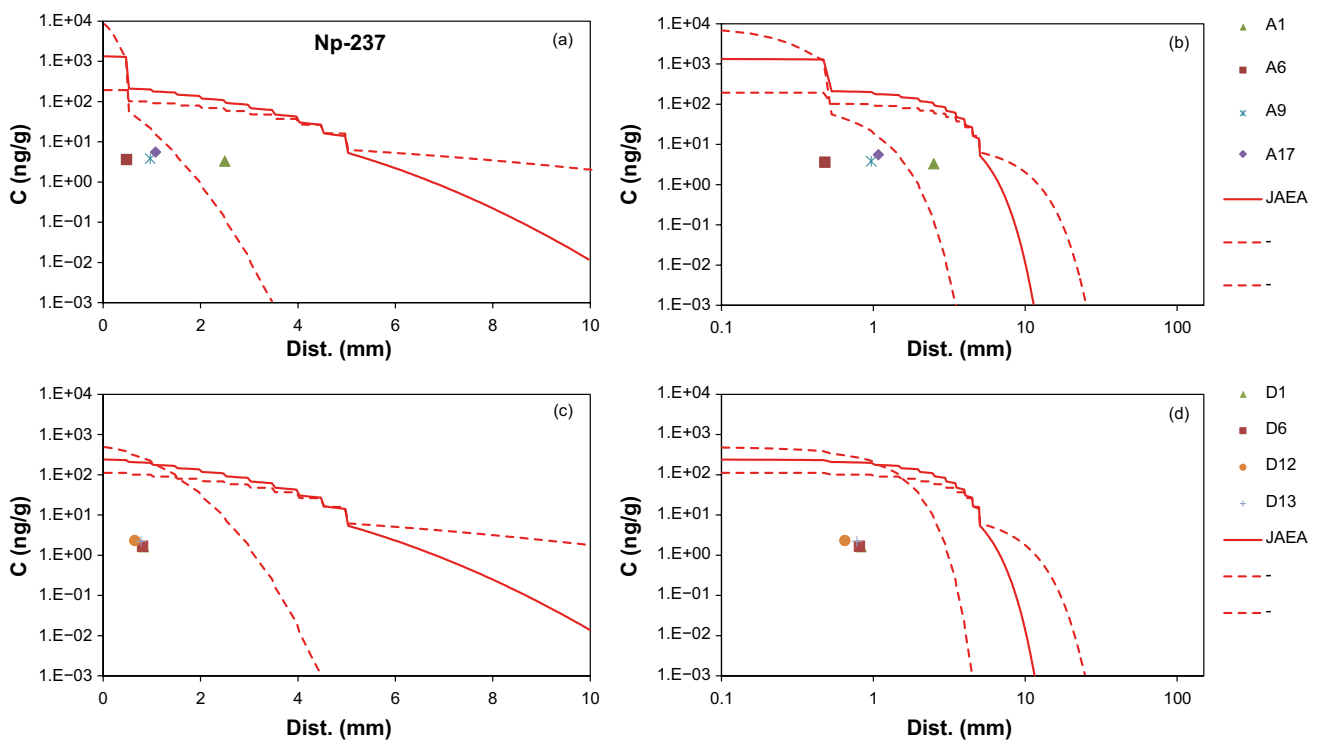


Figure 4-13. Measured (symbols) and calculated (lines) Np-237 tracer profiles for A cores (a,b) and D cores (c,d). Concentrations are in nanograms per gram of rock. All plots show all the measured data.

5 Summary and conclusions

The LTDE-SD experiment was performed at a depth of about 410 m in the Äspö Hard Rock Laboratory between September 27th 2006 and April 12th 2007. A cocktail of radionuclide tracers was circulated for 198 days on the exposed natural surface of a target fracture and in a narrow slim hole drilled in unaltered rock matrix. Overcoring took place shortly after the end of tracer circulation. Together with overcoring, core-sample drilling and slicing took an additional 240 to 290 days after the end of the in situ phase of the experiment.

Within Task 9B, the LTDE-SD in situ test results and supporting laboratory dataset were extended by performing microstructural characterisation of different rock samples and analyses of new cores (see Figure 1-5). In addition, the measured activities in the rock were critically reviewed and updated. The microstructural descriptions of the rock samples were used by several of the teams as the basis for detailed transport models.

The measured tracer activities in the rock samples showed very long profiles (several cm into the rock) for non- or weakly-sorbing tracers (Cl-36, Na-22), but also at low activities for many of the more strongly-sorbing radionuclides. This was an unexpected feature, and one of the main objectives of the modelling exercise was to try to understand these apparently anomalous profiles. However, well into the modelling exercise, re-evaluation of the measurements (see Figure 1-5) led to the identification of probable contamination during sample preparation. Experimental data were completely re-evaluated, leading to the revision of detection limits and the definition of potential contamination levels. After the revision, the anomalous long tails at low activities for strongly sorbing tracers basically disappeared, although a few data points remained for Cs-137 and Ba-133 (close to reported potential contamination levels), Ni-63 and Cd-109. However, most measured data values for strongly-sorbing tracers at long distances (> 10 mm) from the tracer source were now reported to be below detection limits. The few remaining “tail data” for different tracers were not in the same cores, i.e. not related to a possible single structure. Profiles for Cl-36 and Na-22 were not affected by this revision.

Ten different modelling teams provided results for this exercise, using different concepts and codes. An additional team provided results based on conceptual development motivated by this modelling exercise but not matching exactly the conditions of the in situ experiment. These additional results are not discussed in this report. Three main types of models were used: (1) analytical solutions to the transport-retention equations (KTH, HYRL), (2) continuum-porous-medium numerical models (TUL, CTU, GRS, JAEA), and (3) microstructure-based models, accounting for small-scale heterogeneity (i.e. mineral grains, porosities and/or microfracture distributions) and potential centimetre-scale fractures (CFE, A21, KAERI, PROGEO). Different types of zonations in terms of transport and retention parameters have been implemented in continuum-porous-medium and microstructure-based models, including the consideration of fracture coatings (JAEA), narrow (mm-scale) disturbed zones (GRS, JAEA, KAERI) or continuously-changing parameters with distance (TUL, CTU).

The team from KTH performed an estimation of mass balances for the different tracers based on the activities measured after the experiment (reservoir solution, rock matrix, equipment parts, activities removed when sampling). For non- and weakly-sorbing tracers (Cl-36, Na-22), the mass balances were very good. Most of the recovered activities were found in the reservoir, which agreed well with expectations. For cation-exchange tracers (Ba-133, Cs-137, Ra-226), the mass balances were acceptable, since around 80 % of the activities were accounted for, mainly located in the reservoir and in the rock matrix. In contrast, mass balances for surface-complexation ions were rather poor, especially for Co-57, Ni-63, Cd-109 and Gd-153, with more than half of the injected tracer activities not accounted for. The poor mass balance for some of the tracers and the rather constant activities in the reservoir for the non- and weakly-sorbing tracers made it difficult to include the calculation of the evolution of activities in the reservoir in the numerical analyses. Many of the teams actually used either fixed constant activities or prescribed time-dependent activities as reservoir boundary conditions.

For Cl-36 (non-sorbing) and Na-22 (weakly sorbing), two different parts of the tracer profiles in the rock can be distinguished. Commonly, a steeper part within ca 30 mm from the tracer source and an almost flat tail beyond 30 mm can be observed (Figures 4-1 to 4-4). Additionally, and more especially for the case of Cl-36, there is an even steeper segment within ca 5 mm from the tracer

source (Figures 4-3 and 4-4). These more proximal parts of the profiles, up to ca 30 mm, can be well reproduced by the homogeneous models. Results from these homogeneous models fitting the trends in the first 5 mm (Cl-36) require smaller D_a values, pointing to a well defined disturbed zone (DZ). D_a values for distances up to ca 30 mm are consistent with laboratory-derived porosities, effective diffusion coefficients (D_e for iodide and tritium available), and batch-sorption K_d values (Na-22). Parameter values for the more proximal part, within a few mm from the tracer source, result in smaller D_a values.

Models including a disturbed zone (DZ; JAEA, GRS) also capture well this type of profiles, up to ca 30 mm, although different concepts for the changes in D_e , f and K_d with distance have been implemented. D_a values beyond the implemented DZ (5 mm for JAEA, 1 mm for GRS) are consistent with laboratory-derived values. Beyond that distance, the fit is reasonable for Cl-36 (non-sorbing) but not very good for Na-22, with calculated activities dropping quickly with distance.

To fit the flatter ends of the profiles, CTU and TUL had to implement very large D_a values at those distances, not consistent with laboratory-derived values and clearly too large (larger than diffusion coefficients in free water) in some cases. Fitting of those tails by some of the microstructure-based models (CFE, KAERI, PROGEO) was performed by implementing fast transport along microfractures and cm-scale fractures, with no or strongly reduced sorption along these structures in most cases. The model from A21 did not implement such features (Na-22; only intergranular porosity), with results more similar to those from the homogeneous models.

All the other tracers considered in the modelling exercise (Co-57, Ni-63, Ba-133, Cs-137, Cd-109, Ra-226, Np-237) sorb more strongly than Na-22 and their tracer profiles are very different from those of Na-22 and Cl-36. In general, the tracer profiles do not extend beyond 10 mm from the tracer source, although there are some points with measured low activities at larger distances. However, most of the measurements at those distances show readings below detection limits. Also, these few remaining “tail data” for different tracers are not in the same cores, i.e. not related to a possible single structure. Overall, the best fits for the measured profiles within a few mm from the tracer source are achieved by the homogeneous models (constant transport and retention parameters), with D_a values mostly in the 10^{-15} to 10^{-14} m²/s range (10^{-14} to 10^{-13} m²/s for Ba-133; 10^{-14} to 10^{-12} m²/s for Np-237), and overall consistent with laboratory-derived D_e values for HTO and batch-sorption K_d values. Good fits are also achieved by models assuming the presence of a disturbed zone with gradually changing parameters. This observation, together with the fact that most of the measurements above detection limits fall within 5 to 8 mm from the tracer source, and the different trend for the Cl-36 profiles at those distances, suggest the existence of a disturbed zone with a thickness of a few mm and characterised by rather constant (with distance) transport and retention parameters. The longer profiles for Cl-36 and Na-22 point to the properties of an undisturbed rock matrix (not affected by borehole drilling or alteration zones next to fractures) beyond these 5 to 8 mm from the tracer source. Additionally, the flat profile tail ends observed for some of the Na-22 profiles may point to the effect of microfractures and cm-scale fractures (continuum-porous-medium models could not reproduce those tails using realistic parameter values). Remaining “tail data” for some of the strongly-sorbing tracers (notably Cs-137) could also be fitted by models considering the effect of cm-scale fractures or veins (KAERI), although the very flat trend of those remaining points could not be exactly reproduced. Also, many of the samples beyond 10 mm from the tracer source show measurements below detection limit.

The overall result from Task 9B was the understanding of the transport mechanisms and the role of rock structure (i.e. the effects of the disturbed zones and of the micro- and cm-scale fractures) behind the different tracer profiles (non-sorbing, weakly-sorbing and strongly-sorbing) from the LTDE-SD experiment in the tight granodiorite at Äspö. This new insight was allowed first by the re-evaluation and revision of the experimental data (tracer profiles in the rock), which also highlighted the importance of using of blank samples during sample preparation and analysis in future tracer transport experiments. The use of blank samples is essential for the detection of potential contamination or background effects. Another potential improvement could be provided by preparing small-core samples immediately after overcoring. In addition, determination of potential anion exclusion effects could have been achieved if tritium (or another equivalent neutral conservative tracer) had been included in the list of tracers.

In terms of tracer transport and retention, the modelling performed by the different teams allowed the comparison of different model concepts and potential zonations of rock properties. Important features to understand the tracer profiles in the rock were the presence of a disturbed zone close to the tracer source (natural fracture or borehole), with strongly-sorbing-tracer activities restricted to a large degree

to this disturbed zone (at least in the limited time scales of the experiment), and the role of micro- and cm-scale fractures in the formation of the observed long profile tails for weakly-sorbing tracers (Na-22). Additionally, there was an overall compatibility of laboratory-derived transport and retention properties with the observed profiles (with variability according to the the described structural features) supporting the conclusions. Task 9B, and the Task Force GWFTS as a whole, provided the motivation to advance in conceptual and numerical model development for radionuclide transport in tight crystalline rock.

Acknowledgements

The comments from Dr. Kersti Nilsson, the analytical work by VKTA (Task 9B-3 samples, Dresden, Germany) and the constructive review by Dr. Anna-Maria Jakobsson are gratefully acknowledged.

References

SKB's (Svensk Kärnbränslehantering AB) publications can be found at www.skb.com/publications.

Březina J, Stebel J, Flanderka D, Exner P, Hybš J, 2018. Flow123d, Version 2.2.1, User guide and input reference. Technical university of Liberec, Faculty of Mechatronics, Informatics and Interdisciplinary Studies, Liberec, Czech Republic.

GoldSim Technology Group, 2018. User's guide, GoldSim, Probabilistic Simulation Environment. GoldSim Technology Group, Issaquah, WA.

Hammond G E, Lichtner P C, Mills R T, 2014. Evaluating the performance of parallel subsurface simulators: An illustrative example with PFLOTRAN. *Water Resources Research* 50, 208–228.

Hartley L J, 1998. NAPSAC release 4.1 technical summary document. AEA-R&R-0271, AEA Technology, UK.

Hokr M, Havlová V, Vetešník A, Gvoždík L, Milický M, Polák M, Reimitz D, Říha J, Trpkošová D, Višňák J, Vopálka D, 2020. Testing of transport models using foreign in situ experiments. SÚRAO Report 481/2020/ENG, Prague, Czech Republic.

Hokr M, Havlová V, Vetešník A, Gvoždík L, Milický M, Polák M, Reimitz D, Říha J, Trpkošová D, Višňák J, Vopálka D, 2021. Testing of fracture-matrix transport models using in situ data and benchmark problems. Task 9 of SKB Task Force GWFTS – Increasing the realism in solute transport modelling based on the field experiments REPRO and LTDE-SD. SKB P-20-22, Svensk Kärnbränslehantering AB.

Hyman J D, Karra S, Makedonska N, Gable C W, Painter S L, Viswanathan H S, 2015. dfnWorks: A discrete fracture network framework for modeling subsurface flow and transport. *Computers & Geosciences* 84, 10–19.

Iraola A, Trinchero P, Voutilainen M, Gylling B, Selroos J-O, Molinero J, Svensson U, Bosbach D, Deissmann G, 2017. Microtomography-based Inter-Granular Network for the simulation of radionuclide diffusion and sorption in a granitic rock. *Journal of Contaminant Hydrology* 207, 8–16.

Kekäläinen P, 2021. Modelling of the long term diffusion and sorption experiment using an analytically solvable model. Task 9 of SKB Task Force GWFTS – Increasing the realism in solute transport modelling based on the field experiments REPRO and LTDE-SD. SKB P-21-06, Svensk Kärnbränslehantering AB.

Kröhn K-P, 2020. Checking on the consistency of the ‘two-zone model’ for Task 9B – LTDE-SD. Task 9 of SKB Task Force GWFTS – Increasing the realism in solute transport modelling based on the field experiments REPRO and LTDE-SD. SKB P-20-02, Svensk Kärnbränslehantering AB.

Li Q, Ito K, Wu Z, Lowry C S, Loheide II S P, 2009. COMSOL Multiphysics: A novel approach to ground water modeling. *Groundwater* 47, 480–487.

Löfgren M, Nilsson K, 2020. Task description of Task 9B – Modelling of LTDE-SD performed at Äspö HRL. Task 9 of SKB Task Force GWFTS – Increasing the realism in solute transport modelling based on the field experiments REPRO and LTDE-SD. SKB P-17-30, Svensk Kärnbränslehantering AB.

Meng S, Moreno L, Neretnieks I, Liu L, 2020. Modelling matrix diffusion in Task 9B – LTDE-SD. Task 9 of SKB Task Force GWFTS – Increasing the realism in solute transport modelling based on the field experiments REPRO and LTDE-SD. SKB P-20-01, Svensk Kärnbränslehantering AB.

Nilsson K, Byegård J, Selnert E, Widestrand H, Höglund S, Gustafsson E, 2010. Äspö Hard Rock Laboratory. Long Term Sorption Diffusion Experiment (LTDE-SD). Results from rock sample analyses and modelling. SKB R-10-68, Svensk Kärnbränslehantering AB.

Park D K, Ji S-H, 2018. Numerical simulation of anomalous observations from an in situ long-term sorption diffusion experiment in a rock matrix. *Journal of Hydrology* 565, 502–515.

- Park D K, Ji S-H, 2020.** Corrigendum to “Numerical simulation of anomalous observations from an in situ long-term sorption diffusion experiment in a rock matrix” [J. Hydrol.565 (2018) 502–515]. Journal of Hydrology 586, 124758. doi:10.1016/j.jhydrol.2020.124758
- Perko J, Seetharam S C, Mallants D, 2009.** Simulation tools used in long-term radiological safety assessments. Project Near Surface Disposal of Category A Waste at Dessel. NIROND-TR 2008-11 E, ONDRAF/NIRAS, Belgium.
- Schneider A (ed), 2016.** Modelling of data uncertainties on hybrid computers (H-DuR). FKZ 02 E 11062A (BMW), Gesellschaft für Anlagen- und Reaktorsicherheit (GRS) mbH, GRS-392, Germany.
- Svensson U, 2020.** Task 9B – A grain-scale reactive transport model – concepts and tests. Task 9 of SKB Task Force GWFTS – Increasing the realism in solute transport modelling based on the field experiments REPRO and LTDE-SD. SKB P-20-15, Svensk Kärnbränslehantering AB.
- Svensson U, Ferry M, 2014.** DarcyTools: a computer code for hydrogeological analysis of nuclear waste repositories in fractured rock. Journal of Applied Mathematics and Physics 2, 365–383.
- Tachi Y, Ebina T, Takeda C, Saito T, Takahashi H, Ohuchi Y, Martin A J, 2015.** Matrix diffusion and sorption of Cs⁺, Na⁺, I⁻ and HTO in granodiorite: Laboratory-scale results and their extrapolation to the in situ condition. Journal of Contaminant Hydrology 179, 10–24.
- Tachi Y, Ito T, Gylling B, 2017.** Modeling the in situ Long-Term Sorption and Diffusion Experiment (LTDE-SD) at the Äspö Hard Rock Laboratory in Sweden: scaling approach from laboratory to in situ condition. In Proceedings of 16th International Conference on the Chemistry and Migration Behaviour of Actinides and Fission Products in the Geosphere (Migration 2017), Barcelona, Spain, 10–15 September 2017.
- Trincherro P, Molinero J, Deissmann G, Svensson U, Gylling B, Ebrahimi H, Hammond G, Bosbach D, Puigdomenech I, 2017.** Implications of grain-scale mineralogical heterogeneity for radionuclide transport in fractured media. Transport in Porous Media 116, 73–90.
- Vilks P, Miller N H, Stanchell F W, 2005.** Laboratory program supporting SKB’s Long Term Diffusion Experiment. Report 06819-REP-01300-10111-R00, Atomic Energy of Canada Limited.
- Widestrand H, Byegård J, Nilsson K, Höglund S, Gustafsson E, Kronberg M, 2010.** Long Term Sorption Diffusion Experiment (LTDE-SD). Performance of main in situ experiment and results from water phase measurements. SKB R-10-67, Svensk Kärnbränslehantering AB.
- Winberg A, Hermanson J, Tullborg E-L, Staub I, 2003.** Äspö Hard Rock Laboratory. Long-Term Diffusion Experiment. Structural model of the LTDE site and detailed description of the characteristics of the experimental volume including target structure and intact rock section. SKB IPR-03-51, Svensk Kärnbränslehantering AB.
- Wood, 2018.** ConnectFlow technical summary. Release 12.0. Didcot, UK.
- Zheng C, 2010.** MT3DMS v5.3 supplemental user’s guide. Technical Report to the U.S. Army Engineer Research and Development Center, Department of Geological Sciences, University of Alabama.
- Zheng C, Wang P P, 1999.** MT3DMS: A modular three-dimensional multi-species transport model for simulation of advection, dispersion and chemical reactions of contaminants in groundwater systems: documentation and user’s guide. Contract Report SERDP-99-1, University of Alabama.

Summary tables with available measured rock porosities, transport and sorption parameters

Table A1-1 (Widestrand et al. 2010). Summary of the results from measurements of porosity, ϵ , in rock material from KA3065A02, KA3065A03 as well as the rock samples from the Site investigation included in the sorption/diffusion experiments on intact cores. The porosity is expressed in vol.%. The measurement uncertainty of a single porosity value determined by the water saturation method is 0.05 vol.%, given with 1σ confidence. The samples have been divided into four general types: 1, matrix rock; 2, matrix rock with fracture surface on one side; 3, mainly fracture mineralizations and cataclastic rock matrix; 4, strongly altered bedrock.

Rock sample ID	Type of sample	Water saturation measurements (vol.%)				¹⁴ C-PMMA measurements (vol.%)	
		22 mm core diameter	44 mm core diameter	50 mm core diameter	irregular rock samples	22 mm core diameter	irregular rock samples
LTDE-SD samples							
A02:4	1		0.23				
A02:5	1		0.28				
A02:7	1		0.23				
A02:8	1		0.17				
A03:3/Diff I	2	0.33					
A03:4/Diff II	1	0.16					
A03:5/Diff III	1	0.19					
A03:6/Diff IV	1	0.27					
A03:7	1	0.36				0.51	
A03:8	1	0.40				0.61	
A03:10	3/4				2.35		2.4/11*
A03:11	3				5.16		2.0/11*
Forsmark site investigation samples (Selnert et al. 2008)							
KFM02A 276.06	4			18.4			
KFM03A 242.43	1			0.19			
KFM07A 608.75	1			0.29			
KFM09A 713.67	1			0.24			
Oskarshamn site investigation samples (Selnert et al. 2009a)							
KSH01 891.91	1			0.46			
KSH01 981.43	1			0.29			
KLX02 235.08	1			0.39			
KLX04 726.07	1			0.08			
KLX08 417.05	1			0.45			
KLX10 995.79	1			0.06			

* Concerning the PMMA; mean values for the strongly altered bedrock are given to the left and for the cataclastic to the right.

Table A1-2 (Vilks et al. 2005). Summary of iodide diffusion cell data.

Set	Sample	Orientation with Respect to Core Axis	De	Water Immersion Porosity	Rock Capacity Factor	Effective Tortuosity
			(m ² /sec)	(ϵ_c)	(α)	(τ_b)
020205	E-1	parallel	2.88E-14	3.75E-03	1.81E-03	16.35
020205	E-2	parallel	1.80E-14	2.48E-03	1.61E-03	16.82
020205	E-3	parallel	1.82E-14	2.75E-03	1.38E-03	17.60
020205	E-4	parallel	4.75E-14	3.14E-03	2.66E-03	11.64
F 010305	F-1	parallel	1.34E-12	2.80E-03	-	2.07
F 010305	F-2	parallel	4.37E-15	2.59E-03	9.06E-05	34.86
F 010305	F-3	parallel	1.08E-13	2.65E-03	6.74E-03	7.11
F 010305	F-4	parallel	3.86E-14	2.83E-03	1.17E-03	12.26
A 180705	A-1	parallel	5.58E-12	3.11E-03	-	0.32
A 180705	A-2	parallel	2.96E-13	3.35E-03	3.63E-03	4.86
A 180705	A-3	parallel	2.63E-13	3.84E-03	4.54E-03	5.48
A 180705	A-4	parallel	2.98E-12	3.15E-03	3.07E-03	1.11
M 180705	M-1A	perpendicular	1.62E-13	2.84E-03	1.54E-03	5.99
M 180705	M-3A	perpendicular	4.10E-13	3.00E-03	1.84E-03	3.87
M 180705	M-1B	perpendicular	1.34E-13	2.44E-03	1.28E-03	6.11
M 180705	M-3B	perpendicular	3.50E-12	3.10E-03	2.94E-02	1.35
	M-2A	perpendicular		3.40E-03		
	M-2B	perpendicular		3.17E-03		

Table A1-3 (Vilks et al. 2005). Summary of tritium diffusion cell data.

Set	Sample	Orientation with Respect to Core Axis	De	Water Immersion Porosity	Rock Capacity Factor	Effective Tortuosity
			(m ² /sec)	(ϵ_c)	(α)	(τ_b)
020205	E-1	parallel	4.78E-14	3.75E-03	1.91E-03	27.02
020205	E-2	parallel	1.82E-13	2.48E-03	3.96E-03	14.25
020205	E-3	parallel	4.48E-14	2.75E-03	1.97E-03	20.21
020205	E-4	parallel	8.20E-13	3.14E-03	1.80E-02	14.30
F 010305	F-1	parallel	1.50E-12	2.80E-03	-	4.17
F 010305	F-2	parallel	1.29E-14	2.59E-03	4.50E-04	43.22
F 010305	F-3	parallel	1.99E-13	2.65E-03	5.58E-03	11.14
F 010305	F-4	parallel	8.51E-14	2.83E-03	7.84E-04	17.60
A 180705	A-1	parallel	4.61E-11	3.11E-03	-	0.79
A 180705	A-2	parallel	1.16E-12	3.35E-03	1.80E-03	5.18
A 180705	A-3	parallel	4.56E-13	3.84E-03	4.04E-03	8.85
A 180705	A-4	parallel	1.48E-12	3.15E-03	1.50E-03	2.83
M 180705	M-1A	perpendicular	1.06E-12	2.84E-03	2.57E-03	4.99
M 180705	M-3A	perpendicular	1.02E-12	3.00E-03	2.84E-03	5.23
M 180705	M-1B	perpendicular	8.27E-13	2.44E-03	2.96E-03	5.24
M 180705	M-3B	perpendicular	3.77E-12	3.10E-03	4.98E-02	2.77
	M-2A	perpendicular		3.40E-03		
	M-2B	perpendicular		3.17E-03		

Table A1-4 (Widestrand et al. 2010). Results from the batch sorption experiments. The presented K_d values are mean values of two individual measured samples. Contact time: 186 days. Particle size fraction: 1–2 mm.

Radio-nuclide	KA3065A02:1 Red-stained matrix rock		KA3065A02:2 Fracture minerals		KA3065A02:6 Matrix rock		KA3065A03_Batch 1 Matrix rock		KA3065A03_Replica Fracture minerals	
	K_d (m ³ /kg)	+/-	K_d (m ³ /kg)	+/-	K_d (m ³ /kg)	+/-	K_d (m ³ /kg)	+/-	K_d (m ³ /kg)	+/-
Cl-36 ¹⁾							< 1.1E-03		< 8.8E-04	
Na-22	1.7E-04	2.2E-05	3.3E-04	8.3E-04	4.2E-04	9.4E-04	2.8E-04	6.9E-04	-9.6E-05	4.7E-04
Tc-99	2.5E-04	9.8E-05	1.3E-04	3.1E-04	2.3E-04	1.8E-04	2.1E-04	4.6E-05	3.0E-06	5.3E-04
Se-75	1.6E-03	3.0E-03	5.3E-03	4.8E-03	1.4E-03	4.5E-04	1.9E-03	1.5E-03	3.1E-03	4.9E-03
Np-237	1.1E-03	3.0E-04	2.5E-03	8.6E-04	7.2E-04	5.1E-04	6.4E-04	9.4E-05	9.9E-03	9.4E-04
Ba-133	2.0E-03	2.6E-04	9.8E-03	5.8E-04	2.3E-03	2.2E-03	2.0E-03	9.4E-04	1.5E-02	2.5E-03
U-236	1.6E-03	8.3E-04	1.1E-02	3.5E-03	1.1E-03	6.3E-04	9.3E-04	1.1E-04	5.9E-02	2.6E-02
Cd-109	5.9E-03	1.0E-03	2.6E-02	6.7E-04	5.3E-03	4.7E-03	4.0E-03	1.2E-03	9.2E-02	8.2E-02
Ra-226	8.3E-03	1.6E-03	3.7E-02	1.4E-03	7.5E-03	1.4E-03	6.7E-03	5.0E-04	7.5E-02	3.3E-03
Ni-63 ¹⁾	2.5E-02	9.1E-03	4.6E-02	1.6E-02	1.3E-02	5.1E-03	8.2E-03	3.7E-03	2.7E-01	1.2E-01
Co-57	5.2E-02	1.5E-02	2.7E-01	2.4E-03	6.1E-02	2.8E-02	2.6E-02	2.9E-03	5.3E-01	1.7E-01
Cs-137	1.2E-02	4.8E-03	1.0E-01	2.1E-02	3.2E-02	1.1E-02	2.2E-02	3.4E-03	8.6E-01	1.8E-01
Ag-110 m	> 1E-02		> 1E-02		> 1E-02		> 1E-02		> 1E-02	
Gd-153	> 4E-01		> 4E-01		> 4E-01		> 4E-01		> 4E-01	

¹⁾ Based on single samples measured.

Comparison of activity profiles between Data Delivery 11 (start of Task 9B) and Data Delivery 40 (final dataset)

This appendix provides summary plots of A and D core activity profiles for selected radionuclides to illustrate the impact of the revision of data during the task. Table A2-1 summarises the changes for the 5 selected nuclides.

Table A2-1. Summary of changes in radionuclide activity profiles between Data Delivery 11 and Data Delivery 40 for Na-22, Cl-36, Ba-133, Cs-137 and Co-57.

RN	Sorbing	Comparison with A20	Impact of data revision
Na-22	Weakly sorbing	Low levels of activity in A20 relative to that seen in A1, A5 and A6	Estimated levels of sample contamination do not significantly change the observed pattern
Cl-36	Non-sorbing	No activities measured in A20	Practically no change (only new analyses from Task-9B3 cores)
Ba-133	Strongly sorbing	Observed levels of activity in A20 comparable to that seen in other cores beyond 10 mm	Estimated levels of sample contamination change the dataset beyond 10 mm (data no longer reliable)
Cs-137	Strongly sorbing	Observed levels of activity in A20 comparable to that seen in other cores beyond 10 mm	Estimated levels of sample contamination significantly change the dataset beyond 10 mm (data no longer reliable)
Co-57	Strongly sorbing	Observed levels of activity in A20 comparable to that seen in other cores beyond 10 mm	Estimated levels of sample contamination do not significantly change the dataset

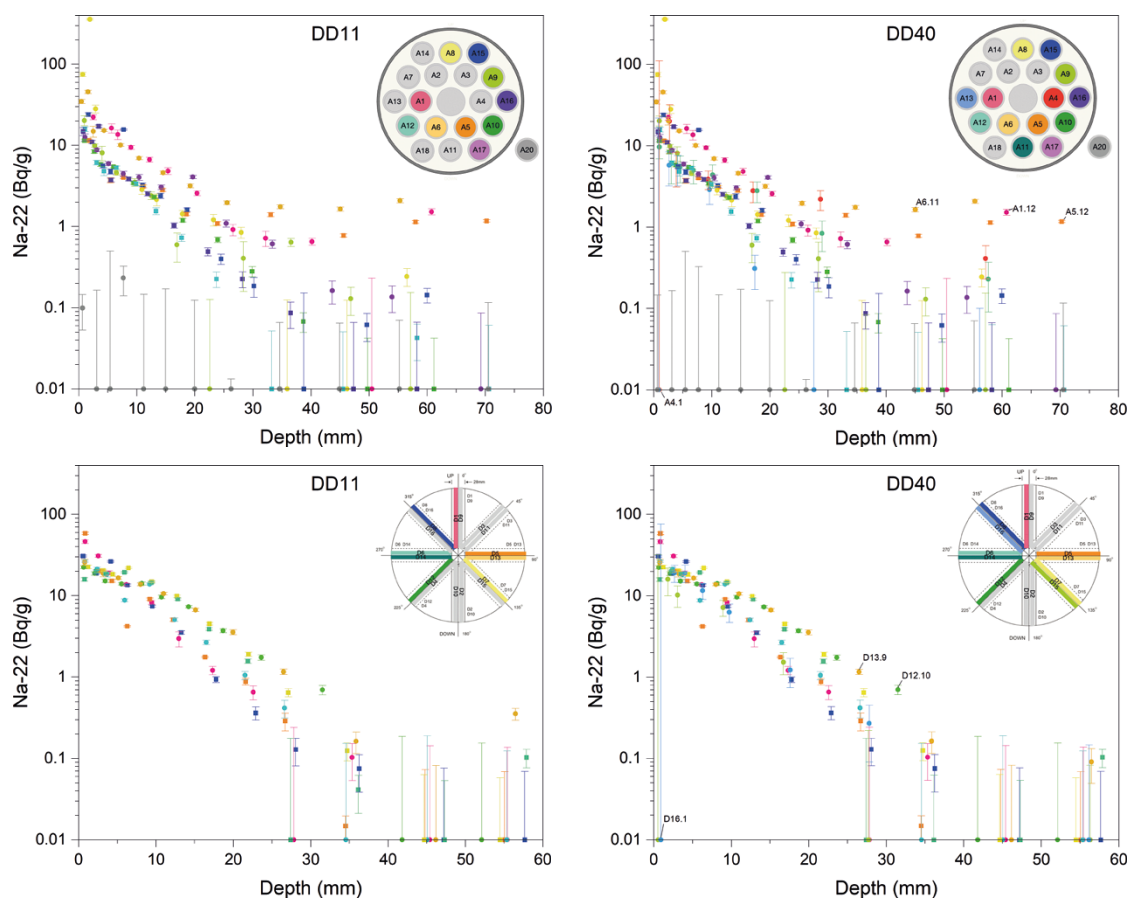


Figure A2-1. Na-22 activity in A and D cores in DD11 and DD40. Data points below detection limit are plotted on the bottom axis of the plots.

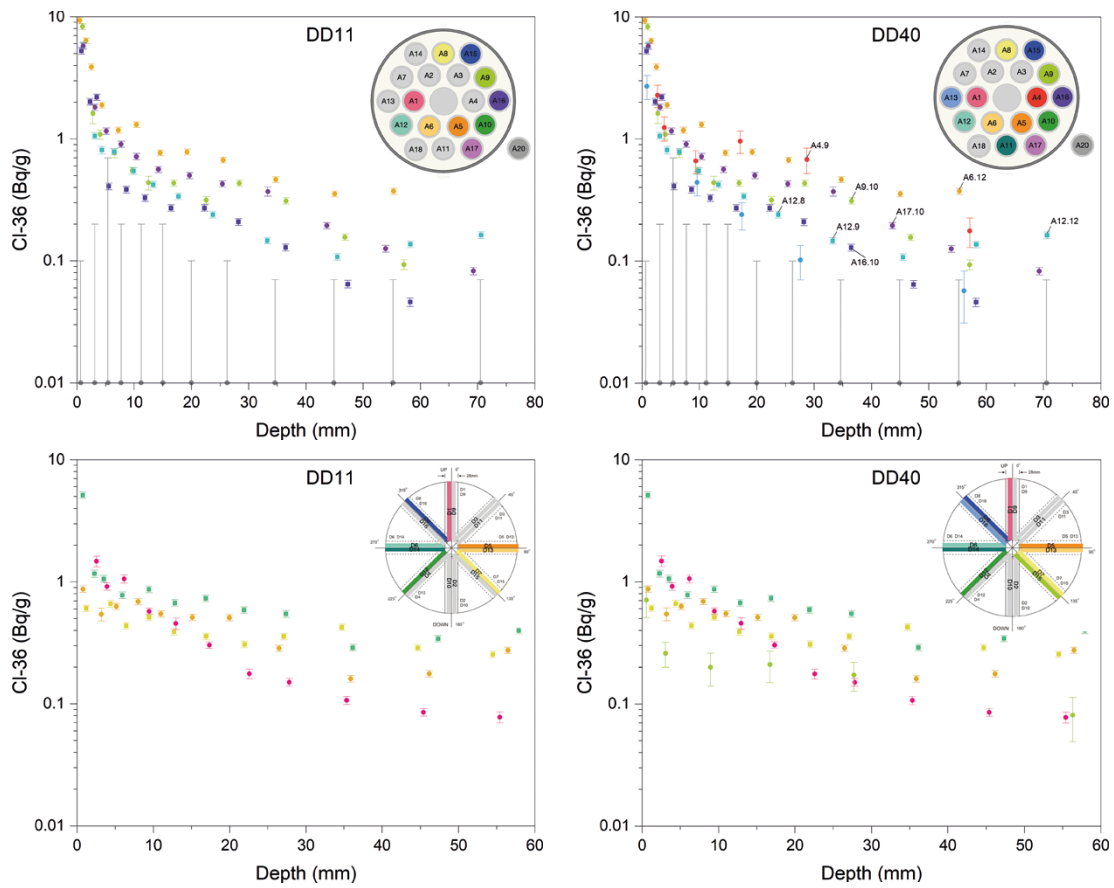


Figure A2-2. *Cl-36 activity in A and D cores in DD11 and DD40. Data points below detection limit are plotted on the bottom axis of the plots.*

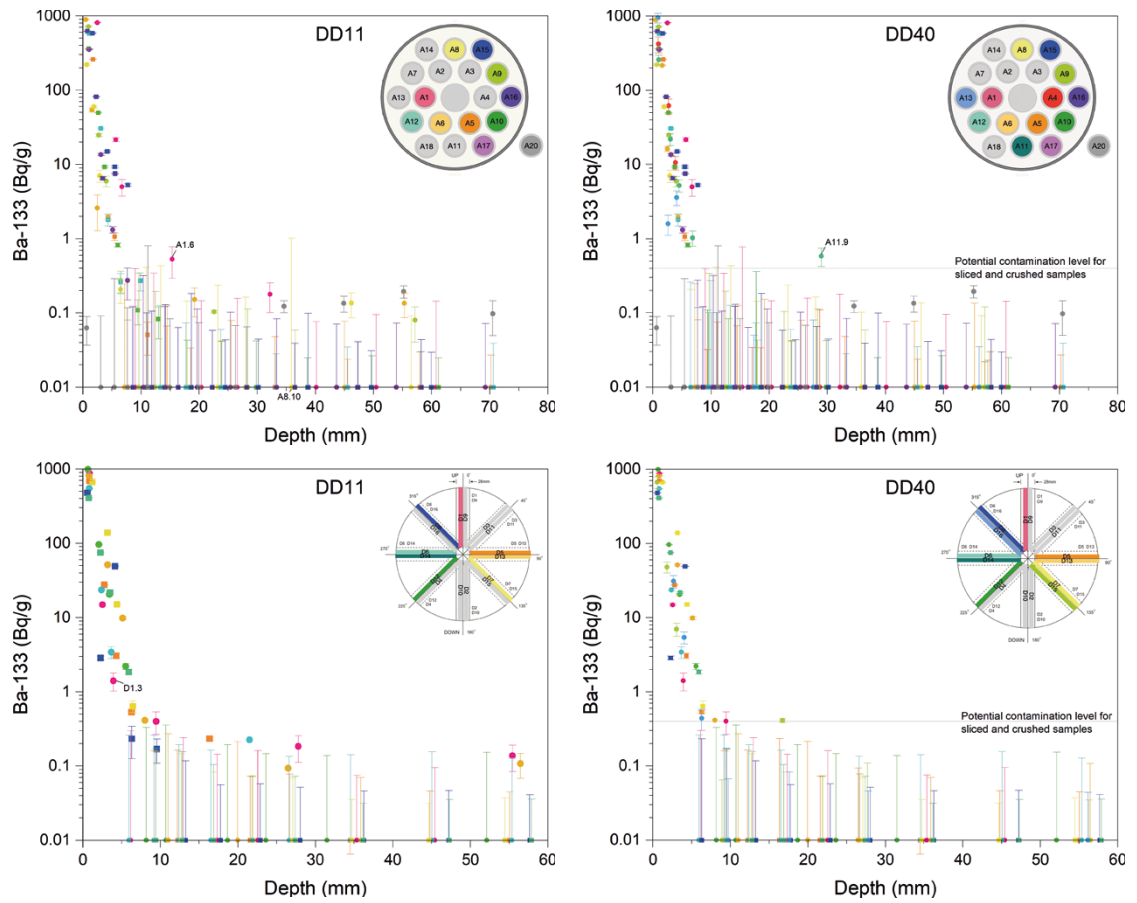


Figure A2-3. *Ba-133* activity in A and D cores in DD11 and DD40. Data points below detection limit (DD11, DD40) or affected by contamination (DD40) are plotted on the bottom axis of the plots.

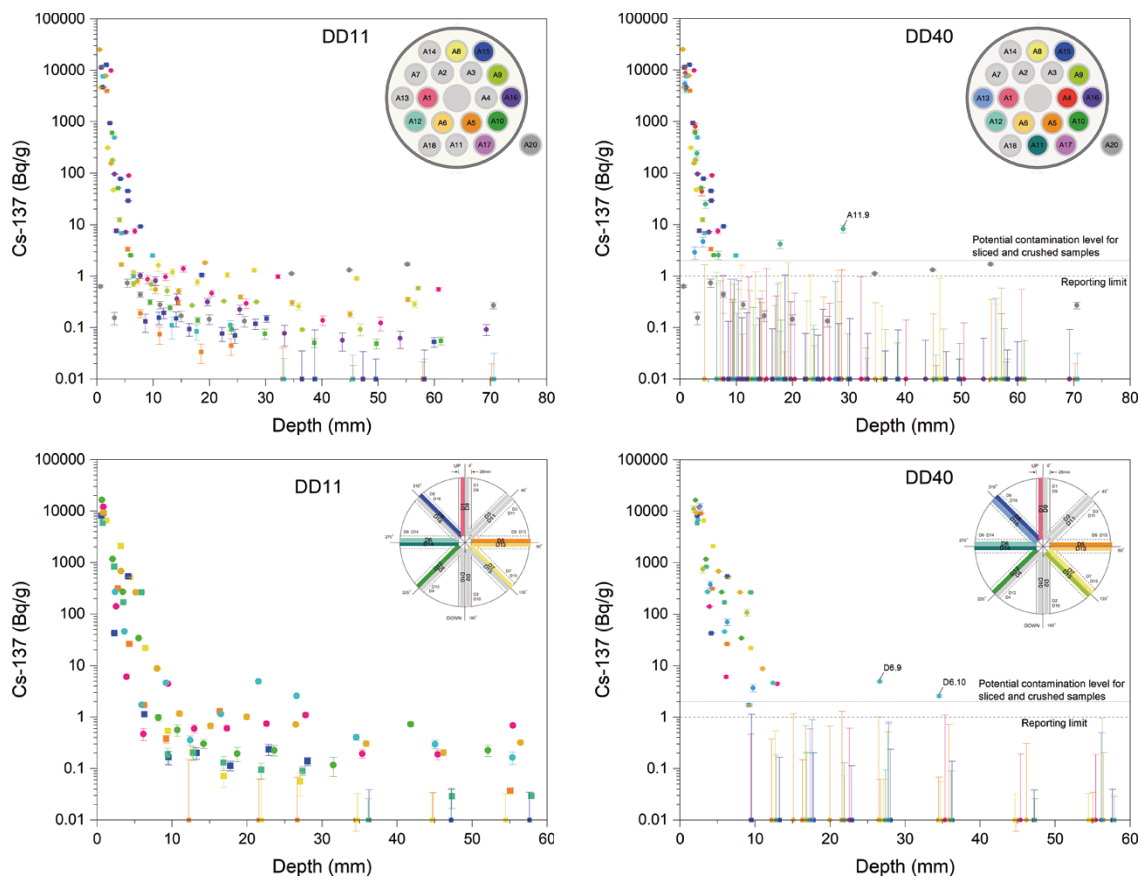


Figure A2-4. Cs-137 activity in A and D cores in DD11 and DD40. Data points below detection limit (DD11, DD40) or affected by contamination (DD40) are plotted on the bottom axis of the plots.

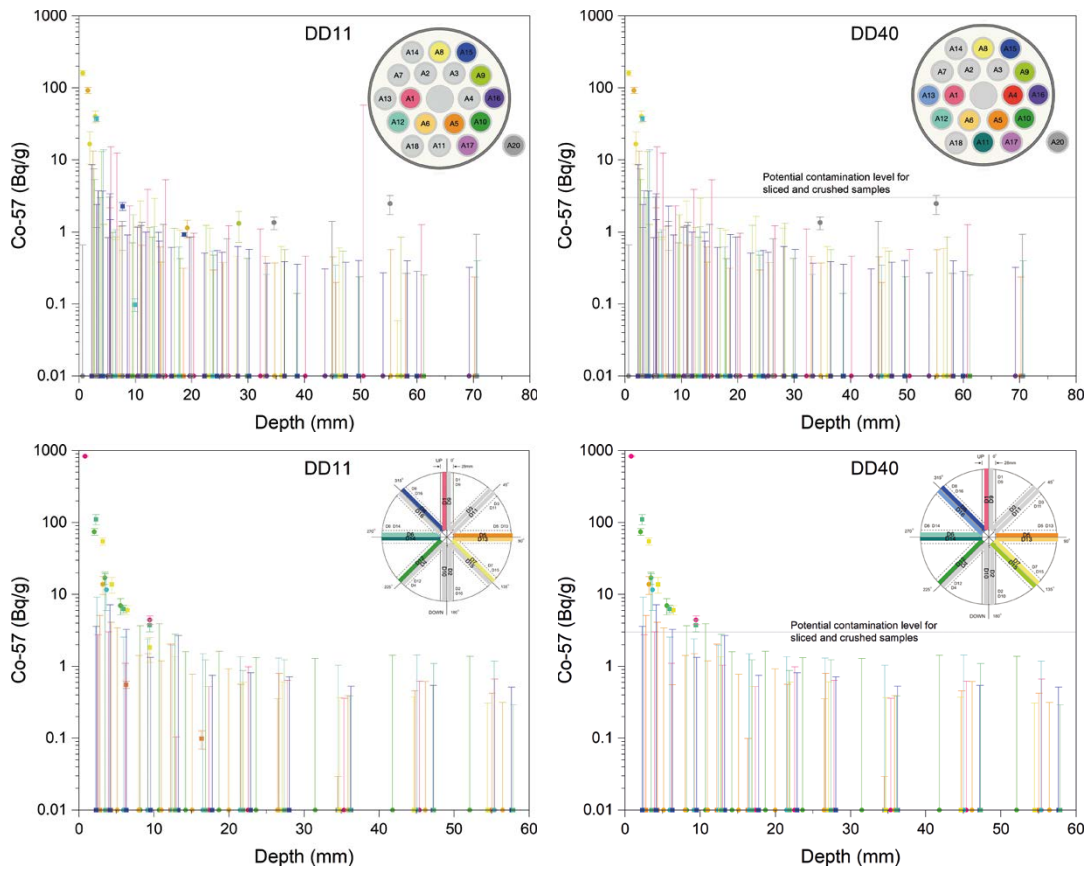


Figure A2-5. Co-57 activity in A and D cores in DD11 and DD40. Data points below detection limit (DD11, DD40) or affected by contamination (DD40) are plotted on the bottom axis of the plots.

